CRINC — REMOTE SENSING LABORATORY

NASA-CR-168576

E85-10019

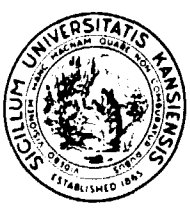

THE UNIVERSITY OF KANSAS CENTER FOR RESEARCH, INC.

2291 Irving Hill Drive—Campus West
Lawrence, Kansas 66045

ACTIVE MICROWAVE MEASUREMENTS OF SEA ICE UNDER FALL CONDITIONS THE RADARSAT/FIREX FALL EXPERIMENT

R.G. Onstott
Y.S. Kim
R.K. Moore

Remote Sensing Laboratory
Center for Research, Inc.
The University of Kansas
Lawrence, Kansas 66045-2969

RSL Technical Report
RSL TR 331-30/578-Final

June 1984

Supported by:

OFFICE OF NAVAL RESEARCH
Department of the Navy
800 N. Quincy Street
Arlington, Virginia 22217

Contract N00014-76-C-1105

and

NASA HEADQUARTERS
Washington, D.C.

Contract NAGW-334

This investigation was supported by:

U.S. Agencies:

Office of Naval Research
National Aeronautics and Space Administration

Canadian Agencies:

Atmospheric Environment Service (Ottawa)
Atmospheric Environment Service (Winnipeg)
Radar Satellite Program
Polar Continental Shelf Project

ACKNOWLEDGEMENTS

Acknowledgements are due to a large number of individuals and organizations who provided support during the Mould Bay October 1981 Field Investigation. They are:

(1) A.E.S. staff at Mould Bay (O.I.C.P. Gunst, H.E.O.M. Norman)
(2) A.E.S. staff at Resolute Bay (O.I.C.C. Hannah)
(3) Arctic Weather Center, Edmonton
(4) Auto-Concrete Curb Ltd.
(5) Bradley Air Services (Resolute Bay)
(6) Polar Continental Shelf Project (Ottawa)
(7) Quasar Aviation Ltd.
(8) Technical Field Support Services (E.M.R.)

ABSTRACT

During October 1981, the University of Kansas Remote Sensing Laboratory conducted a series of measurements of the active microwave properties of sea ice under fall growing conditions. These measurements, which focused on the characteristics of multiyear and newly formed ice, were made as part of the FIREX/RADARSAT Experiment Program, and were coordinated with an intensive ice characterization program led by Dr. Rene O. Ramseier of AES/RADARSAT Canada. This program was based at the High Arctic Weather Station on Prince Patrick Island. Ice in the inland waters of Mould Bay, Crozier Channel, and Intrepid Inlet and ice in the Arctic Ocean near Hardinge Bay was investigated.

Active microwave data were acquired using the University of Kansas helicopter-borne scatterometer (HELOSCAT) which operated at frequencies between 4 and 18 GHz, at angles from 5° to 70°, and at like- and cross-antenna polarizations.

Results show that multiyear ice frozen in grey or first-year ice is easily detected under cold fall conditions due to greater than 6 dB contrasts at most incidence angles. Contrast improves with increasing frequency. Backscatter behavior at C-band frequencies is more similar to that at Ku-X-band than L-band frequencies. Multiyear ice returns were dynamic due to response to two of its scene constituents, ice mounds which produce strong returns and meltpools which produce weaker returns. Variations in grey and first-year ice returns are, in comparison, much less. Floe boundaries between thick and thin ice are well defined with a characteristically brief, high contrast radar response. Multiyear pressure ridge returns are similar in level to background ice returns. Backscatter from homogeneous first-year ice is seen to be primarily due to surface scattering, and variation due to small-scale surface roughness changes is shown to result in an overall spread of 3-4 dB. Operation at 9.6 GHz is more sensitive to the detailed changes in scene roughness, while operation at 5.6 GHz seems to track roughness changes less ably, but provides greater absolute level shifts. Grey ice backscatter is demonstrated to be dependent upon the state of deformation.

TABLE OF CONTENTS

1.0 INTRODUCTION.....1

2.0 THE RADAR SCATTEROMETER.....2

3.0 EXPERIMENT DESCRIPTION.....5

4.0 DESCRIPTION OF THE BACKSCATTER DATA.....9

5.0 EXPERIMENT RESULTS.....10

- 5.1 Intrepid Inlet - An Old Multiyear Floe Frozen in Grey Ice.....13
- 5.2 Multiyear Pressure Ridge.....16
- 5.3 Mould Bay - First-Year Ice.....16
- 5.4 Hardinge Bay - Shorefast Ice.....22
- 5.5 Lake Ice.....23
- 5.6 Summary.....27
  - 5.6.1 Frequency Response.....27
  - 5.6.2 Angular Response.....32
  - 5.6.3 Contrast.....37

6.0 CONCLUSIONS.....39

REFERENCES.....43

APPENDICES.....44

LIST OF TABLES

TABLE 1 HELOSCAT III System Specifications.....3

TABLE 2: Summary of Data Acquisition by Helicopter-Borne Scatterometer.....7

TABLE 3: Mould Bay Field Investigation Personnel.....9

TABLE 4: Distance Between Mould Bay Site Markers Based on SLAR Imagery.....10

TABLE 5: Ice Characterization Measurements for Mould Bay First-Year Ice on 19 Oct.....19

LIST OF FIGURES

FIGURE 2.1: University of Kansas Helicopter-Borne Scatterometer Mounted on Bell Model 206.....4

FIGURE 3.1: Experiment Site Location Map.....6

FIGURE 4.1: Mould Bay First-Year Ice Flight Line.....11

FIGURE 4.2: HELOSCAT Flight Line of an Old Multiyear Floe Frozen in Grey Ice Located in Intrepid Inlet.....11

FIGURE 4.3: HELOSCAT Flight Line for Old Shorefast Ice Located in Hardinge Bay.....12

FIGURE 5.1: Profile of a Composite Multiyear Ice Floe at (a) 5.6 GHz and (b) 9.6 GHz.....14

FIGURE 5.2: Typical Profile of a Multiyear Pressure-Ridge.....17

FIGURE 5.3(a): Profiles Across the Mould Bay with = 20, F=5.6 and 9.6 GHz and Average ° for Each Interval and Sample Snow and Ice Depths.....20

FIGURE 5.3(b): Average Scattering Cross-Sections for Individual Zones Across Mould Bay at (a) 5.6 and (b) 9.6 GHz; HH-Polarization; and 20°, 40° and 60°.....21

FIGURE 5.4(a) Profile of Old Shorefast Ice in Hardinge Bay at 9.6 GHz, VV-Polarization and 40°.....24

FIGURE 5.4(b): Scattering Cross-Section Frequency Response for Old Shorefast Ice in Hardinge Bay at VV-Polarization at 40° (1) and 70° (2).....25

FIGURE 5.5: A Profile of Lake Ice, With and Without Snow Cover.....26

FIGURE 5.6: Scattering Cross-Section Frequency Response of MY, FY and GY Ice at VV and HH Polarizations and 0°.....28

FIGURE 5.7: Scattering Cross-Section Frequency Response of MY, FY and GY Ice at VV and HH Polarizations and 10°.....28

FIGURE 5.8: Scattering Cross-Section Frequency Response of MY, FY and GY Ice at VV and HH Polarizations and 20°.....29

FIGURE 5.9: Scattering Cross-Section Frequency Response

of MY, FY and GY Ice at VV and HH Polarizations and 30°.....29

FIGURE 5.10: Scattering Cross-Section Frequency Response of MY, FY and GY Ice at VV and HH Polarizations and 40°.....30

FIGURE 5.11: Scattering Cross-Section Frequency Response of MY, FY and GY Ice at VV and HH Polarizations and 50°.....30

FIGURE 5.12: Scattering Cross-Section Frequency Response of MY, FY and GY Ice at VV and HH Polarizations and 60°.....31

FIGURE 5.13: Scattering Cross-Section Frequency Response of MY, FY and GY Ice at VV and HH Polarizations and 70°.....31

FIGURE 5.14: Scattering Cross-Section Frequency Response of MY, FY, GY and SF at 40° and VV-Polarization.....33

FIGURE 5.15: Scattering Cross-Section Angular Response of MY, FY and GY Ice at VV and HH Polarizations and 5.2 GHz.....34

FIGURE 5.16: Scattering Cross-Section Angular Response of MY, FY and GY Ice at VV and HH Polarizations and 9.6 GHz.....34

FIGURE 5.17: Scattering Cross-Section Angular Response of MY, FY and GY Ice at VV and HH Polarizations and 13.6 GHz.....35

FIGURE 5.18: Scattering Cross-Section Angular Response of MY, FY and GY Ice at VV and HH Polarizations and 16.6 GHz.....35

FIGURE 5.19: Radar Contrast Between MY and FY Ice at VV Polarization.....38

FIGURE 5.20: Radar Contrast Between MY and GY Ice at HH Polarization.....38

1.0 INTRODUCTION

Radar measurements of sea ice were made at four sites during the FIREX/ RADARSAT October 1981 Fall Experiment at Mould Bay, N.W.T., Canada. The observed ice types included multiyear, first-year, grey and very old shore-fast.

These measurements were made to address the needs, associated with the study of sea-ice-covered waters, which are important in meeting the requirements of a future SAR satellite program. Before a research or operational SAR or RAR (Synthetic- or Real-Aperture Radar) can occur, an adequate knowledge of the backscatter coefficients of ice features of interest is necessary for the definition of satellite or aircraft parameters. They are also a significant source of information for the interpretation of data products from existing and future sensors. Comprehensive backscatter measurements and ice characterization programs enhance our ability to understand and study the radar-ice interaction process.

The University of Kansas scatterometer measurements have been made over a wide range of frequencies (L-C-X-Ku-bands). In contrast, previous investigations have been limited to one or two frequencies. What was known prior to the time of this program's first measurements was that frequencies above 9 GHz have shown the ability to discriminate between different ice types, at least under winter and spring conditions, while frequencies below 1.5 GHz have not. No data were available at that time in the region between 1.5 and 9 GHz. The University of Kansas measurement program was proposed to make C-band measurements and fill this gap. Since 9 GHz is perhaps the best frequency to use for discriminating ice types, while 1.5 GHz is unsatisfactory, an optimum frequency somewhere between 1.5 and 9 GHz might have been present, or, at least, the use of C-band may give results that will be more like the 9 GHz

good results than the not-so-usable 1.5 GHz results. Since the character of the radar backscatter changes so much over this gap in frequency coverage (wavelength changes by a factor of 6:) additional measurements were needed to determine just where the ability to discriminate drops off as one goes down from 9 GHz.

Also, what is the impact of season on the ability to discriminate ice types Because the physical/electrical properties of ice are influenced by season, it is necessary to have a seasonally dependent description of backscatter properties. This was the aim of the first measurement program, which included the use of a wide range of frequencies, angles, and polarizations coupled with intensive ice characterizations to be undertaken during fall conditions.

2.0 THE RADAR SCATTEROMETER

The active sensor used in this experiment program was a multifrequency, multi-polarization, and multi-angle-of-incidence frequency-modulated continuous-wave (FM-CW) calibrated radar (scatterometer). Frequency bands of operation included: C-band (4-8 GHz), X-band (8-12 GHz) and Ku-band (12-18 GHz) (see Table 1 for system specifications). Polarization capabilities included HH, VV and HV (H = horizontal, V = vertical; the first letter identifies transmitted polarization and the second identifies received polarization). Angles of incidence could be selected from 5° to 70° (measured with respect to vertical). The radar was flown using a Bell Model 206 helicopter at 15 to 30 meters, with the antennas mounted so that the radar was side-looking (see Figure 2.1).

TABLE 1
HELOSCAT III SYSTEM SPECIFICATIONS

Type	FM-CW
Frequency Range	4-18 GHz
Modulating Waveform	Triangular
FM Sweep	800 MHz
Transmitter Power	14-19dBm
Intermediate Frequency	50 kHz
IF Bandwidth	13.5 kHz
Antennas:	Log-Periodic Feed Reflectors
Polarization	VV
Size	46 cm
Beamwidths	6.4°, 4.4°, 3.8° and 3.4° at 4.8, 7.2, 9.6 and 13.6 GHz
Polarization	HH
Size	61 cm
Beamwidths	4.0°, 3.4°, 2.5° and 1.9° at 4.8, 7.2, 9.6 and 13.6 GHz
Polarization	Cross
Size	46 cm and 61 cm
Beamwidths	5.6°, 3.8°, 3.0° and 2.6° at 4.8, 7.2, 9.6 and 13.6 GHz
Incidence Angles	5° to 70° from nadir
Calibration:	
Internal	Signal injection (delay line)
External	Luneberg lens
Altitude	30 m for θ = 10° to 50° 15 m for θ = 60° and 70°

Internal calibration necessary for short-term variations in the radar was accomplished by passing the radar signal through a delay line of known loss. External calibration for the overall system calibration was performed by measuring the return from a Luneberg lens of known radar cross-section.

FIGURE 2.1

University of Kansas Helicopter-Borne Scatterometer
Mount on Bell Model 206

3.0 EXPERIMENT DESCRIPTION

The October 1981 investigation was conducted as part of the FIREX/ RADARSAT Experiment Series supported by U.S. and Canadian agencies. The High Arctic Weather Station (Mould Bay: 76°, 14' N, 119° 20' W) located on Prince Patrick Island was used as the base of operations. A map showing the location of this camp at Mould Bay and some of the areas surrounding it is in Figure 3.1. One of the prime advantages of working at this location was the high probability that multiyear ice would be accessible. Lack of accessible multi-year ice had had major impacts on the overall success of previous experiments.

A summary of backscatter measurements and descriptions of the five sites examined at various times during the experiment period are presented in Table 2. Four types of sea ice were investigated: multiyear, first-year, grey and shorefast. Lake ice and an old weathered pressure ridge were also examined.

The experiment procedure in data acquisition was for a HELOSCAT flight line to be established at the four ice sites and full-length profiles of the flight line made at 5.2 and 9.6 GHz (frequencies similar to those allocated for satellite sensor operation), at HH-polarization, and at as many angles as was possible. The data base was further expanded by adding additional frequencies and polarizations.

Several additional investigations were carried out by other investigators as part of the Mould Bay program. A study was made of the mechanical strength of first-year and multiyear ice. These samples, collected from the backscatter study areas, were also used to study the microstructure of the ice sheet.

SLAR imagery was acquired by the Atmospheric Environment Ice Reconnaissance Aircraft. Data obtained prior to the beginning of the field investigation were used in preliminary planning. Imagery acquired during the

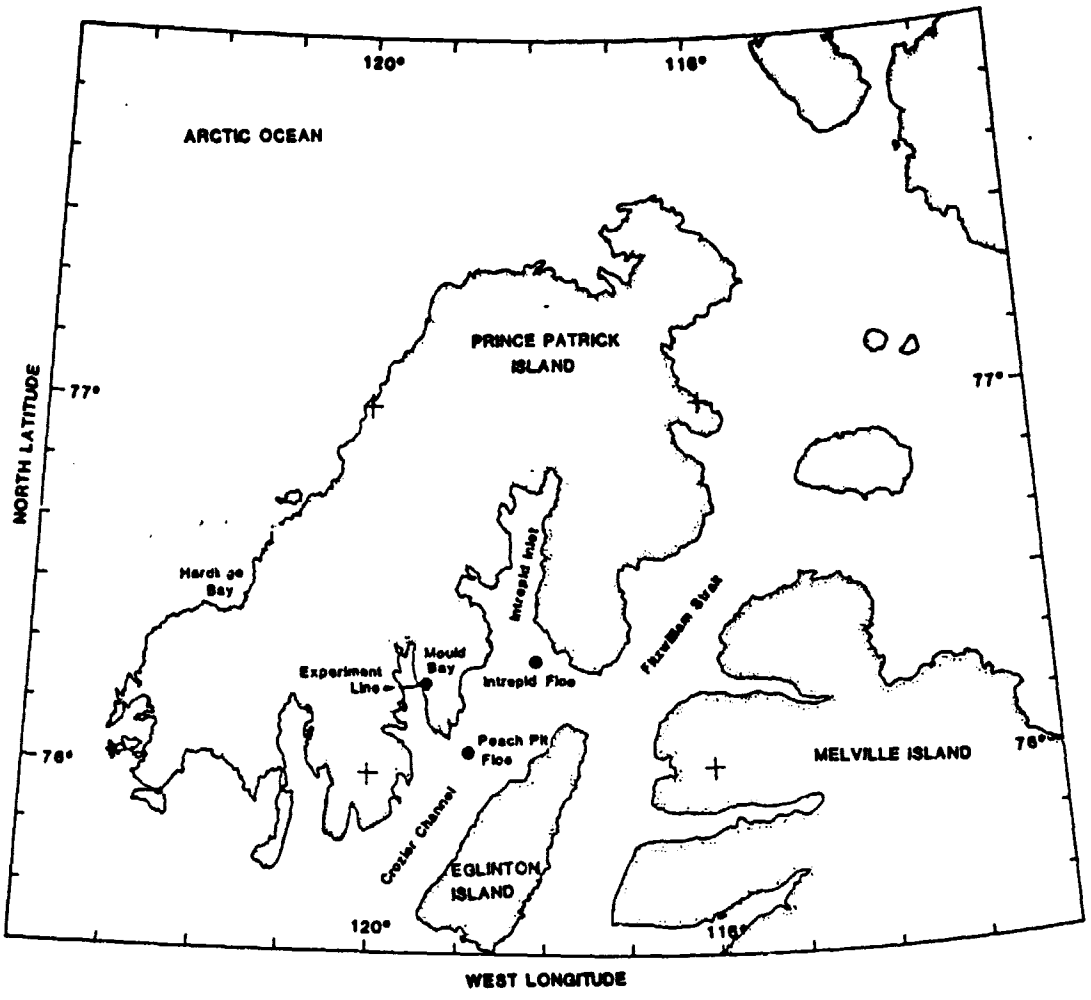

FIGURE 3.1

Experiment Site Location Map

TABLE 2

SUMMARY OF DATA ACQUISITION BY HELICOPTER-BORNE SCATTEROMETER

Date	Site Location	Frequency (GHz)	Polarization	Angle (Degrees)
10/18/81	Mould Bay -FY-	5.6 9.6 5.6	HH HH Cross	0, 10, 20, 40, 60 20, 40, 60 20
10/19/81	Mould Bay -FY-	5.6, 9.6 4-18 5.6	Cross VV,HH HH	20, 40, 60 10-70 0, 10
10/22/81	Intrepid Inlet -multiple ice cat.-	4-18	HH	10-40
10/23/81	Intrepid Inlet -multiple ice cat.-	4-8 5.6 8-18 9.6	HH HH HH VV,HH,Cross	50-70 70 50, 60 50
10/24/81	Intrepid Inlet -multiple ice cat.-	5.6,7.2,9.6,13.6 4-18	VV VV	40 10-70
10/24/81	Intrepid Inlet -Large MY Pressure Ridge-	5.6,7.2,9.6,13.6 9.6,13.6	VV VV	40 70
10/24/81	Landing Lake -Bare + Snow-Covered Fresh Water Ice-	4-18 5.6,9.6,13.6	VV VV	40, 70 40
10/24/81	Hardinge Bay -shorefast-	4-18	VV	30, 40, 60, 70

experiment period was used for the coordination of on-site efforts, for studies of what constituted anomalies and representative ice, and for future radar-ice interaction studies.

The U.S. Navy P-3 acquired data with a millimeter-wave imaging radiometer [1] for the purpose of demonstrating that sea ice can be measured accurately from the air, day or night, and in all types of weather.

An intensive effort, coordinated by R.O. Ramseier, was made to support the radar backscatter measurements and the aircraft overflights with detailed ice characterization information, and to study the physical/chemical properties of the ice in the region [2]. Measurements included the following:

(1) Air temperature.

(2) Snow temperature.

(3) Snow salinity.

(4) Description of the construction of the snow layer.

(5) Description of slush layers.

(6) Ice surface roughness.

(7) Construction of the interface between the ice and snow.

(8) High resolution salinity profile of the ice sheet.

(9) Temperature profile of the ice sheet.

(10) Description of the construction of the ice sheet.

(11) Ice thickness.

Ice conditions at Mould bay were not as expected. Ice in the bay had evacuated during the summer, leaving only occasional pieces of multiyear ice grounded near the shore. At the start of October, the ice in the bay was 24-cm-thick homogeneous first-year ice. The inland waters contained a variety of multiyear floes frozen in grey ice.

An unseasonably warm weather system (a record high of -1° C was recorded on October 6) occurred during the first third of the month. This caused a slush layer (1.5 cm) to form at the snow-ice interface. As the month progressed, temperatures returned to normal (low of -30° C).

A list of the persons who participated in the Mould Bay investigation is shown in Table 3.

TABLE 3
MOULD BAY FIELD INVESTIGATION PERSONNEL

Mr. Ken W. Asmus	AES	Ice Observation and Analysis
Ms. Susan A. Digby	RADARSAT	Field Support and Data Coordinator
Mr. Vince Garbowski	Quasar	Helicopter Mechanic
Ms. I. Kilukishak	ARE	Ice Laboratory Technician
Mr. Y.S. Kim	U of KS	Scatterometry
Mr. M. Komangapik	ARE	Ice Laboratory Technician
Mr. S. Koonark	ARE	Ice Laboratory Technician
Mr. Howard Massecar	Quasar	Helicopter Pilot
Dr. Robert G. Onstott	U of KS	Scatterometry
Dr. Rene O. Ramseier	AES	Project Leader
Dr. Nirmal Sinha	NRC	Mechanical Properties
Mr. Larry Solar	AES	Ice Observation and Analysis Deputy Project Leader

4.0 DESCRIPTION OF THE BACKSCATTER DATA

Data and results not found in the main body of this report may be found in the Appendices. Scattering cross-section frequency response data have been regressed and coefficient tabulated in Appendix 1; mean scattering cross-sections tabulated as a function of frequency, polarization and incidence angle in Appendix 2; some related statistical descriptions in Appendix 3; contrasts between ice types tabulated in Appendix 4; two additional angular responses in Appendix 5; and scattering cross-section profiles obtained by transversing the flight lines in Appendix 6. The data stream was annotated with solid vertical lines to indicate the occurrence of site markers or change

in ice type. After October 18, target-encoding did not function properly, making some data analysis more intensive. However, changes in ice type were very often readily detected due to easily recognizable changes in backscatter level. These transitions are shown as dashed lines on the profile plots.

Location of the 11 site markers on the Mould Bay flight line is shown in Figure 4.1 (also see Table 4), the Intrepid Inlet flight line in Figure 4.2, and the Hardinge Bay flight line in Figure 4.3.

TABLE 4
DISTANCE BETWEEN MOULD BAY SITE MARKERS BASED ON SLAR IMAGERY

Marker Designation Kansas	CDN	Distance from Marker No. 1 -meters-
1	1	0
2	2	492
3	3	985
4	4	1717
5	5	2298
6	6	2822
7	6A	3409
8	6B	3990
9	7	4596
10	7A	6313
11	8	7980
SHORE	SHORE	8081

5.0 EXPERIMENT RESULTS

Multiyear ice frozen in grey ice, a large weathered multiyear pressure-ridge, first-year ice with varying degrees of surface roughness, shorefast ice, and lake ice were investigated.

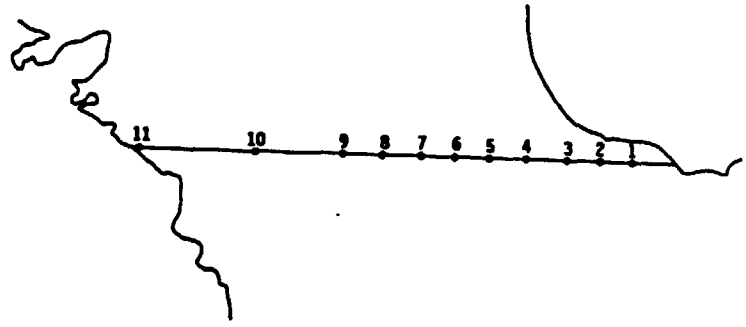

FIGURE 4.1
Mould Bay First-Year Ice Flight Line

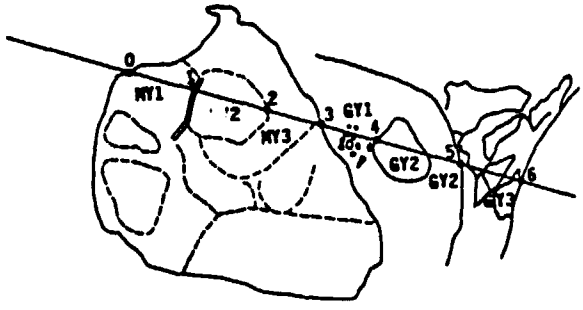

FIGURE 4.2
HELOSCAT Flight Line of an Old Multiyear Floe Frozen
in Grey Ice Located in Intrepid Inlet

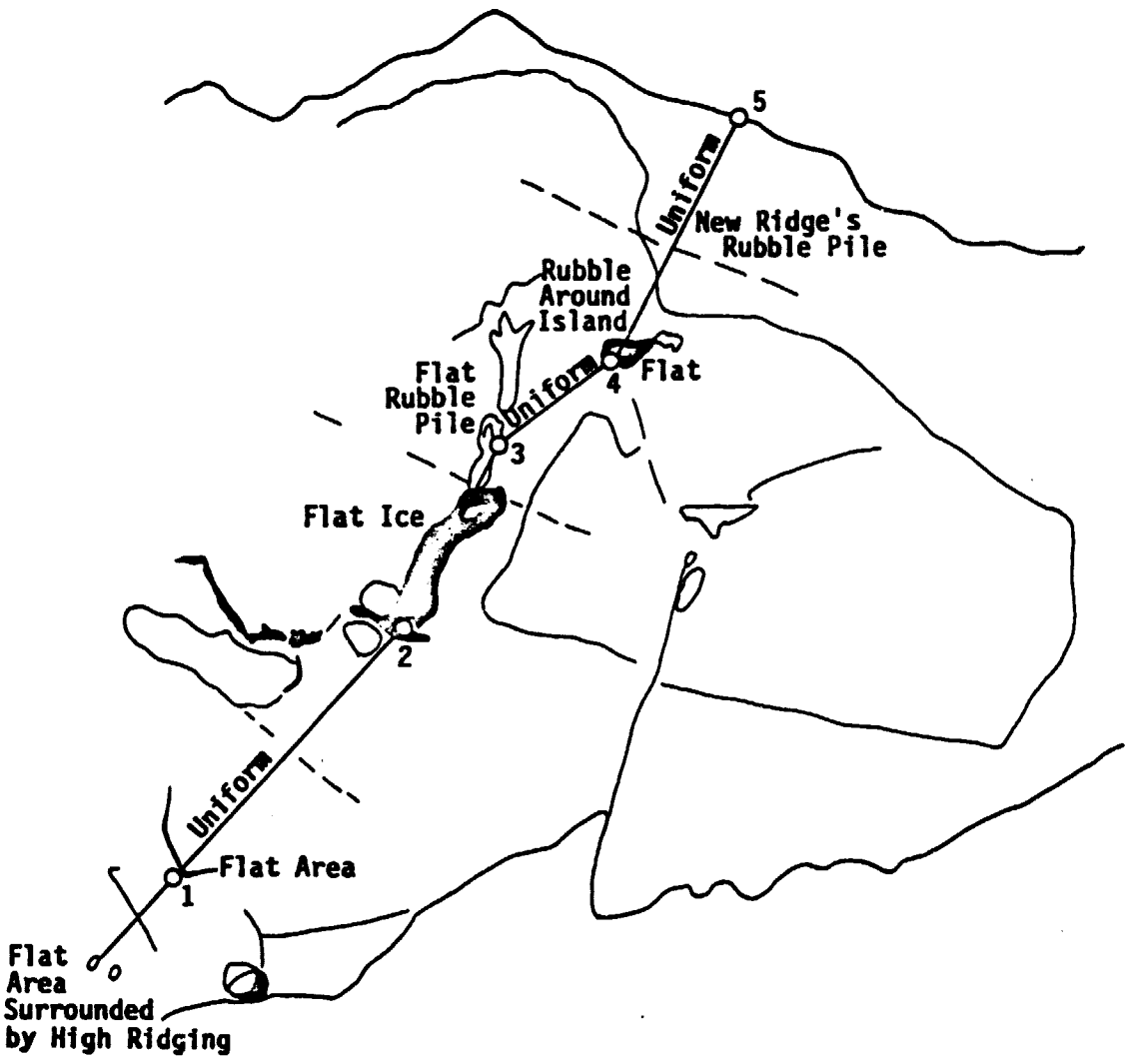

FIGURE 4.3

HELOSCAT Flight Line for Old Shorefast Ice

Located in Hardinge Bay

5.1 Intrepid Inlet - An Old Multiyear Floe Frozen in Grey Ice

This site, located in the mouth of Intrepid Inlet, is composed of an old multiyear floe frozen into grey ice. This floe is distinguished by two prominent features: a massive hummock of over 7 m relief and a km-long old, weathered ridge with 6 m peaks. It is composed of expanses of low undulating, well-rounded ice, and areas comprised of blocks cemented into the top portion of the ice sheet.

Figures 5.1(a) and (b) are representative 5.6 and 9.6 GHz radar responses of the ice features found along the multiyear-grey ice flight line. Examination of the HELOSCAT profiles and aerial photography yields much information as to the features to which the radar responds. Multiyear returns are very dynamic, showing that there are at least two scenes which contribute to the backscatter response of multiyear ice. These wide variations occur because ice mounds provide strong returns while the smooth fresh-water ice in the meltpools provide weak returns.

The large old multiyear floe is made up of smaller floes and zones which have different large-scale surface roughnesses. The first zone (MY1, S0.0 to S1.0) has prominent melt features. It has fewer (but larger) meltpools and larger ice mounds than the second zone encountered along the flight line (MY2; S1.0 to F2.0). This zone is characterized by a more uniform population of meltpools and ice mounds, although, in some areas, meltpools are strung together to form much larger pools with small ice mounds framing individual pools. A large meltpool near the center of MY1 is identifiable as a 7 dB notch of significant spatial duration. The larger meltpool formation in MY2 provides an even weaker return with 13 dB of contrast between it and surrounding ice. Returns from ice mound features in both MY1 and MY2 provide similar backscatter levels.

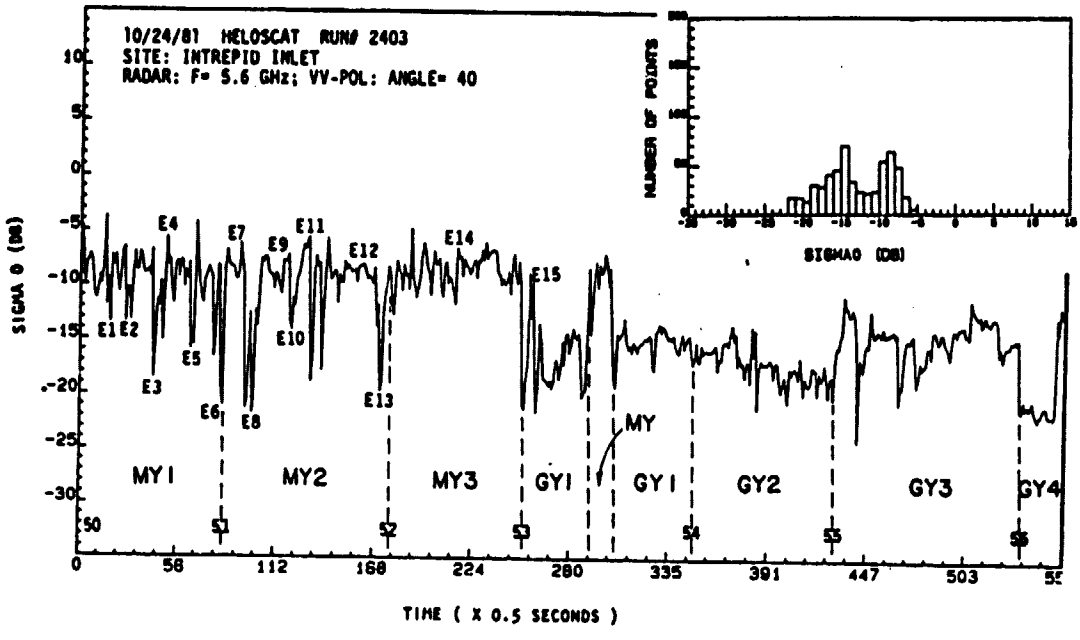

(a)

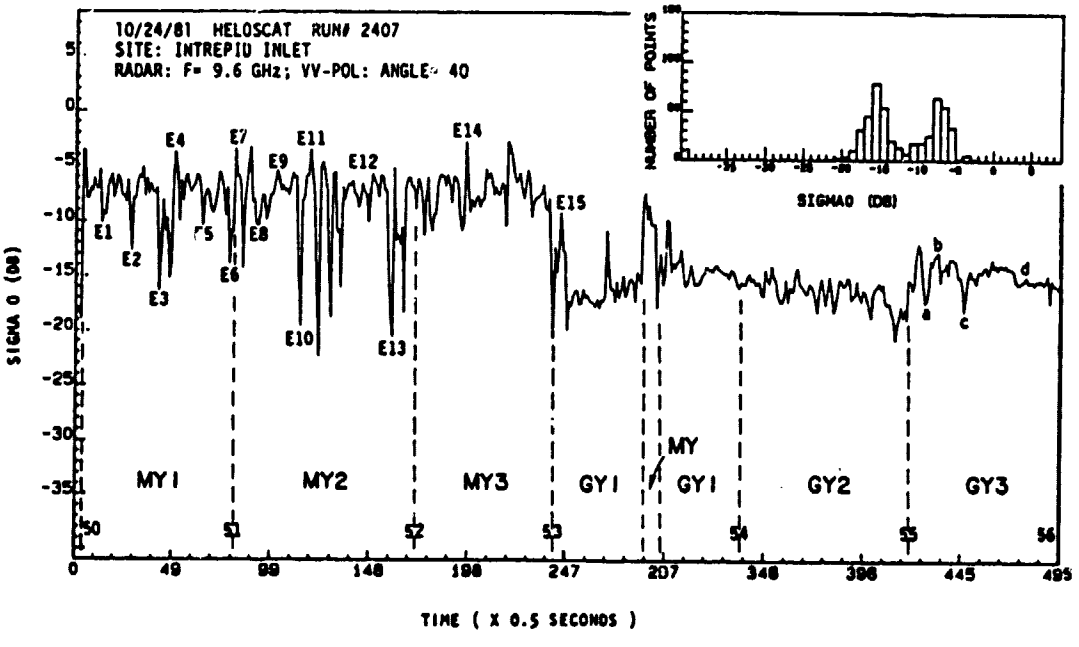

(b)

FIGURE 5.1
Profile of a Composite Multiyear Ice Floe at (a) 5.6 GHz and (b) 9.6 GHz

The third zone (MY3; S2.0-S3.0) is representative of another category of multiyear ice. The first half (S2.0-S2.5) contained ice similar to MY1. The second half, however, was rougher topographically and exhibited few, if any, meltpools. The radar response in this area is more uniform and does not show the weak returns which correspond to meltpools. The overall backscatter level is similar to that of the ice mound features seen in MY1 and MY2 and the variation in the radar response is significantly less.

Grey ice returns are 5 to 12 dB lower than multiyear ice returns. Grey ice scattering cross-sections are very dependent upon the state of deformation, or rafting. Undisturbed grey ice (F4.6-F5.0) produces returns which are about 10-12 dB lower (at 40°-VV) than those for multiyear ice mounds. Heavily rafted grey ice (F5.0-F6.0) produces returns which are 3-5 dB higher than smooth grey ice. Lightly rafted grey ice (F4.0-F4.6) produce returns which fall midway between the other two cases. The multiyear fragment found near the border of the multiyear floe (F3.0-F4.0) is easily detected in the lightly rafted grey ice background. Mean scattering cross-sections for multiyear and grey ice as a function of frequency and incidence angle, together with the other ice types, will be further discussed.

Comparison of the textures or standard deviations of returns of multiyear ice and grey ice is interesting in that it quantifies the dynamic nature of multiyear and the less-dynamic nature of grey ice. The standard deviation of the multiyear ice portion of the flight line at 9.6 GHz VV-polarization, and 40° is 3.4 dB, while it is 1.5 dB for the grey ice portion of the flight line. Wide variation in the passive response of multiyear ice was also noted in the NRL P-3 imagery [1].

The multiyear floe boundary is well-defined on the HELOSCAT profiles, and show up to 14 dB transitions when crossing the border between the grey ice and

the multiyear ice. This high contrast appears to be due to the large-scale roughness of strewn blocks at the multiyear ice edge and the much smoother grey ice.

5.2 Multiyear Pressure Ridge

The old weathered, multiyear pressure ridge located at the border between MY1 and MY2 is not detectable by backscatter level, but is by its spatial extent. Scattering levels are similar to those of the much smaller ice mounds. If it was not known to exist it would be difficult to be certain that this feature was a pressure ridge. It is, however, accented with boundaries of low return. This has been observed in many SAR and SLAR images. From aerial photographs, it is seen that the skirts of the ridge terminate into meltpond features, which are more prevalent in number at the ridge boundary than elsewhere on the floe.

Measurements were also made parallel to the ridge as shown in Figure 5.2. These measurements show that the overall backscatter from the ridge is slightly lower than the mean return from the background multiyear ice. Variation in the parallel transect returns is typically 5 to 10 dB.

5.3 Mould Bay - First-Year Ice

Homogeneous first-year ice, located in Mould Bay, has tnicknesses ranging from 35 to 46 cm with a 40-cm average thickness. Snow cover ranges from 2 to 11 cm with a 1-cm average depth. Average salinity in its top few mm is $14^{o}/oo$, in its top 4 cm $9^{o}/oo$, and in its bottom layer is $18^{o}/oo$. The snow cover has three defined ice layers. The top 3 cm is made up of lightly compressed snow composed of 1 mm or less diameter ice crystals. The next .5 cm layer is composed of frozen slush. The bottom 1 cm is composed of the

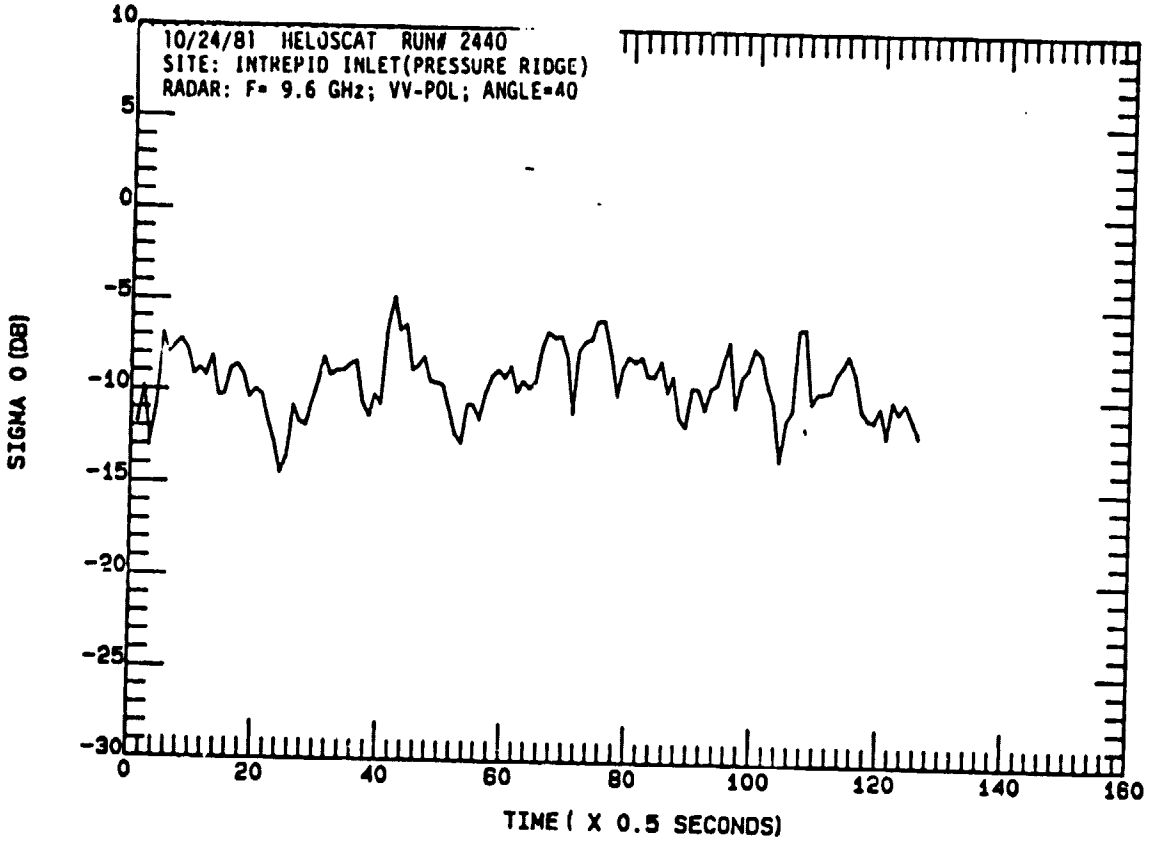

FIGURE 5.2

Typical Profile of a Multiyear Pressure-Ridge

remnants of old frost flowers growths. The ice surface small-scale roughness varies from very rough, 1-2 cm roughness elements (primarily due to rafting and development of pancake ice when the ice sheet was initially forming) to very smooth (where the newly formed ice was shielded from the agitation effects of the wind). Table 5 summarizes ice characterization measurements made on 19 October.

An 8 km, 10 zone flight line was positioned across Mould Bay. Ice characterizations were performed in each zone. The HELOSCAT data was encoded so that it can be compared to the characterizations. Figure 5.3 shows returns at 5.6 and 9.6 GHz, HH-polarization and 20°. Examination reveals that the radar is sensitive to the variations in the small-scale roughness of the otherwise homogeneous first-year ice which is visually masked by a 4 cm snow layer. The variation in small-scale surface roughness accounts for 3 to 4 dB shifts in the backscatter levels along the flight line. The slightly rafted area near the start of the flight line provides the largest radar return. If this zone is not included with the others, variation about the mean cross-section of the ice sheet is easily within 1 dB. The responses at 20° and 5.6 and 9.6 GHz are nearly identical. A major difference between the way the radar, operating at these two frequencies, views the ice sheet is that the 5.6 GHz responses show a slightly larger absolute level difference between the rough and smooth ice responses. However, operation at the higher frequency shows more sensitivity to changes in small-scale surface roughness of the smooth ice.

TABLE 5
ICE CHARACTERIZATION MEASUREMENTS FOR MOULD BAY
FIRST-YEAR ICE ON 19 OCTOBER

Site Notation	Thickness (cm) Ice	Snow	Temperature °C Air	Ice (1cm)	Salinity - °/oo Snow (Top)	Snow (Bottom)	Ice (4cm)	Comments
1	46	3	-14	-15	16	20	7	Area of heavy rafting. Roughness elements of 1-2cm hts.
2	44	5	-14	-11	5	2	10	Snowpack composed of 1mm or smaller ice crystals.
3	40	7	-13	-14	20	16	8	Area which is slightly rough and has light rafting. Occasional MY chunks in this area.
4	35	3	-14	-10	20	14	10	Area which has very smooth, occasionally rafted ice.
5	40	3	-13	-15	17	18	9	Area of rough ice and little rafting. Roughness elements of 1 cm heights.
6	40	4	-12	-14	7	24	10	Area of smooth ice with occasional small rafts.
7	38	3	-14	-13	15	22	9	Area of flat ice which has a pitted surface. Bubbles also exist in upper part of ice sheet. Ice has fine fracture line running in HELOSCAT flight line direction.
8	40	4	-14	-13	9	19	10	Area of flat ice which has a pitted surface. Bubbles also exist in upper part of ice sheet.
9	37	3	-14	-14	11	19	8	Area of flat ice. Upper layer of ice sheet lacks bubbles seen in locations 6,7, and 8.
10	38	3	-13	-13	16	20	7	Area of flat ice. Bubbles also exist in ice sheet upper part.
11	38	3	-13	-14	17	20	8	
Avg.	40	4	-13	-13	14	18	9	

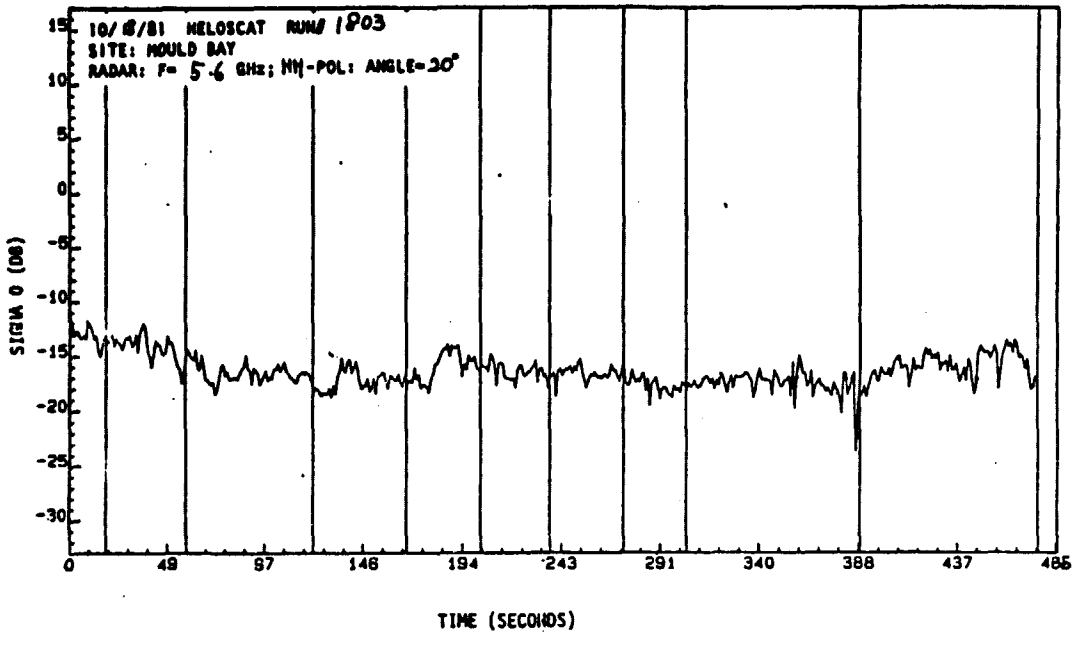

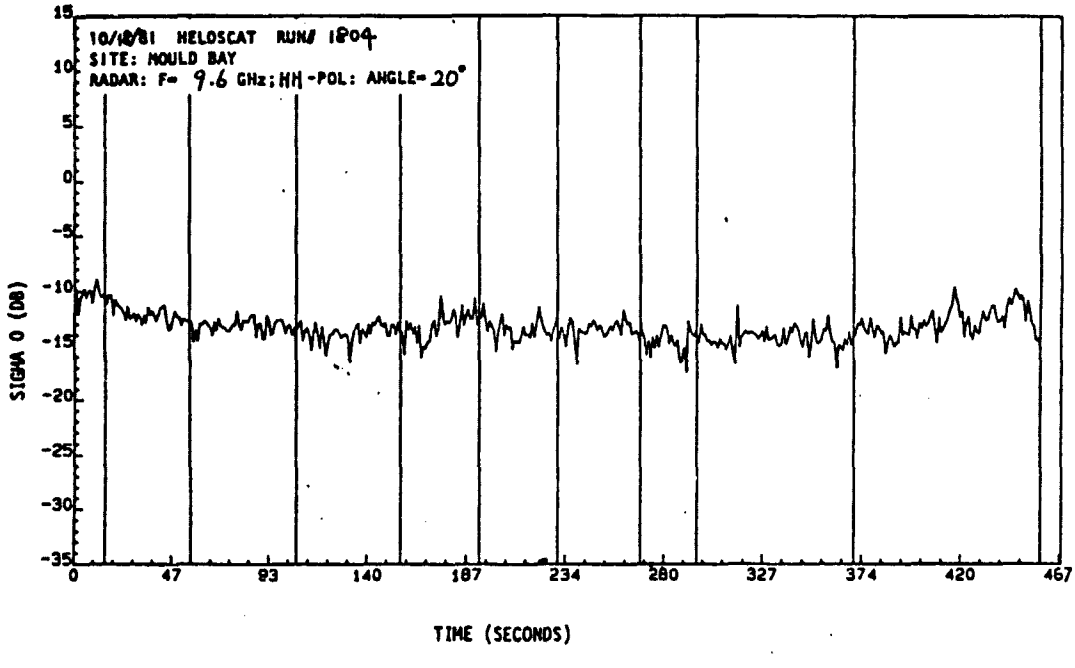

FIGURE 5.3(a)
Profiles Across the Mould Bay with $\theta = 20°$, F = 5.6 and 9.6 GHz, and Average σ^0 for Each Interval and Sample Snow and Ice Depths

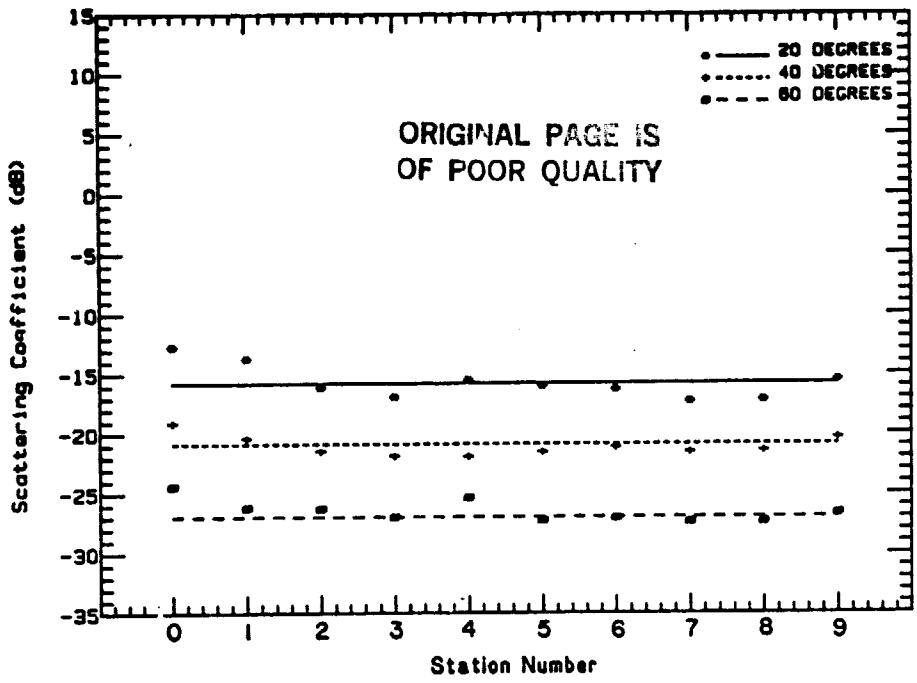

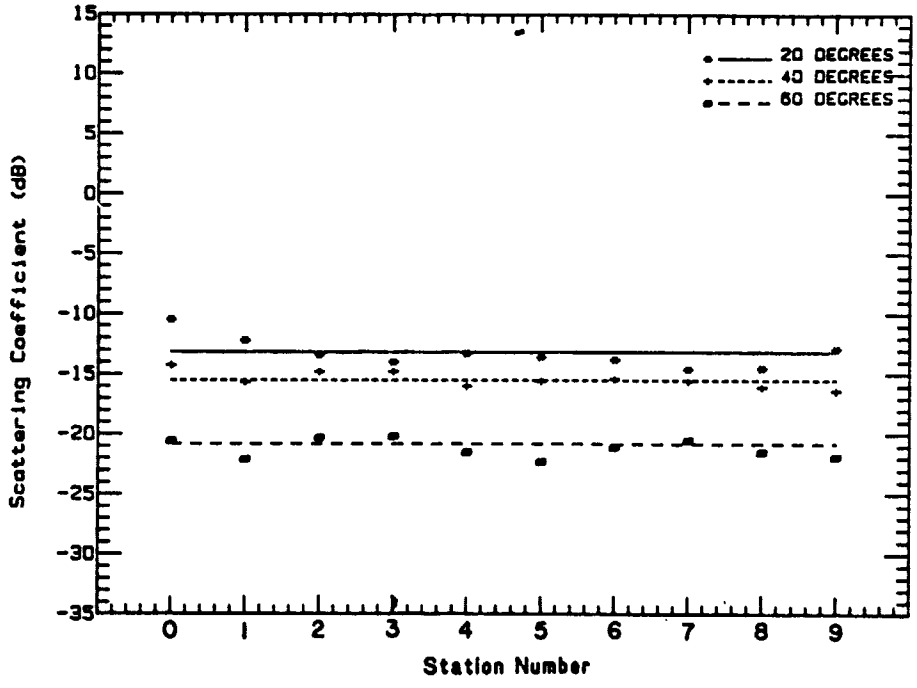

FIGURE 5.3(b)
Average scattering cross-sections for individual zones across Mould Bay at (a) 5.6 and (b) 9.6 GHz; HH-polarization; and 20°, 40° and 60°

Figure 5.3 also shows snow and ice thickness for the 10 segments across Mould Bay. Visual inspection reveals that the backscatter response does not respond to changes in snow depth or ice thickness. The best correlation between the ice physical properties and backscatter response is with surface roughness, which supports empirically that surface scattering is the dominant scattering mechanism for first-year ice, although the existence of the snowpack and the frozen slush layer may influence the surface scatter response and provide a small volume scattering component which may reduce the expected separation in the absolute level between smooth and rough ice without a snow cover for large angles. This conclusion is arrived at by comparing the difference in absolute level for smooth and rough ice at 20° and 60°. This result is important and requires further examination and study.

5.4 Hardinge Bay - Shorefast Ice

Data from very old landfast ice located near Hardinge Bay was collected. The HELOSCAT flight line begins at a lake-like feature which is surrounded by high ridging with rubble stacked to heights estimated at 7-8 m. The next zone is composed of alternating hummocks and meltponds, and terminates into an island, with rubble piled to 2 m around the perimeter, which is surrounded by smooth fresh-water ice. One ridge which runs perpendicular to the flight line occurred near the zone's center. The next zone is composed of alternating hummocks and meltponds which change to multiyear floes and old ridges, then to new ridges and rubble piles. The radar frequency is changed at 10 sec intervals throughout the flights, but with careful study the uniform ice, ridged ice, and flat ice features can be detected. Shorefast ice was found to have absolute scattering cross-section levels similar to multiyear ice. A radar profile normalized to 9.6 GHz, 40°

and VV-polarization is illustrated in Figure 5.4. Examination of the data at 40° and 70° and VV-antenna polarization shows that there are three basic features in the shorefast region: (1) ice that is ridged or stacked, (2) uniform ice which has alternating ice mounds and meltpools, and (3) smooth fresh water ice. Ridged ice produces returns that are 5-9 dB stronger than uniform ice; flat ice produces returns that are 7-11 dB lower at 40° and 4 to 7 dB lower at 70°.

5.5 Lake Ice

A profile of fresh water ice (Landing Lake: salinity = 1.4°/oo) at 5.6 and 9.6 GHz, VV-polarization, and 40° is shown in Figure 5.5. A flight line was constructed so that both snow-covered lake ice and bare lake ice with occasional snow patches were observed. The effect of the snow cover is quite apparent when examining the profiles. The presence of snow adds 2-4 dB at 5.6 and 9.6 GHz to the radar cross-section of bare lake ice. Snow drifts which run across the bare zone of the lake readily stand out in the profiles. The radar operating at 5.6 GHz appears more sensitive to the presence of snow. This illustrates the influence snow under cold conditions for ice which has smooth and rough surfaces. At the lower frequency, the wavelength is large and the lake-ice surface will appear smoother to the radar than if operating at 9.6 GHz. The influence of snow has been shown to be most dramatic on smooth surfaced ice [3]. Backscatter from fresh water lakes can be enhanced if volume scattering in the snow layer is greater than the bare ice alone. The effect of the snow layer may be less for an ice sheet with a rough surface if the radar cross-section of the ice sheet is on the order of or larger than the radar cross-section of the snow contribution.

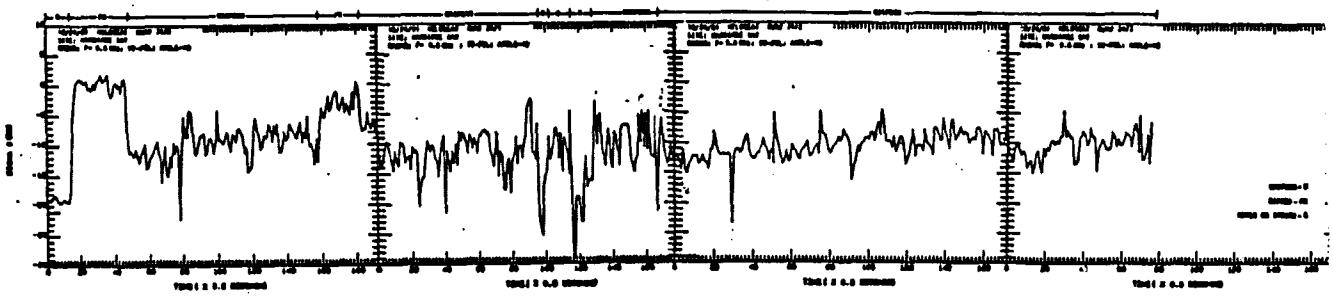

FIGURE 5.4(a)
Profile of old shorefast ice in Hardinge Bay at
9.6 GHz, VV-polarization and 40°

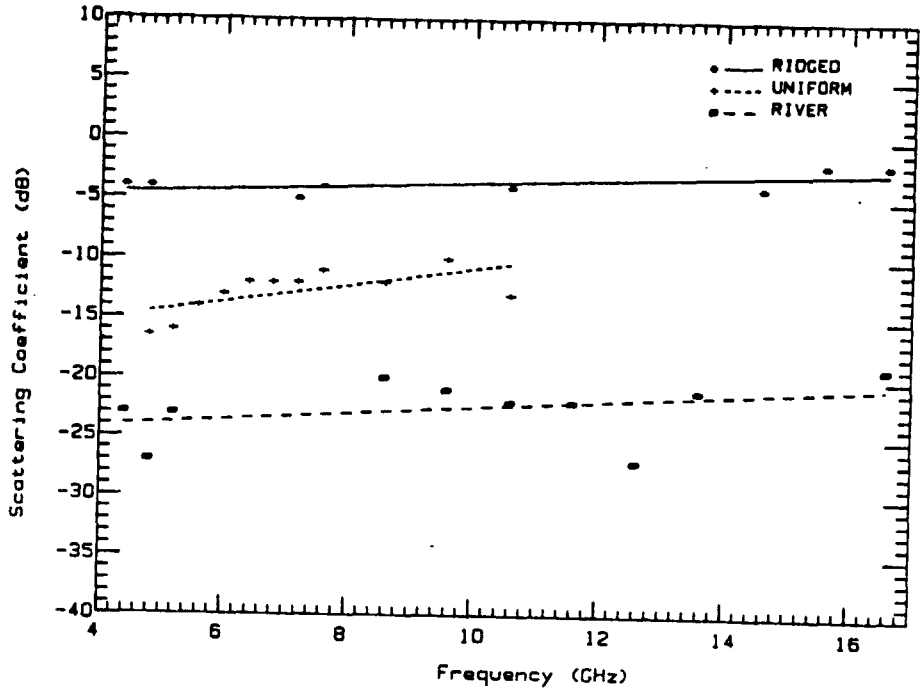

(1)

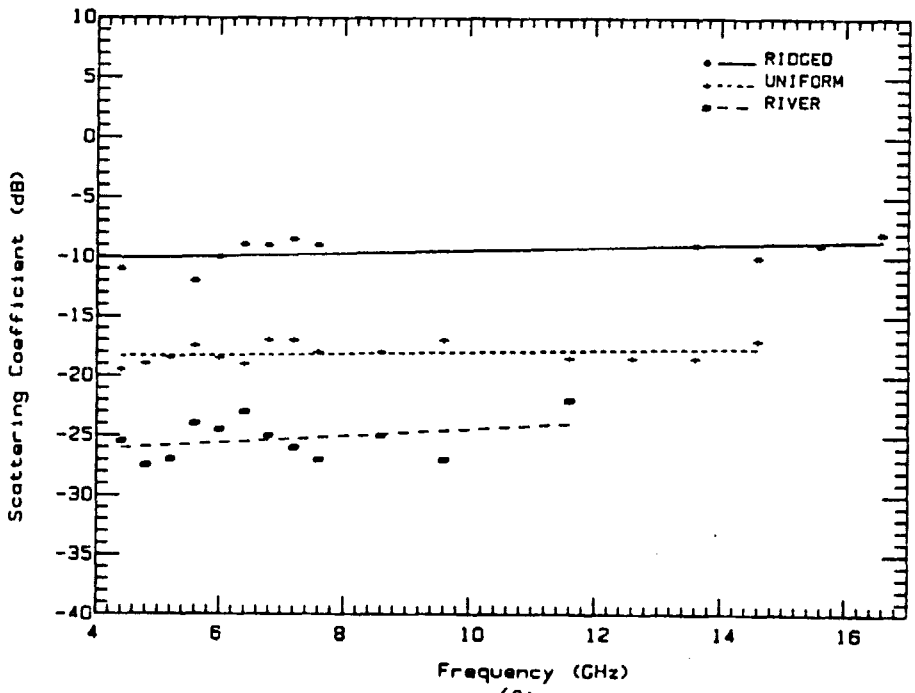

(2)

FIGURE 5.4(b)
Scattering Cross-Section Frequency Response for Old Shorefast Ice
In Hardinge Bay at VV-Polarization at 40° (1) and 70° (2)

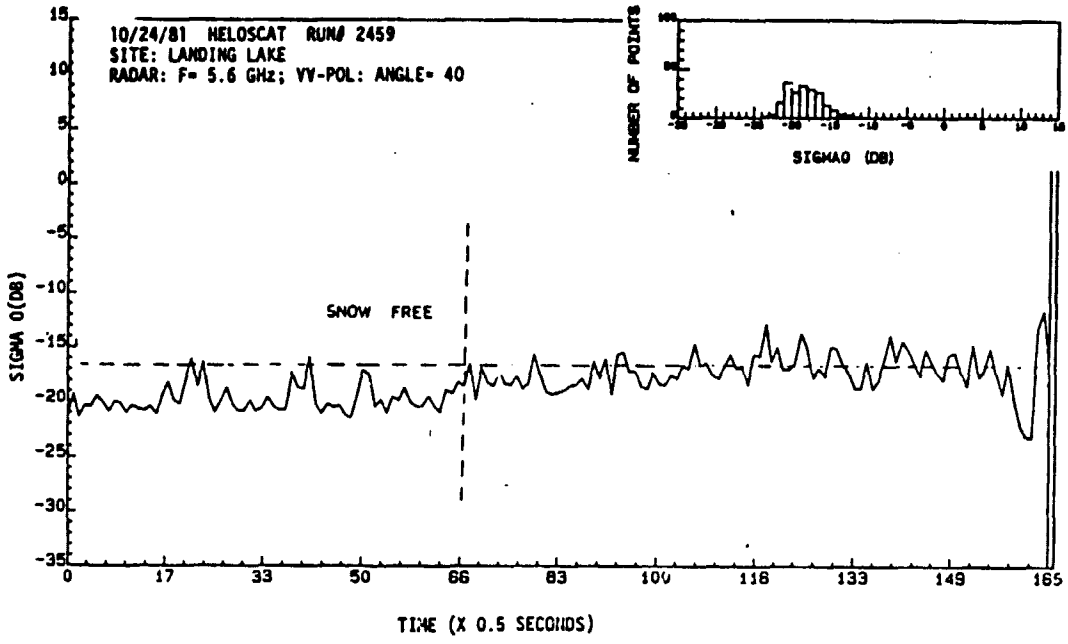

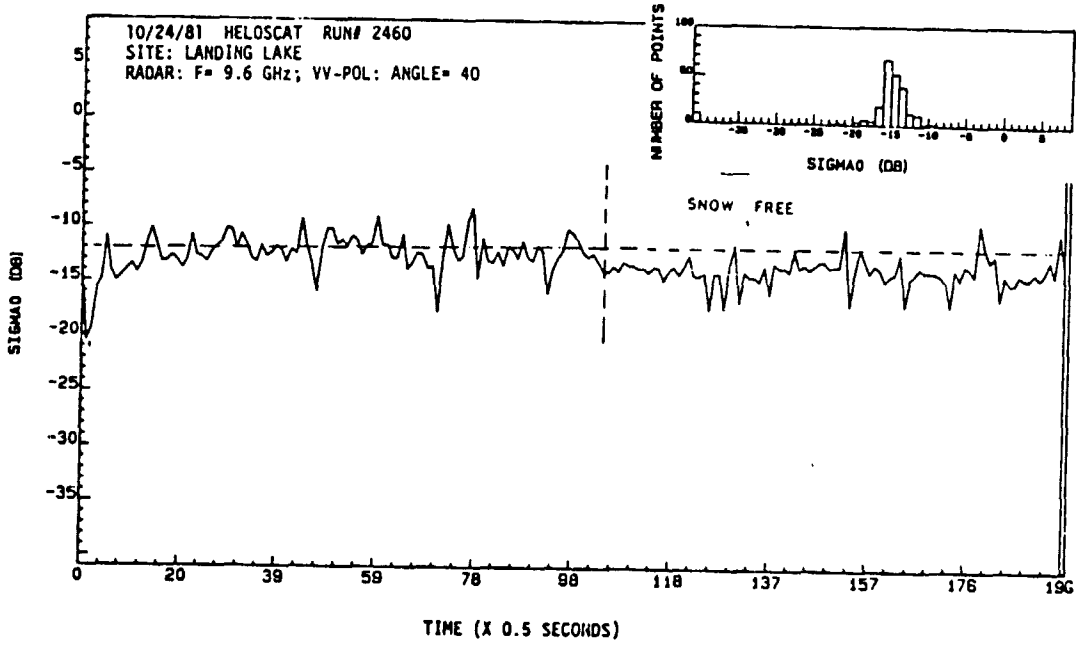

FIGURE 5.5
A Profile of Lake Ice, With and Without Snow Cover

5.6 Summary

5.6.1 Frequency Response

The frequency responses of the average scattering cross-sections are shown in Figures 5.6 to 5.13 for multiyear ice with VV- and HH-polarization, first-year ice with VV-polarization, and grey ice with HH-polarization at angles from 0° to 70°.

At vertical incidence the frequency responses for both MY-VV and FY-VV are not heavily frequency independent; cross-sections fall within a 3 dB interval across the entire frequency range. Cross-sections for these two ice types are also very similar in that the spread between trend lines ranges from 1-3 dB.

The scattering cross-sections of the various ice types tend to come together in the region from 10° to 15° incidence. This is demonstrated in Figure 5.7 for MY-HH and GY-HH. Their responses are very similar at all frequencies at 10°, but, as is shown in the other figures, their cross-sections will rapidly diverge as the angle is increased. The remainder of the figures show that MY-VV and MY-HH are very similar in their absolute level and are nearly identical at the Ku-X-band frequencies. However, as the frequency approaches the lowest C-band frequency, MY-HH cross-sections decay at a much greater rate than MY-VV and this divergence grows as the angle is increased. Because of this, MY-HH has a greater spread in cross-sections over the entire range of angles from 0° to 70° than MY-VV at C-band frequencies while at Ku-X-band frequencies the overall range of cross-sections are nearly identical.

Both first-year and grey ice cross-sections have a much greater dynamic range at these angles. When their frequency response trends are examined as a function of angle, it is seen that first-year and grey ice are similar, and that they have a different type of response than multiyear. First-year ice

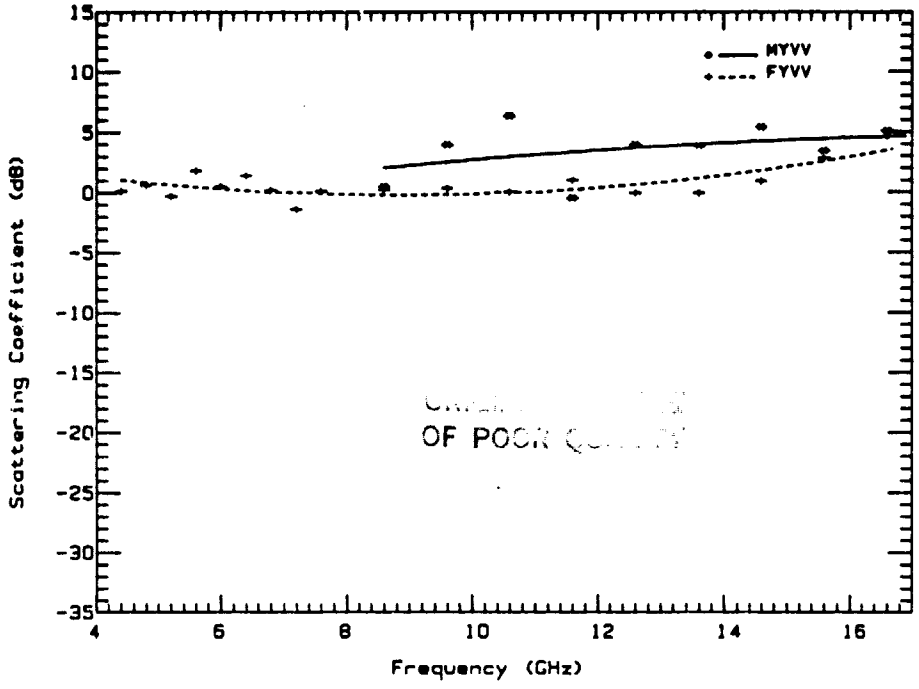

FIGURE 5.6
Scattering cross-section frequency response of MY, FY and GY ice at VV and HH polarizations and 0°

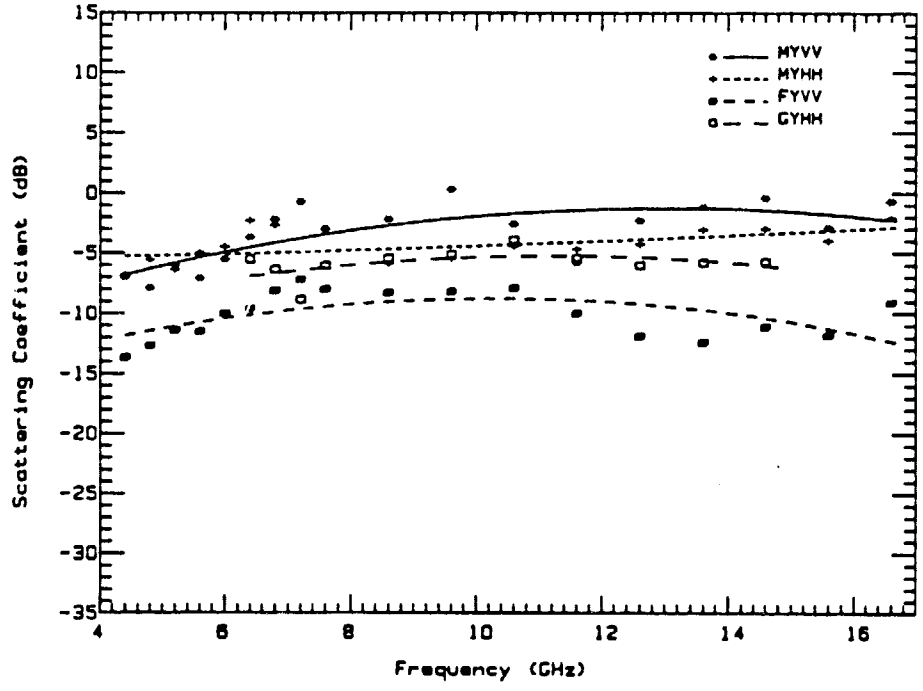

FIGURE 5.7
Scattering cross-section frequency response of MY, FY and GY ice at VV and HH polarizations and 10°

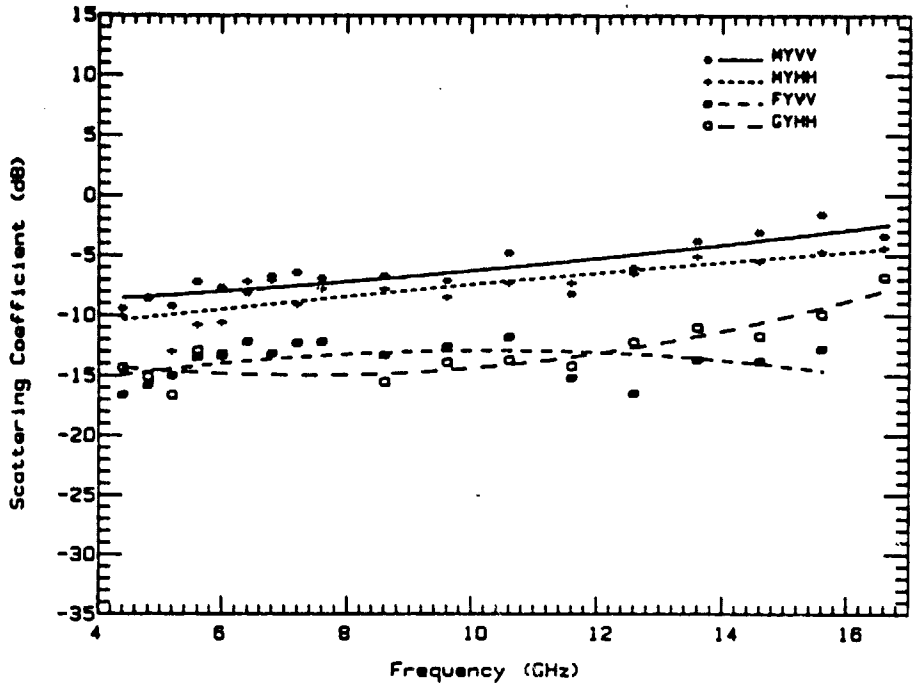

FIGURE 5.8
Scattering cross-section frequency response of MY, FY and GY ice at VV and HH polarizations and 20°

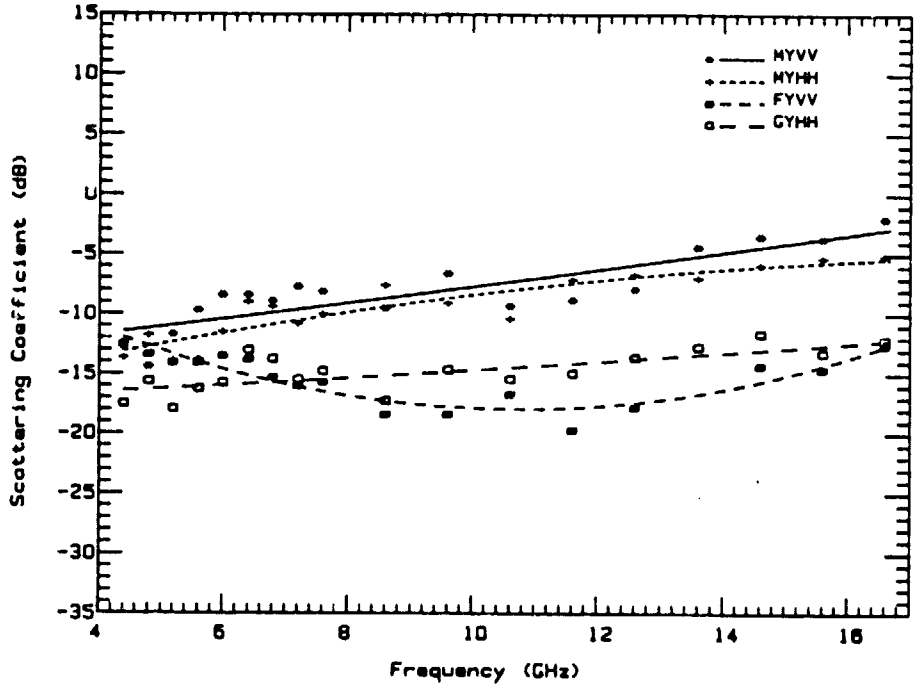

FIGURE 5.9
Scattering cross-section frequency response of MY, FY and GY ice at VV and HH polarizations and 30°

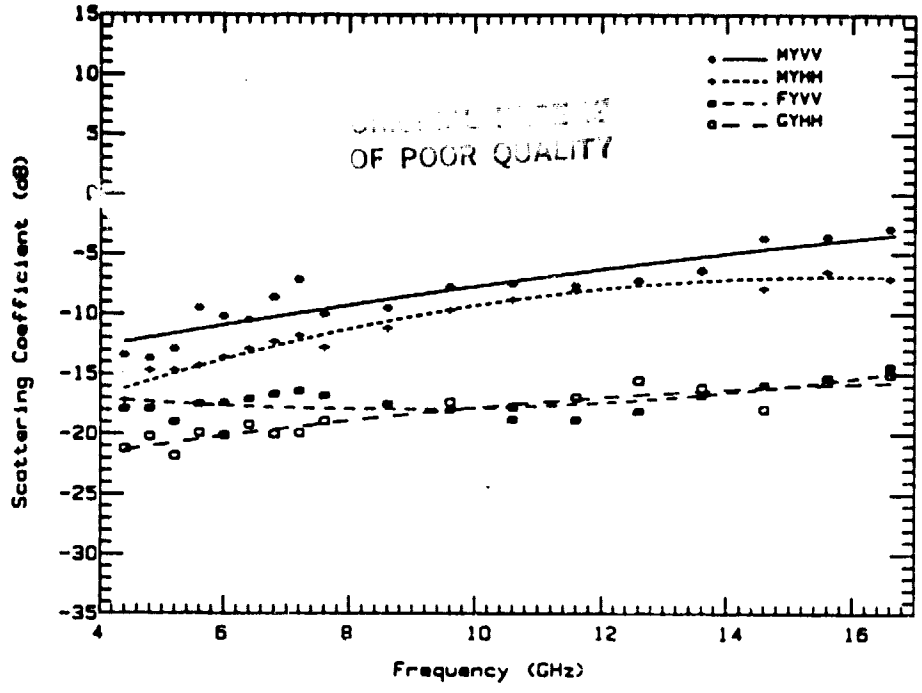

FIGURE 5.10
Scattering cross-section frequency response of MY, FY and GY ice at VV and HH polarizations and 40°

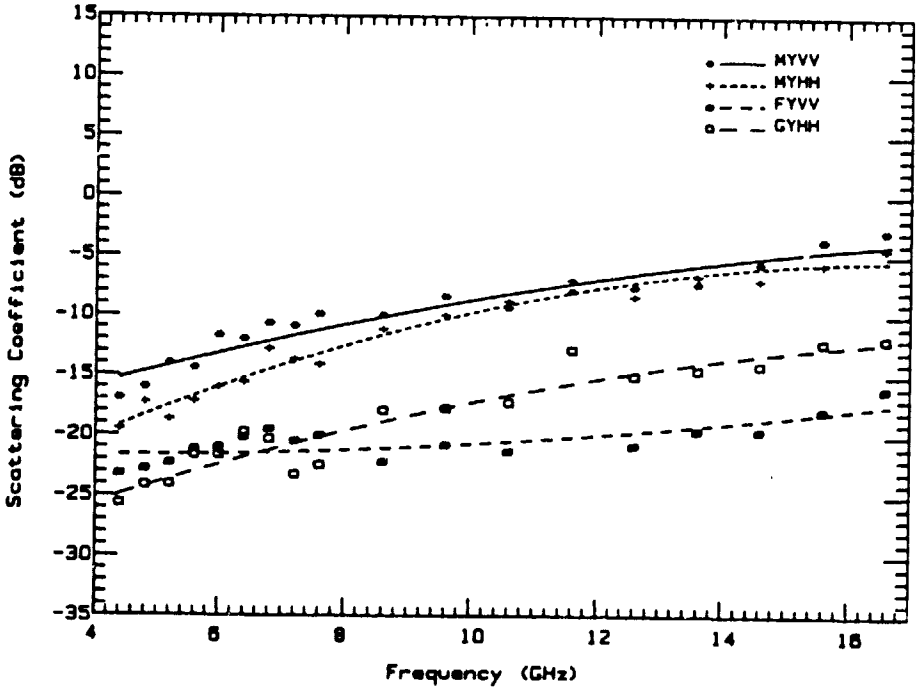

FIGURE 5.11
Scattering cross-section frequency response of MY, FY and GY ice at VV and HH polarizations and 50°

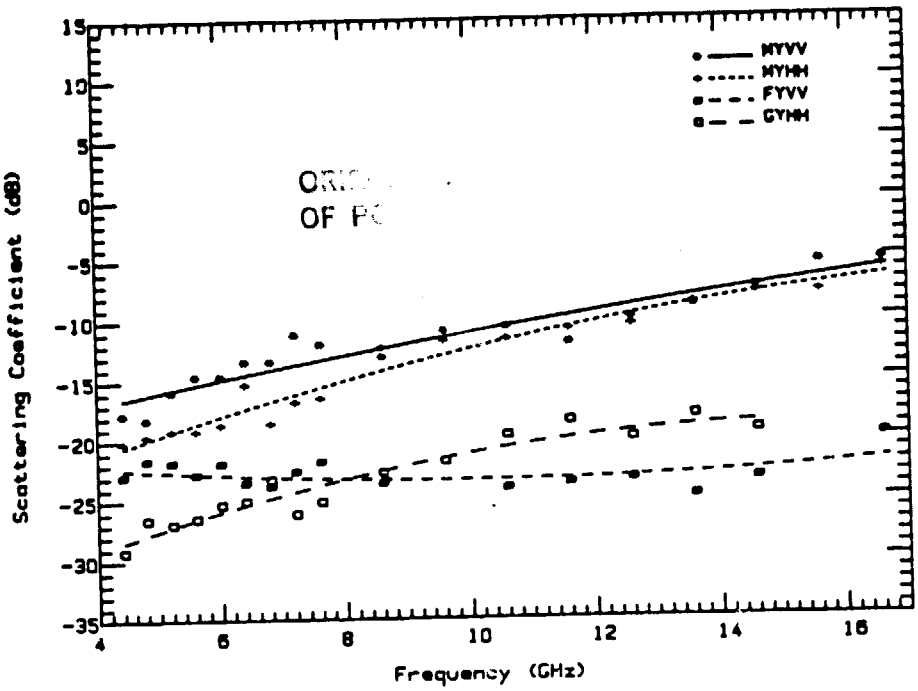

FIGURE 5.12
Scattering cross-section frequency response of MY, FY and GY ice at VV and HH polarizations at 60°

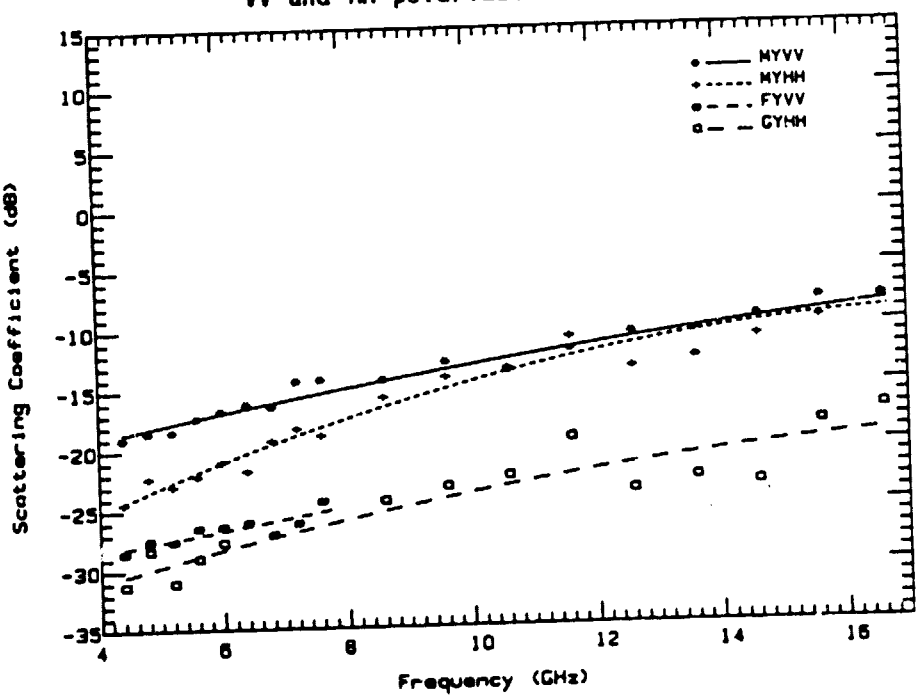

FIGURE 5.13
Scattering cross-section frequency response of MY, FY and GY ice at VV and HH polarizations at 70°

frequency responses tended to be flat while grey ice responses showed a greater tendency for higher cross-sections with increasing frequency.

Scattering cross-sections for multiyear, first-year, grey, shorefast and pressure-ridged ice is shown at 40° and VV-polarization in Figure 5.14. Multiyear and pressure-ridged ice provides the strongest returns while first-year ice produces the weakest. Grey ice returns are similar to those from first-year ice at the lower frequencies, but increased more rapidly with frequency till they fall midway between multiyear and first-year ice returns. Shorefast ice returns are slightly lower, 1-3 dB, than multiyear ice returns, especially at the higher freqeuencies.

5.6.2 Angular Response

The angular responses for multiyear ice with VV- and HH-polarization, first-year ice with VV-polarization, and grey ice with HH-polarization are shown in Figures 5.15 to 5.18 for 5.2, 9.6, 13.6 and 16.6 GHz. Responses at other frequencies in the 4-18 GHz range tend to be very similar to their nearest frequency neighbor.

Much information about the backscatter mechanisms is revealed through examination of the angular responses of each ice type. Backscatter from sea ice is described through the actions of three mechanisms. The roughness of the sea-ice surface and its dielectric properties provide a contribution in the form of surface scattering. The existence of scattering centers of sizes similar to the electromagnetic wavelength in the medium provide a contribution in the form of volume scattering. The third mechanism is the absorption of the energy in the medium. This absorption may take place when the medium is lossy or which has internal scattering. In many cases in nature all of these mechanisms are at play; however, what is important in understanding the

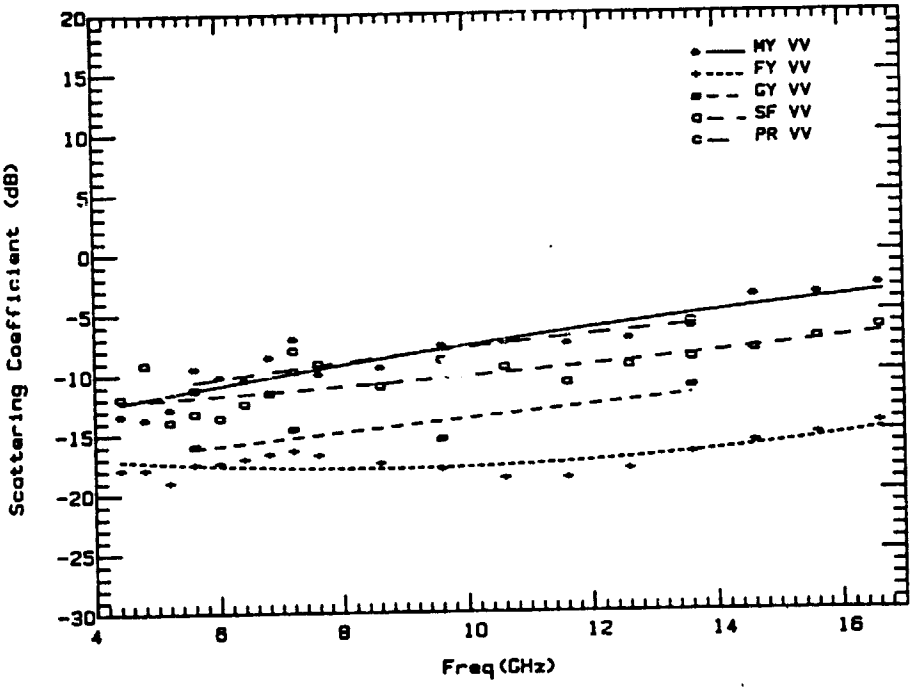

FIGURE 5.14
Scattering Cross-Section Frequency Response of MY, FY, GY and SF at 40° and VV-Polarization

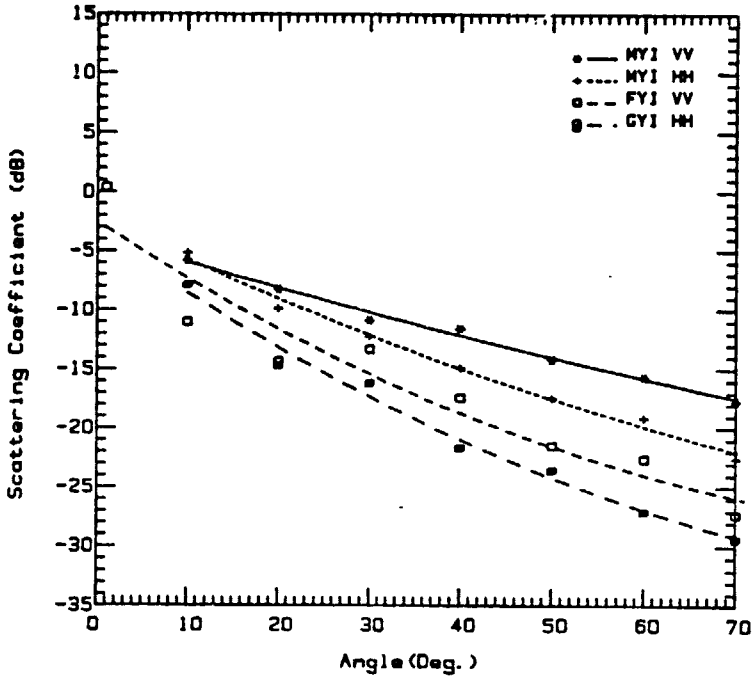

FIGURE 5.15
Scattering cross-section angular response of MY, FY and GY ice at VV and HH polarizations and 5.2 GHz

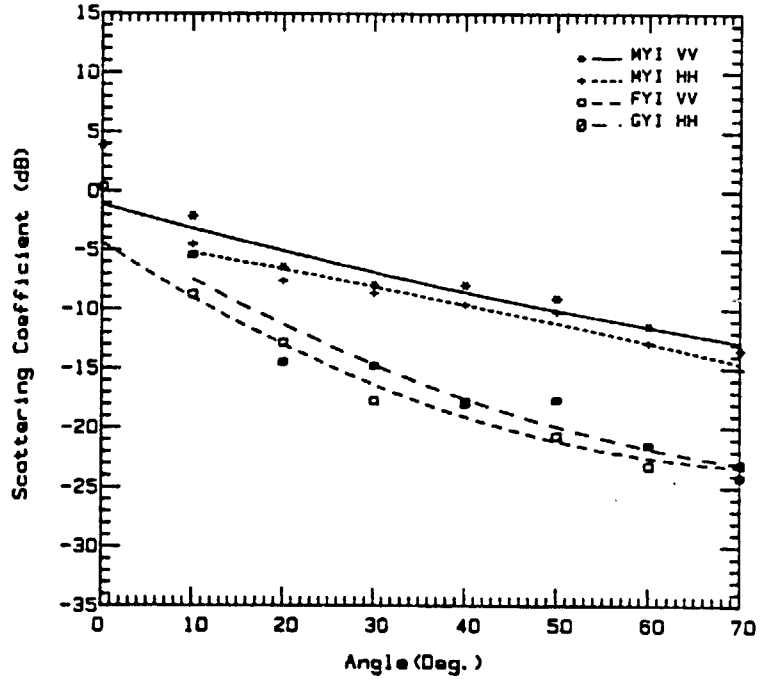

FIGURE 5.16
Scattering cross-section angular response of MY, FY and GY ice at VV and HH polarizations and 9.6 GHz

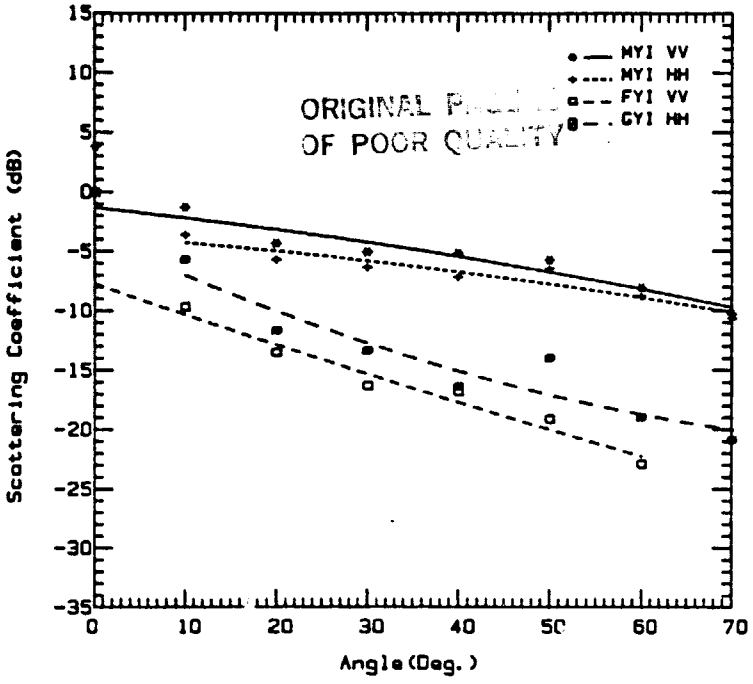

FIGURE 5.17
Scattering cross-section angular response of MY, FY and GY ice at VV and HH polarizations and 13.6 GHz

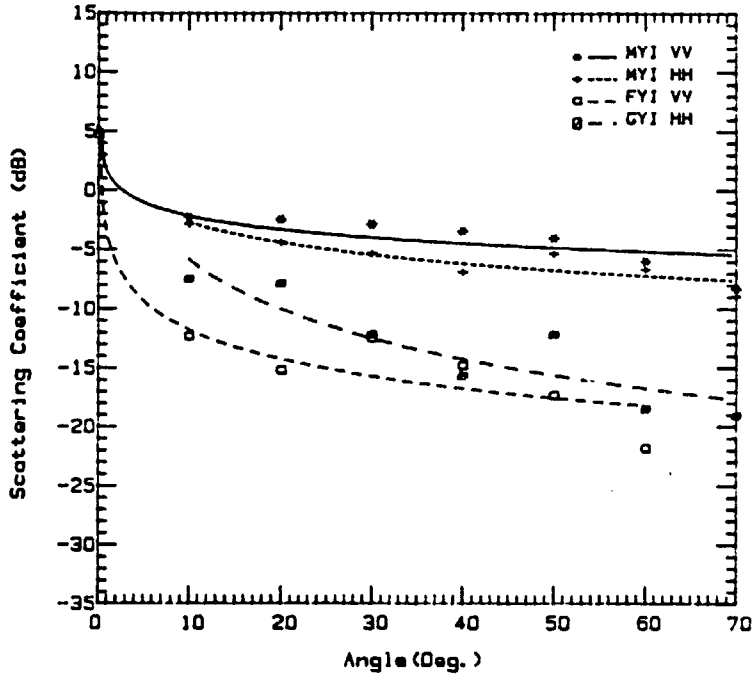

FIGURE 5.18
Scattering cross-section angular response of MY, FY and GY at VV and HH polarizations and 16.6 GHz

interaction process is the ability to describe the most dominant mechanism or dominant combination of mechanisms.

Analysis of the sea ice response under cold, late-fall conditions (temperatures greater than -20° C) shows that volume scattering dominates the backscatter process for multiyear ice and that surface scattering dominates the backscatter from first-year and grey ice. Surface scattering produces its most significant returns near vertical. After 20° to 30°, even for very rough surfaces, returns become very weak and decay rapidly with increasing angle. This is the phenomenon observed for first-year and grey ice. As the radar wavelength decreases, the influence of the small-scale surface roughness becomes greater, producing an angular response which decays less rapidly past vertical, and volume scattering from the thin snow layer or the upper few centimeters of the ice may begin to become more important. Results demonstrate the above well.

Volume scattering produces an angular response which is more angle independent. Near vertical, surface and volume scattering often work together. Results show multiyear returns are significantly greater than those of the thinner ice types. This suggests the presence of a volume scattering component since the ice surfaces do not exhibit a small-scale surface roughness which is extraordinarily different than that observed for the thinner ice types. The noticeably less-rapidly varying angular-response suggest strongly that volume scattering is the prime contributor to the backscatter process. As frequency is increased it is observed that the slope of the angular response became significantly less. At 16.6 GHz, for example, the slope is 2 dB/30° between 20° and 50°. For a scene with a high absolute level this argues for a strong volume scattering contribution. First-year ice shows a somewhat similar plateau but at levels 12 dB lower illustrating weak

scattering mechanisms. This also serves to demonstrate the relationship between the size of the scattering center and the wavelength of the energy within the medium. As frequency is increased, the radar wavelength decreasing proportionally, the scattering centers in the scattering volume become more influential and may produce a larger volume scattering contribution. Results demonstrate this effect well. The response of multiyear ice and the thinner ice types have a relatively similar slope but are offset in absolute level (at least 5 dB). Here the volume scattering contribution will be weaker at the lower frequencies than at higher frequencies due to the significant scale difference between wavelength and the scattering center sizes.

5.6.3 Contrast

Multiyear returns were greater than those from the thinner ice types. The contrast between multiyear and first-year ice at vertical polarization as a function of angle and frequency is shown in Figure 5.19. The contrast between multiyear and grey ice at horizontal polarization as a function of angle and frequency is shown in Figure 5.20. The ability to discriminate among these ice types was dependent upon angle, frequency, and polarization. Results show that contrast tends to increase with increasing frequency. This is the predominant trend for angles greater than 20°. Observation of the frequency-response trends show a convex response for 10° and 20° and a concave response for angles 30° to 60° for MY-VV and FY-VV. These two trends demonstrate the effects of operation in the anglular regions near vertical and away from vertical. Operation at the higher Ku-band frequencies provides an extra 1-2 dB contrast on top of the 11-14 dB contrast already present at 60°. Contrast is improved with increasing angles to 60°. These results are not conclusive as to whether there is an improvement by operating at 70°.

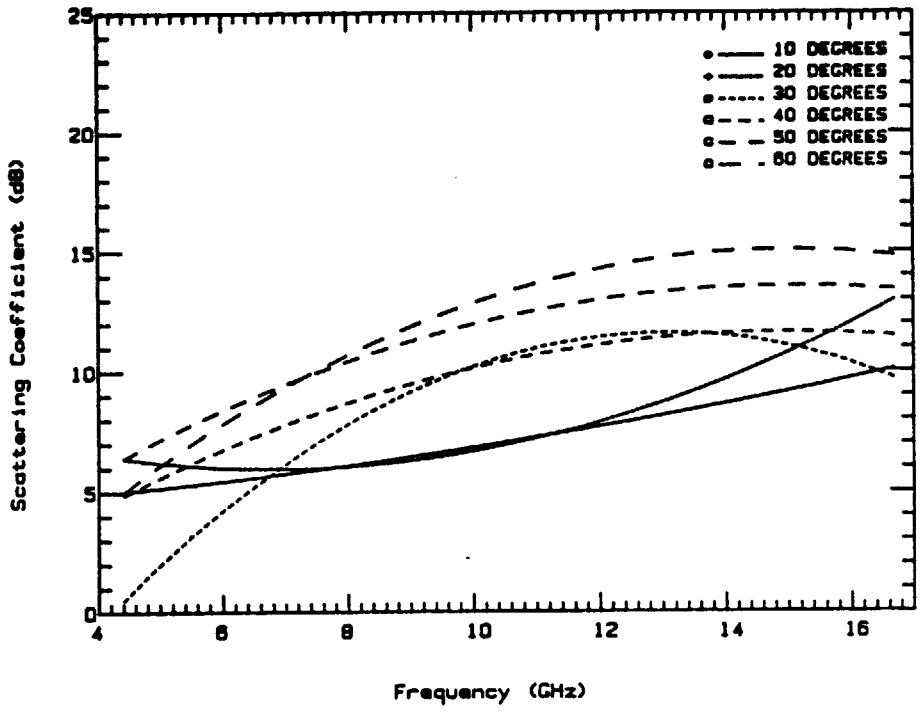

FIGURE 5.19
Radar contrast between MY and FY ice at VV-polarization

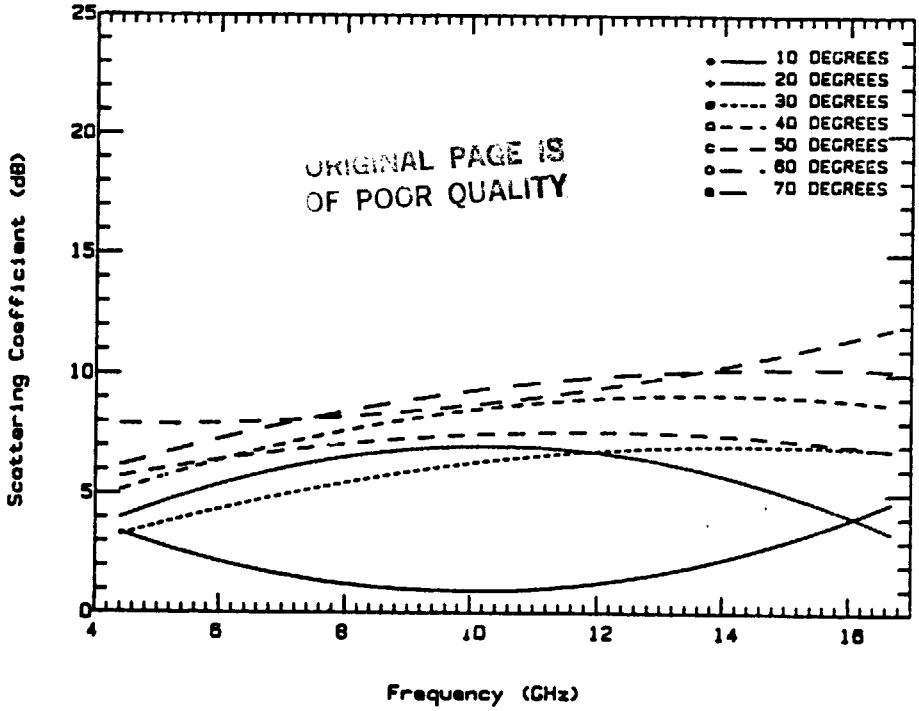

FIGURE 5.20
Radar contrast between MY and GY ice at HH-polarization

Examination of low frequency data for VV-polarization and angular response trends would, however, suggest that an improvement at 70° is expected.

To illustrate the influence this has on the ability to discriminate, 5 and 10 GHz contrasts are compared at 40°. For MY-VV and FY-VV the contrast at 5 GHz was 6 dB while at 10 GHz it was 10 dB. For MY-HH and GY-HH the contrast at 5 GHz was 6 dB while at 10 GHz it was 8 dB. There is some difficulty in arriving at the proper interpretation of these results. Examination of imagery obtained by the AES Electra over the ice sites discussed above shows that similar backscatter levels were obtained for FY-HH and GY-HH at 10 GHz. This would suggest, although not conclusively, that operation at VV would add an additional 20 percent in contrast. Following this argument further, operating at even higher frequencies would add an additional 100 percent over operation at 5 GHz.

Few measurements were made at cross-polarization due to encountered time constraints. Comparisons are unfortunately limited to 9.6 GHz and 50°. Contrast between multiyear ice and first-year ice is 12.4 dB at VV-polarization and 14.5 dB at VH-polarization. Contrast between multiyear ice and grey ice is 7.8 dB at HH-polarization and 8.0 dB at VH-polarization. Based upon these two measurements which include many spatial samples, contrast is very similar when operating at either like- or cross-polarization, and may be improved from .2 to 2.1 dB by operating at cross-polarization.

6.0 CONCLUSIONS

Active microwave measurements of sea ice under cold, late fall conditions were made during October 1981 at sites located near Mould Bay, N.W.T., Canada. The measurements were coordinated with an extensive ice characterization program. Results for data acquired at frequencies between 4

and 18 GHz, at angles from 5° to 70°, and at like- and cross-polarizations indicate the following. Multiyear ice frozen in grey or first-year ice is easily detectable based upon the intensity of the radar return. Contrasts at most frequencies and angles are often much greater than 6 dB. The greatest contrast was about 15 dB. The contrast between thick and thin ice returns improved with increasing frequency. The rate of increase was greatest at the lowest frequencies and slows at the higher frequencies. Most importantly, operation at C-band frequencies, a possible candidate for satellite operation, is very similar to operation at X-band frequencies. There is a demonstrated ability to discriminate ice types, but contrast between thick and thin ice may be reduced by a factor of 2. Fortunately, operation at C-band is dissimilar to operation at L-band where thick first-year and multiyear ice returns for flat ice are very similar, if not identical.

Multiyear ice returns are very dynamic. This is due to the contrast between the radar responses of two of its major ice features, meltpools and ice mounds. Meltpools, composed of smooth fresh water ice, produce low returns because backscatter is due primarily to surface scattering from the ice and a weak volume scatter from its snowpack. The ice mounds which produce much stronger returns have both surface scattering and dominate volume scatter. The presence of these two features produce significant variation in returns for multiyear ice. In imagery this is seen as well-defined texture. Scene variation for grey and first-year ice may be much less. Ice which is rafted when mixed among ice which is homogeneous also shows significant variation in return strength.

The boundary between the multiyear ice floe which is frozen into the grey ice is readily detectable in the radar profile. There is often a brief, high contrast response associated with this transition region. Contrast at this

boundary is often significantly greater than that found elsewhere. The cause of this tendency has not been defined as yet, but may be answered with some further study. It is expected that deformation and/or strewn blocks of ice at the edge, possibly in combination with a brief zone of smooth thin ice is responsible.

A large, old multiyear pressure ridge in a multiyear ice background is found to produce returns very similar to its background ice. Because the ridge is well-weathered, which reduces possible peculiar returns from edges of ice blocks, and since volume scattering is fairly insensitive to incidence angle, it may be expected that old pressure ridge features will have returns not radically different from its background ice. As grazing angles are used it is also expected that ridge returns will become much stronger when compared to the flat ice. In addition, melt features at the skirts of the ridge may make identification possible by providing a feature composed of a bright linear feature sandwiched between weak linear features.

Returns from homogeneous first-year ice can be characterized as being dominated by surface scattering effects since the ice is highly saline and thereby lossy. Regional variations in the scattering cross-sections of homogeneous first-year ice are seen to be due primarily to local small-scale surface-roughness conditions. Level shifts of 3 to 4 dB are noted for roughnesses which range from very smooth to ice which has 1-2 cm roughness elements. The light snow cover may also act to absorb radar energy due to the migration of salt into the snowpack. A comparison of 5.6 and 9.6 GHz results is interesting in that it appears that operation at the higher frequency more closely tracks the changes in surface roughness, but use of the lower frequency provides more dynamic range between the smooth and rough ice.

Very limited cross-polarization measurements indicate that contrast is similar to that of like-polarization, but with a potential improvement of 2 dB.

The best comparison of all three polarizations is made of multiyear and grey ice at 9.6 GHz and 50°. Contrasts of 7.7, 8.0 and 8.0 were measured for VV-, HH-, and VH-polarizations, respectively.

REFERENCES

[1] Troy, B.E., Jr., J.P. Hollinger, M.C. Hartman, R.O. Ramseier and S.A. Digby, "Preliminary Report on Passive Microwave and Millimeter Wave Measurements of Arctic Sea Ice, October/November 1981," NRL Memorandum Report 4861, July 16, 1982.

[2] Digby, S.A., "Mould Bay Sea Ice Experiment I October 1981: Experiment Summary and Surface Characteristics Report 82-15," RadarSat Report 82-15, no date.

[3] Kim, Y.S., "Theoretical and Experimental Study of Radar Backscatter from Sea Ice," Ph.D. Thesis, University of Kansas, Lawrence, Kansas, January 1984.

APPENDICES

APPENDIX 1
Regression Equation and Constants

The regression equation for the frequency response of the scattering coefficient is of the form:

$$\sigma^{o}(dB) = A\ f^{2} + B\ f + C$$

where f = frequency in GHz.

(1) Constants for MY Ice; Polarization = VV

Angle (°)	A	B	C
0	-2.1435 E-2	0.8635	- 3.8008
10	-6.8313 E-2	1.9152	-14.235
20	-1.3117 E-2	-0.2194	- 9.7575
30	4.2909 E-2	0.6144	-14.248
40	-1.5641 E-2	1.0569	-16.684
50	-3.8019 E-2	1.7158	-22.064
60	-1.6306 E-2	1.2059	-21.525
70	-2.3022 E-2	1.2598	-23.708

(2) MY Ice; Polarization = HH

Angle (°)	A	B	C
10	6.5283 E-3	6.1816 E-2	- 5.688
20	-7.0721 E-3	0.6318	-13.01
30	-3.2588 E-2	1.3229	-18.34
40	-7.1911 E-2	2.2692	-24.78
50	-8.3419 E-2	2.8834	-30.26
60	-4.6966 E-2	2.1222	-28.99
70	-7.3242 E-2	2.7933	-35.15

(3) First-Year Ice; Polarization = VV

Angle (°)	A	B	C
0	0.0625	-1.1092	4.686
10	-8.9634 E-2	1.840	-18.20
20	-1.1886 E-2	0.2435	-14.777
30	4.1932 E-2	-0.8869	-11.575
40	0.03583	-0.5659	-15.638
50	5.2778 E-2	-0.777	-18.606
60	3.3443 E-2	-0.6636	-20.116
70	1.8333 E-2	0.6842	-31.485

(4) Grey Ice; Polarization = HH

Angle (°)	A	B	C
10	-3.3384 E-2	0.6973	- 8.991
20	8.0183 E-2	-1.1571	-10.817
30	4.6624 E-3	0.2482	-17.602
40	-2.6048 E-2	1.0097	-25.276
50	-0.04959	2.0819	-33.097
60	-7.3897 E-2	2.3615	-37.403
70	6.9326 E-2	-0.5464	-27.114

APPENDIX 2
Mean Cross-Sections

Average σ^0 (dB): HELOSCAT Results

(1) Multiyear ice, HH polarization

(GHz)	10°	20°	30°	40°	50°	60°	70°
4.4	-6.8	-10.1	-13.7	-17.2	-19.5	-20.2	-24.4
4.8	-5.6	- 8.5	-11.8	-14.7	-17.3	-19.6	-22.3
5.2	-6.4	-13.0	-13.9	-14.7	-18.7	-19.2	-23.0
5.6	-5.0	-10.8	-13.8	-14.3	-17.2	-19.2	-22.2
6.0	-4.5	-10.6	-11.5	-13.6	-16.0	018.7	-21.0
6.4	-2.3	- 7.2	- 9.0	-12.9	-15.6	-15.3	-21.8
6.8	-2.7	- 7.1	- 9.4	-12.3	-12.8	-18.6	-19.3
7.2		- 9.1	-10.8	-11.8	-13.7	-16.8	-18.3
7.6		- 7.8	-10.0	-12.8	-14.1	-16.5	-18.9
8.6	-5.9	- 7.8	- 7.6	-11.2	-11.2	-12.3	-15.8
9.6	-5.5	- 8.5	- 9.1	- 9.7	-10.0	-11.8	-14.2
10.6	-4.5	- 7.3	-10.4	- 8.8	- 8.8	-11.7	-13.5
11.6	-4.7	- 7.3	- 7.1	- 8.0	- 7.0	-10.9	-11.0
12.6	-4.3	- 6.5	- 6.7	- 7.3	- 8.4	-10.6	-13.6
13.6	-3.1	- 5.1	- 7.0	- 6.5	- 6.7	- 8.8	-10.6
14.6	-3.0	- 5.5	- 5.9	- 7.9	- 7.0	- 8.0	-11.1
15.6	-4.0	- 4.7	- 5.3	- 6.5	- 5.7	- 8.0	- 9.7
16.6	-2.1	- 4.4	- 5.1	- 7.1	- 4.4	- 6.0	- 7.9

(2) Grey Ice: HH polarization

(GHz)	10°	20°	30°	40°	50°	60°	70°
4.4		-14.4	-17.6	-21.3	-25.7	-29.3	-31.3
4.8		-15.2	-15.7	-20.3	-24.2	-26.6	-28.4
5.2		-16.7	-18.0	-21.9	-14.1	-27.0	-31.1
5.6		-13.0	-16.3	-20.0	-21.7	-26.5	-29.1
6.0		-13.3	-15.8	-20.2	-21.7	-25.4	-27.8
6.4	-5.6	-13.1	-19.3	-19.8	-25.1		
6.8	-6.4	-13.8	-20.1	-20.4	-23.3		
7.2	-8.9	-15.5	-20.0	-23.3	-26.2		
7.6	-6.1	-14.8	-19.0	-22.5	-25.2		
8.6	-5.5	-15.6	-17.3		-18.0	-22.8	-24.5
9.6	-5.2	-14.0	-14.7	-17.4	-17.8	-21.9	-23.4
10.6	-4.0	-13.8	-15.5	-17.8	-17.3	-19.8	-22.6
11.6	-5.5	-14.3	-15.0	-17.0	-12.9	-18.6	-19.5
12.6	-6.1	-12.3	-13.7	-15.6	-15.1	-20.1	-23.9
13.6	-5.9	-11.1	-12.8	-16.2	-14.6	-18.2	-22.9
14.6	-5.8	-11.8	-11.7	-18.0	-14.2	-19.5	-23.4
15.6		-10.0	-13.3	-15.7	-12.3	-18.4	
16.6		- 6.9	-12.2	-15.1	-12.0	-17.2	

(3) First-year ice, HH polarization

(GHz)	20°	40°	60°
5.6	-15.8	-20.9	-25.9
9.6	-13.2	-15.5	-20.8

(4) Multiyear ice, VV polarization

(GHz)	0°	10°	20°	30°	40°	50°	60°	70°
4.4		-7.0	-9.4	-12.8	-13.4	-16.9	-17.8	-19.0
4.8		-7.9	-8.6	-14.4	-13.7	-16.0	-18.2	-18.5
5.2		-6.0	-9.2	-11.7	-12.9	-14.0	-15.9	-18.4
5.6		-7.1	-7.2	- 9.7	- 9.5	-14.4	-14.6	-17.3
6.0		-5.5	-7.7	- 8.4	-10.2	-11.7	-14.6	-16.7
6.4		-3.7	-8.1	- 8.4	-10.5	-12.0	-13.4	-16.2
6.8		-2.2	-6.7	- 8.9	- 8.6	-10.7	-13.4	-16.4
7.2		-0.7	-6.4	- 7.7	- 7.1	-10.9	-11.2	-14.3
7.6		-3.0	-6.9	- 8.1	-10.0	- 9.9	-12.0	-14.2
8.6	0.5	-2.2	-6.7	- 9.5	- 9.5	-10.0	-13.1	-14.3
9.6	3.9	0.3	-7.1	- 6.6	- 7.7	- 8.4	-11.0	-12.9
10.6	6.3	-2.6	-4.8	- 9.3	- 7.5	- 9.3	-10.7	-13.7
11.6	-0.5	-5.8	-8.2	- 8.8	- 7.6	- 7.9	-12.0	-12.0
12.6	3.9	-2.3	-6.0	- 7.9	- 7.2	- 7.6	-10.0	-10.7
13.6	3.8	-1.2	-3.8	- 4.4	- 6.3	- 7.3	- 9.0	-12.8
14.6	5.4	-0.4	-3.1	- 3.5	- 3.7	- 5.6	- 7.5	- 9.4
15.6	3.4	-2.9	-1.6	- 3.7	- 3.6	- 3.7	- 5.5	- 8.0
16.6	5.1	-0.7	-3.4	- 2.0	- 2.9	- 2.9	- 5.4	- 8.1

(5) First-year ice, VV polarization

(GHz)	10°	20°	30°	40°	50°	60°	70°
4.4	-13.7	-16.6	-12.5	-17.9	-23.2	-22.9	-28.5
4.8	-12.7	-15.8	-13.4	-17.0	-22.8	-21.6	-27.5
5.2	-11.4	-15.0	-14.1	-19.0	-22.3	-21.8	-27.6
5.6	-11.5	-13.5	-14.1	-17.5	-21.2	-22.8	-26.5
6.0	-10.0	-13.4	-13.5	-17.4	-21.0	-21.9	-26.4
6.4	- 9.6	-12.2	-13.8	-17.1	-20.2	-23.9	-26.1
6.8	- 8.1	-13.2	-15.3	-16.7	-19.5	-23.8	-27.1
7.2	- 7.2	-12.3	-16.0	-16.4	-20.5	-22.6	-26.2
7.6	- 8.0	-12.2	-15.7	-16.8	-20.0	-21.8	-24.4
8.6	- 8.3	-13.3	-18.4	-17.5	-22.2	-23.6	
9.6	- 8.2	-12.6	-18.4	-18.0	-20.8		
10.6	- 7.9	-11.8	-16.7	-18.8	-21.3	-24.1	
11.6	-10.0	-15.2	-19.7	-18.8	-23.7		
12.6	-11.9	-16.5	-17.8	-18.1	-20.8	-23.4	
13.6	-18.4	-13.7	-16.8	-19.6	-24.8		
14.6	-11.1	-13.8	-14.3	-15.9	-19.6	-23.4	
15.6	-11.8	-12.8	-14.6	-15.3	-17.9	-21.0	
16.6	- 9.1		-12.6	-14.4	-16.1	-19.9	

(6) Shore-fast ice, VV polarization

(GHz)	30°	40°	60°	70°
4.4	-11.9	-12.0	-14.2	-20.3
4.8	-11.0	- 9.2	-15.8	-20.8
5.2	- 9.4	-14.0	-16.8	-20.7
5.6	-10.7	-13.3	-17.9	-17.9
6.0	- 8.6	-13.7	-12.3	-15.4
6.4	- 8.0	-12.5	-15.9	-15.1
6.8	- 8.0	-11.6	-14.5	-13.6
7.2	- 7.3	- 9.8	-13.0	-12.4
7.6	- 7.1	- 9.2	-14.0	-14.1
8.6	- 8.6	-11.1	-14.8	-16.8
9.6	- 8.8	- 8.9	-11.8	-15.6
10.6	- 7.3	- 9.6	- 8.0	-13.1
11.6	-10.9	-10.9	-13.1	-15.8
12.6	- 9.6	- 9.5	-13.3	-14.6
13.6	- 6.0	- 8.9	- 8.6	-17.2
14.6	- 4.1	- 8.2	- 7.3	-12.4
15.6	- 4.8	- 7.3	- 7.3	-10.5
16.6	- 2.6	- 6.4	- 5.4	-11.0

(7) Lake ice, VV polarization

(GHz)	40°	70°
4.4	-21.7	-28.6
4.8	-19.7	-27.9
5.2	-18.6	-26.2
5.6	-18.5	-26.4
6.0	-16.2	-25.9
6.4	-16.0	-25.0
6.8	-16.7	-25.2
7.2	-15.7	-24.2
7.6	-15.9	-23.8
8.6	-12.8	-24.8
9.6	-12.6	-19.3
10.6	-11.1	-18.3
11.6	-10.9	-22.5
12.6	- 8.8	-26.3
13.6	- 7.8	-24.8
14.6	- 5.6	-17.1
15.6	- 5.1	-19.9
16.6	- 2.8	-17.6

(8) Grey ice, VV polarization

(GHz)	40°	50°
5.6	-16.0	
7.2	-14.6	
9.6	-15.5	-16.1
13.6	-11.2	

(9) Pressure-ridge, VV polarization

(GHz)	40°	70°
5.6	-11.3	
7.2	- 8.1	
9.6	- 9.0	-13.8
13.6	- 5.9	-11.3

(10) First-year ice, VH polarization

(GHz)	20°	40°	60°
5.6	-22.9	-28.4	-34.0
9.6	-19.3	-22.8	-27.7

(11) Multiyear/grey ice, VH polarization, 50°

9.6 GHz	-10.8/-18.8

APPENDIX 3
Statistics

(1) Multiyear/Grey Ice (Intrepid Inlet)

Run	Freq. (GHz)	Pol.	Angle	Avg. σ^0	Min.	Std. Max.	Dev.	# of Data Pts.	Target
2303	5.6	HH	50°	-21.4	-30.4	-13.8	2.8	184	GY
2305	5.6	HH	60°	-18.4	-27.9	-13.3	2.2	187	MY
				-26.	-33.7	-23.4	1.3	151	GY
2308	5.6	HH	70°	-29.6	-41.5	-23.2	2.0	180	GY
				-21.5	-33.7	-12.6	2.6	260	MY
2315	9.6	HH	50°	- 9.8	-20.1	- 6.9	2.1	172	MY
				-17.8	-21.3	-15.8	1.0	66	GY
2316	9.6	VV	50°	-16.1	-22.7	-14.2	1.2	124	GY
				- 8.4	-20.8	- 3.9	2.6	181	MY
2403	5.6	VV	40°	- 9.5	-22.4	- 4.4	3.2	244	MY
				-16.6	-21.8	-13.6	1.7	116	Smooth GY
				-16.	-24.7	-11.4	2.6	252	Whole GY
2404	7.2	VV	40°	-14.6	-19.5	-10.8	1.8	180	GY
				- 7.1	-23.4	- 1.5	3.4	250	MY
2407	9.6	VV	40°	- 7.7	-22.7	- 3.2	3.4	230	MY
				-15.5	-21.2	-10.2	1.5	198	GY
2408	13.6	VV	40°	-11.2	-17.8	-5.	1.5	120	GY
				- 6.3	-14.5	-2.	2.5	290	MY

(2) Multiyear pressure ridge (Intrepid Inlet)

Run	Freq. (GHz)	Pol.	Angle	Avg. σ^0	Min.	Std. Max.	Dev.	# of Data Pts.	Target
2438	5.6	VV	40°	-11.3	-24.4	-5.1	2.5	80	
2439	7.2	VV	40°	- 8.1	-23.	-5.3	2.7	112	
2440	9.6	VV	40°	- 9.	-14.4	-3.6	1.9	128	
2441	13.6	VV	40°	- 5.9	-11.8	-2.4	1.5	128	
2443	13.6	VV	70°	-11.3	-21.9	-3.6	2.3	157	
2444	9.6	Vv	70°	-13.8	-26.8	-9.	2.7	96	

(3) Lake ice (Landing Lake)

Run	Freq. (GHz)	Pol.	Angle	Avg. σ^o	Min.	Max.	Std. Dev.	# of Data Pts.	Target
2447	8.6	VV	40°	-12.7	-23.5	- 4.3	2.7	186	Whole line
				-12.9	-23.5	- 5.6	3.1	92	Snow free
				-12.4	-22.3	- 4.3	2.0	93	Snow covered
2459	5.6	VV	40°	-18.7	-23.1	-13.	2.2	165	Whole (part)
				-18.4	-23.9	-12.3	2.3	200	Whole
				-19.5	-23.1	-13.	2.3	66	Snow free
				-18.3	-22.2	-13.5	1.9	98	Snow covered
2460	9.6	VV	40°	-11.8	-19.9	- 3.3	1.9	196	Whole (part)
				-11.4	-19.9	- 3.3	2.	100	Snow covered
				-12.2	-16.7	- 6.8	1.8	95	Snow free
2461	13.6	VV	40°	- 7.8	-12.	- 4.3	1.4	160	Whole

(4) First-year ice (Mould Bay)

Run #	Freq.	Pol.	Angle	Avg. σ^0	Min.	Max.	Std. Dev.	# of Pts.	Target
1803	5.6 GHz	HH	20°	-12.7	-14.9	-11.1	1.0	38	0
				-13.7	-17.7	-11.4	1.3	82	1
				-16.1	-18.3	-13.7	0.9	128	2
				-16.9	-19.1	-14.5	1.0	94	3
				-15.5	-18.5	-13.0	1.4	74	5
				-16.0	-18.6	-14.0	0.9	70	6
				-16.3	-18.6	-14.6	0.7	74	7
				-17.3	-19.9	-15.6	0.8	64	8
				-17.2	-24.5	-14.4	1.2	172	9
				-15.5	-22.6	-13.0	1.5	176	10
1804	9.6	HH	20°	-10.5	-13.3	- 8.9	1.0	32	0
				-12.2	-14.0	- 9.5	0.9	84	1
				-13.4	-16.9	-11.5	0.9	104	2
				-14.0	-17.5	-12.3	1.0	100	3
				-13.3	-17.2	-10.6	1.4	76	5
				-13.6	-17.2	-11.0	1.1	76	6
				-13.8	-17.6	-11.8	1.0	80	7
				-14.6	-18.3	-12.5	1.4	56	8
				-14.5	-24.4	-10.0	1.5	150	9
				-12.9	-16.5	- 9.2	1.4	178	10
1805	9.6	HH	20°	-10.8	-19.8	- 8.3	1.6	80	0
				-12.1	-14.6	- 8.9	1.2	70	1
				-13.7	-19.6	-12.4	1.3	94	2
				-14.1	-16.5	-11.8	0.9	84	3
				-13.2	-17.1	-10.8	1.4	84	5
				-13.7	-18.7	-11.7	1.2	76	6
				-13.4	-20.6	-11.0	1.3	66	7
				-14.0	-19.9	- 9.5	1.5	56	8
				-14.6	-22.5	-11.8	1.6	110	9
				-12.6	-16.4	- 5.1	1.7	176	10
1808	5.6	HH	40°	-19.1	-23.5	-16.6	1.2	92	0
				-20.4	-28.7	-17.6	1.5	86	1
				-21.5	-23.1	-20.0	0.6	106	2
				-21.9	-23.7	-20.0	0.7	104	3
				-21.6	-24.3	-18.9	1.0	76	6
				-21.2	-23.2	-19.7	0.8	58	7
				-21.6	-23.5	-20.6	0.7	56	8
				-21.5	-26.2	-18.6	1.2	148	9
				-20.4	-25.1	-15.0	1.6	202	10
1811	9.6	HH	40°	-14.3	-19.2	-12.6	1.0	72	0
				-15.7	-18.3	-13.6	0.8	68	1
				-14.8	-17.6	-12.4	0.6	110	2
				-14.8	-17.2	-13.4	0.9	76	3
				-16.0	-22.0	-13.8	1.4	92	6
				-15.6	-22.9	-14.0	1.3	84	7
				-15.4	-18.3	-13.5	0.9	60	8
				-16.1	-20.6	-14.4	0.9	174	9
				-16.4	-19.8	-13.0	0.8	172	10
1813	5.6	HH	60°	-24.4	-26.4	-22.1	0.9	80	0
				-26.2	-29.5	-23.1	1.3	92	1
				-26.3	-28.8	-24.8	0.7	120	2
				-27.0	-29.8	-24.6	0.9	102	3
				-25.4	-28.0	-22.4	1.2	80	5
				-27.3	-30.0	-25.0	1.2	60	6
				-27.1	-29.7	025.8	0.8	72	7
				-27.4	-31.0	-25.9	0.9	58	8
				-27.4	-29.8	-25.3	0.9	150	9
				-26.7	-32.3	-23.4	1.6	174	10
1815	9.6	HH	60°	-20.6	-22.4	-18.9	0.8	50	0
				-22.1	-24.5	-20.1	1.0	102	1
				-20.3	-23.3	-18.3	0.8	142	2
				-20.2	-25.2	-18.2	1.2	106	3
				-21.5	-25.1	-19.4	1.1	78	5
				-22.3	-27.5	-19.4	1.6	82	6
				-21.1	-25.1	-19.4	1.4	80	7
				-20.5	-24.2	-17.7	1.3	68	8
				-21.5	-25.7	-18.7	1.1	184	9
				-21.9	-25.6	-19.5	1.1	156	10
1902	5.6	VH	20°	-22.9	-34.	-16.	---	1002	whole flight line
1904	9.6	VH	20°	-19.3	-36.6	- 8.3	1.9	949	
1906	5.6	VH	40°	-28.4	-36.4	-14.9	1.6	992	
1908	9.6	VH	40°	-22.8	-37.1	-12.9	1.7	976	
1910	5.6	VH	60°	-32.8	-42.7	-14.4	2.6	1050	
1912	9.6	VH	60°	-27.7	-32.6	-19.4	1.3	894	

APPENDIX 4
Contrasts and Contrasts Regression Equations

(1) Difference between multiyear and first-year ice, VV polarization

(GHz)	10°	20°	30°	40°	50°	60°	70°
4.4	6.7	7.3	- 0.3	4.5	6.4	5.1	9.4
4.8	4.8	7.2	- 1.1	4.2	6.9	3.4	9.0
5.2	5.4	5.8	2.4	6.1	8.4	5.9	9.3
5.6	4.4	6.3	4.4	8.0	6.8	9.1	9.2
6.0	4.4	5.6	5.1	7.2	9.3	7.3	9.7
6.4	5.8	4.1	5.4	6.6	8.2	10.1	9.9
6.8	5.9	6.5	6.5	8.1	8.8	10.4	10.7
7.2	6.5	5.8	8.4	9.4	9.6	11.4	11.9
7.6	5.0	5.3	7.6	6.8	10.1	9.7	10.2
8.6	6.1	6.6	8.8	8.0	12.2	10.4	
9.6	8.5	5.6	11.8	10.2	12.4		
10.6	5.2	7.0	7.4	11.4	12.0	13.4	
11.6	4.1	7.0	10.9	11.2		11.7	
12.6	9.6	10.5	9.9	10.9	13.3	13.4	
13.6	11.2	9.9	10.4	12.4	15.9		
14.6	10.7	10.6	10.9	12.3	14.0	15.9	
15.6	8.9	11.2	10.9	11.7	14.3	15.5	
16.6	8.5		10.6	11.5	13.3	14.6	

(2) Difference between multiyear and grey ice, HH polarization

GHz	10°	20°	30°	40°	50°	60°	70°
4.4		4.3	3.9	4.1 6.2	9.1	6.9	
4.8		6.7	3.9	5.6 6.9	7.0	6.1	
5.2		3.7	4.1	7.2 5.4	7.8	8.1	
5.6		2.2	2.5	5.7 4.5	7.3	6.9	
6.0		2.7	4.3	6.6 5.7	6.7	6.8	
6.4	3.3		4.1	6.4 4.2	9.8		
6.8	3.7		4.4	7.8 7.6	4.7		
7.2			4.7	8.2 9.6	9.4		
7.6			4.8	6.2 8.4	8.7		
8.6	-0.4	7.8	9.7	6.8	10.5	8.7	
9.6	-0.3	5.5	5.6	7.7 7.8	10.1	9.2	
10.6	-0.5	6.5	5.1	9.0 8.5	8.1	9.1	
11.6	0.8	7.0	7.9	9.0 5.9	7.7	8.5	
12.6	1.8	5.8	7.0	8.3 6.7	9.5	10.3	
13.6	2.8	6.0	5.8	9.7 7.9	9.4	12.3	
14.6	2.8	6.3	5.8	10.1 7.2	11.5	12.3	
15.6		5.3	8.0	9.2 6.6		8.7	
16.6		2.5	7.1	8.0 7.6		9.3	

APPENDIX 5
Angular Responses

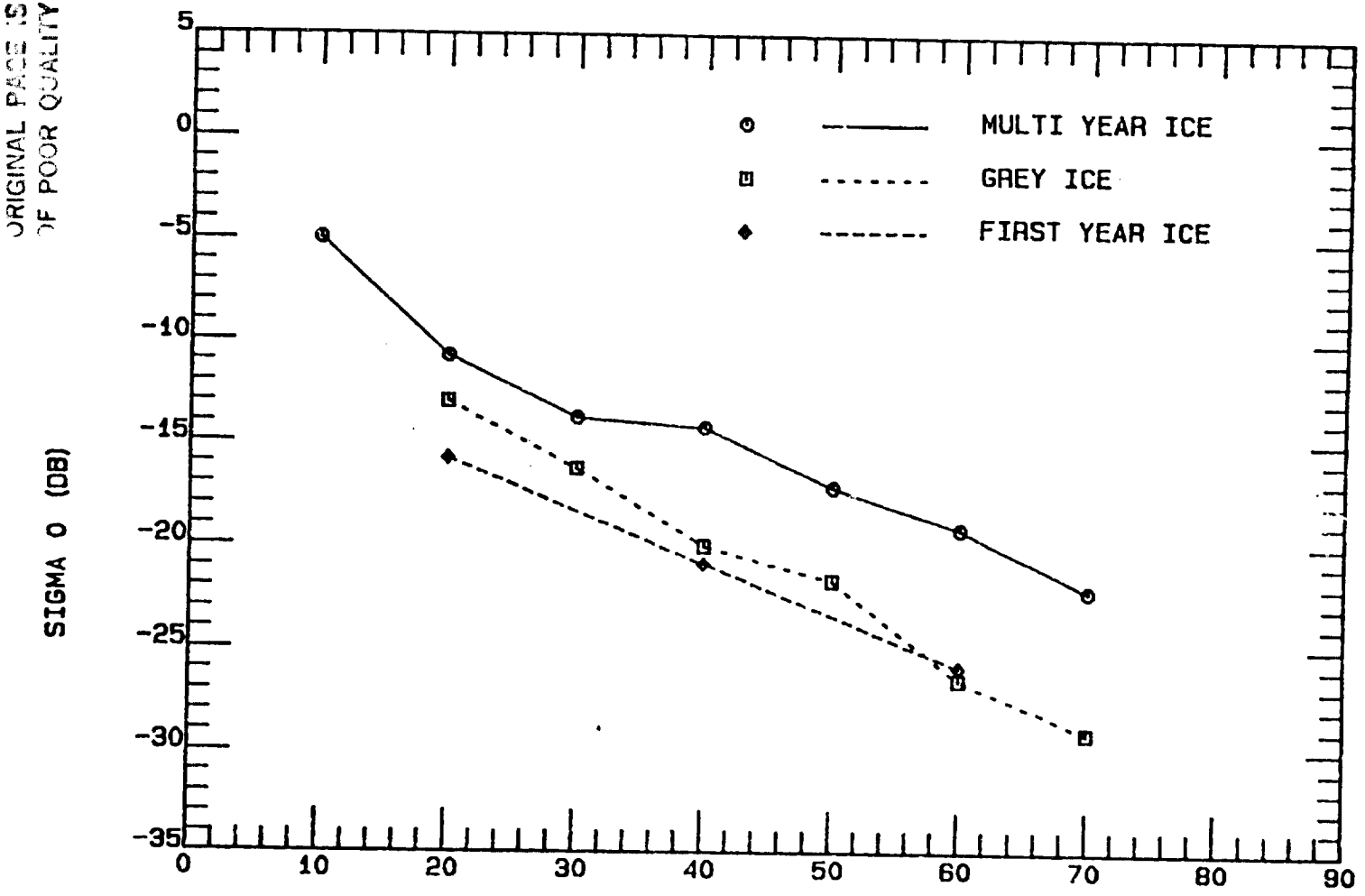

FREQUENCY= 5.6 GHZ, POL=HH, MOULD BAY, OCT. 1981

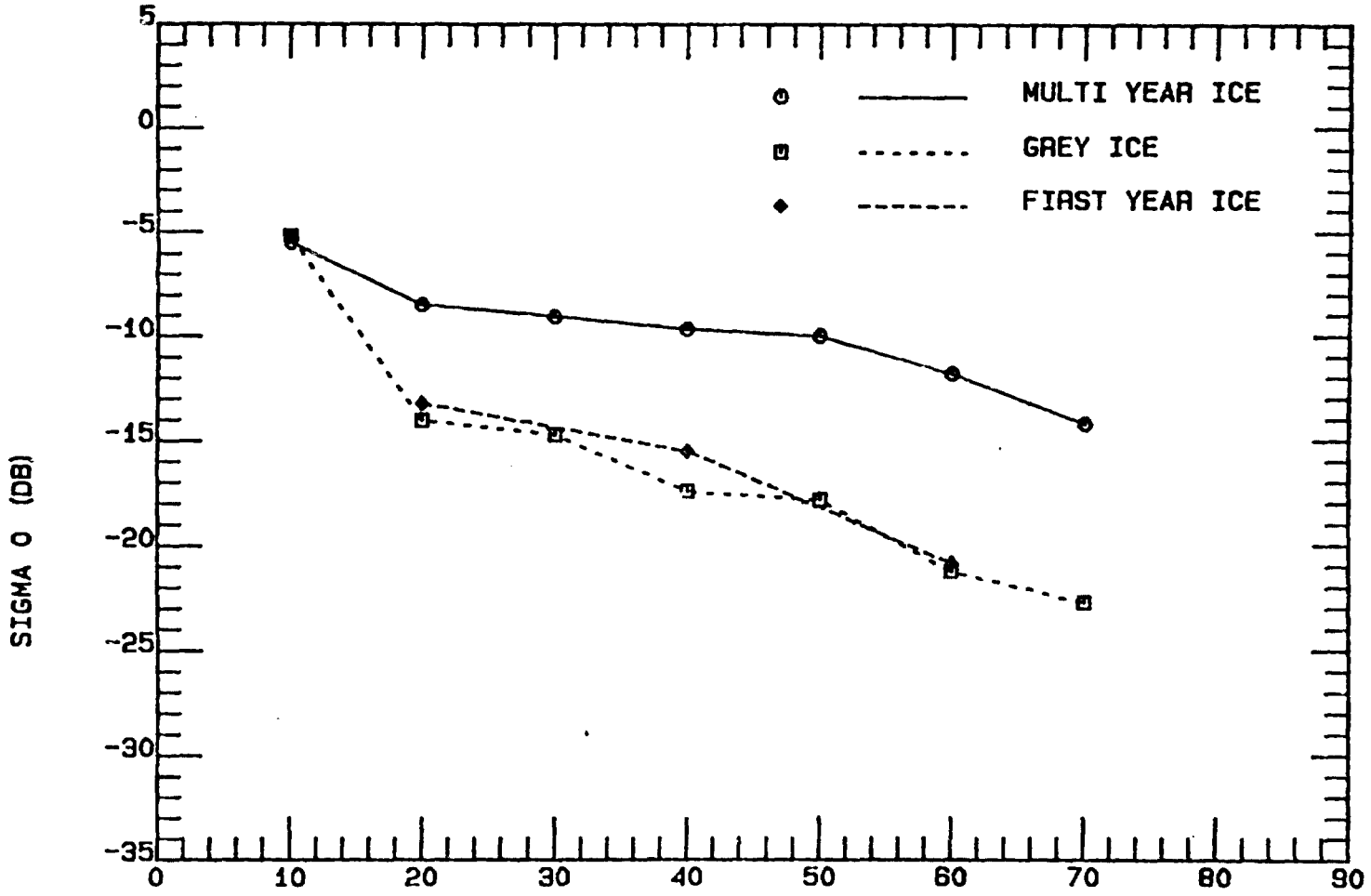

FREQUENCY= 9.6 GHZ, POL=HH, MOULD BAY, OCT. 1981

APPENDIX 6
Profiles

1)	10/18/81	Mould Bay first-year ice		
		HH-Pol.;	5.6, 9.6 GHz	20°, 40°, 60°
		Run #'s:	1803, 1804, 1805, 1808, 1811, 1313, 1815	
		Histograms		
2)	10/19/81	Mould Bay first-year ice		
		VH-Pol.;	5.6, 9.6 GHz	20°, 40°, 60°
		Run #'s:	1902, 1904, 1906, 1908, 1910, 1912	
		Histograms		
3)	10/22/81	Intrepid Inlet, multiyear/grey ice		
		HH-Pol.;	C- and Ku-X-band	10°, 20°, 30°, 40°
		Run #'s:	2202, 2205, 2208, 2209, 2212, 2213, 2214, 2217	
4)	10/23/81	Intrepid Inlet, multiyear/grey ice		
		HH,VV,VH-Pol.;	C- and Ku-X-band	50°, 60°, 70°
		Run #'s:	2302, 2303, 2304, 2305, 2306, 2307, 2308, 2311, 2312, 2313, 2314, 2315, 2316, 2317	
		Histograms for 2315, 2316, 2317		
5)	10/24/81	Intrepid Inlet, multiyear/grey ice		
		VV-Pol.;	5.6, 7.2, 9.6, 13.6 GHz	40°
		Run #'s:	2403, 2404, 2407, 2408	
		Intrepid Inlet, multiyear ice		
		VV-Pol.;	C- and Ku-X-band	30°, 40°, 70°
		Run #'s:	2419, 2420, 2424, 2435, 2430, 2432	
		Intrepid Inlet, multiyear pressure-ridge		
		VV-Pol.;	5.6, 7.2, 9.6, 13.6 GHz	40°, 70°
		Run #'s:	2438, 2439, 2440, 2441, 2443, 2444	
		Histograms		
		Landing Lake, lake ice		
		VV-Pol.;	5.6, 8.6, 9.6 GHz	40°
		Run #'s:	2447, 2459, 2460	
		Hardinge Bay, shorefast ice		
		VV-Pol.;	C- and Ku-X-band	40°, 70°
		Run #'s:	2470, 2471, 2472, 2473, 2474, 2475, 2478, 2479, 2480, 2481	

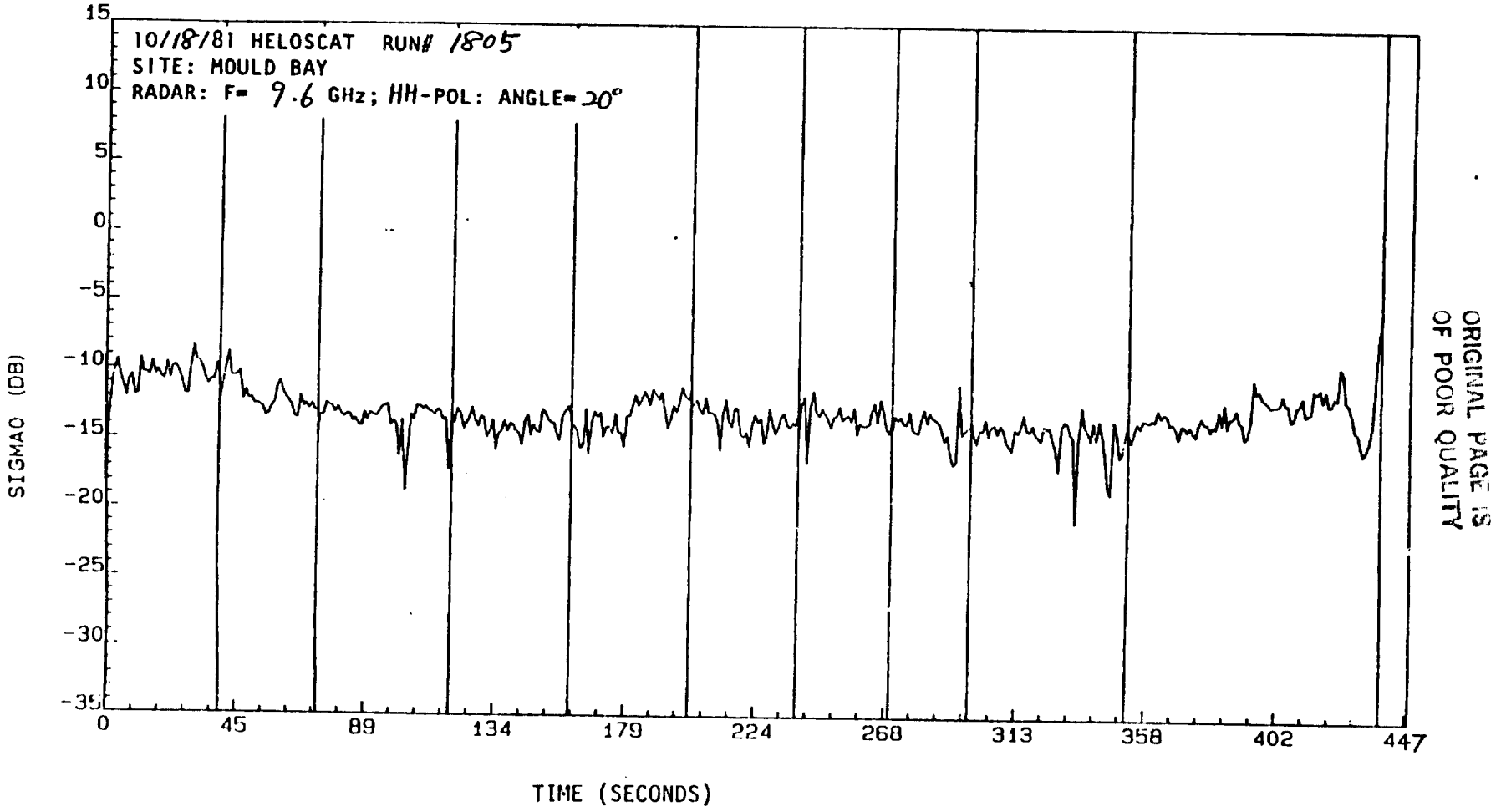

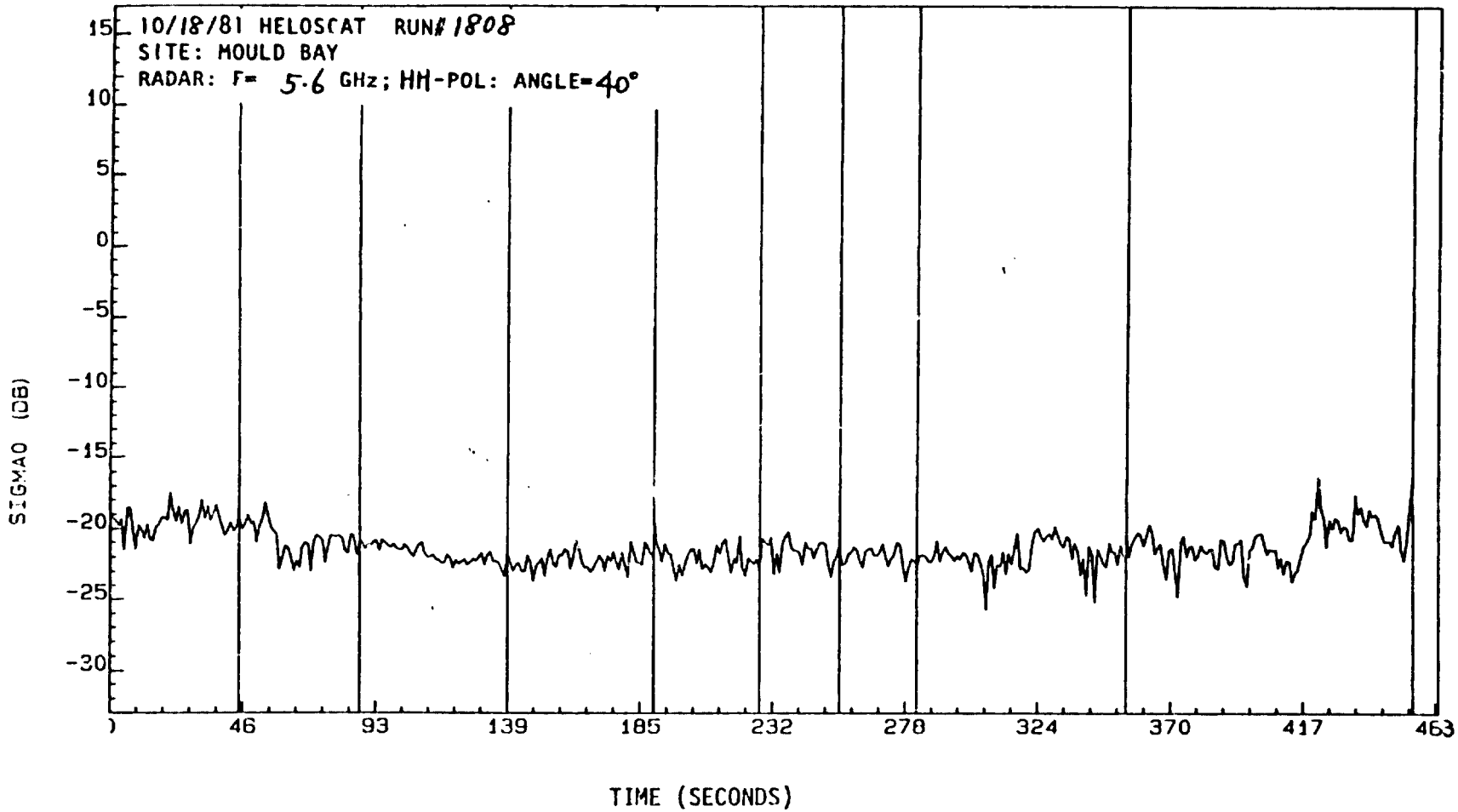

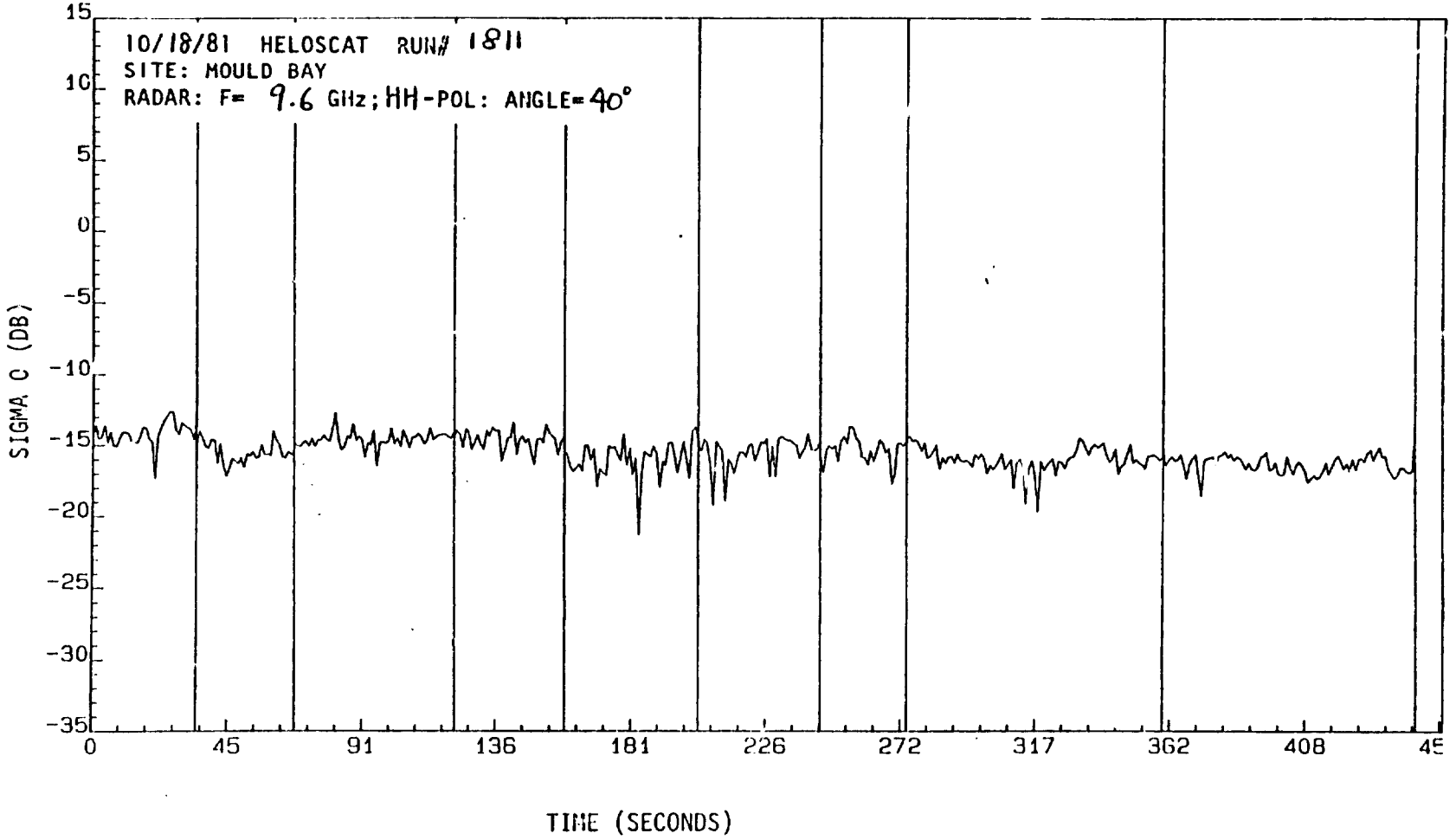

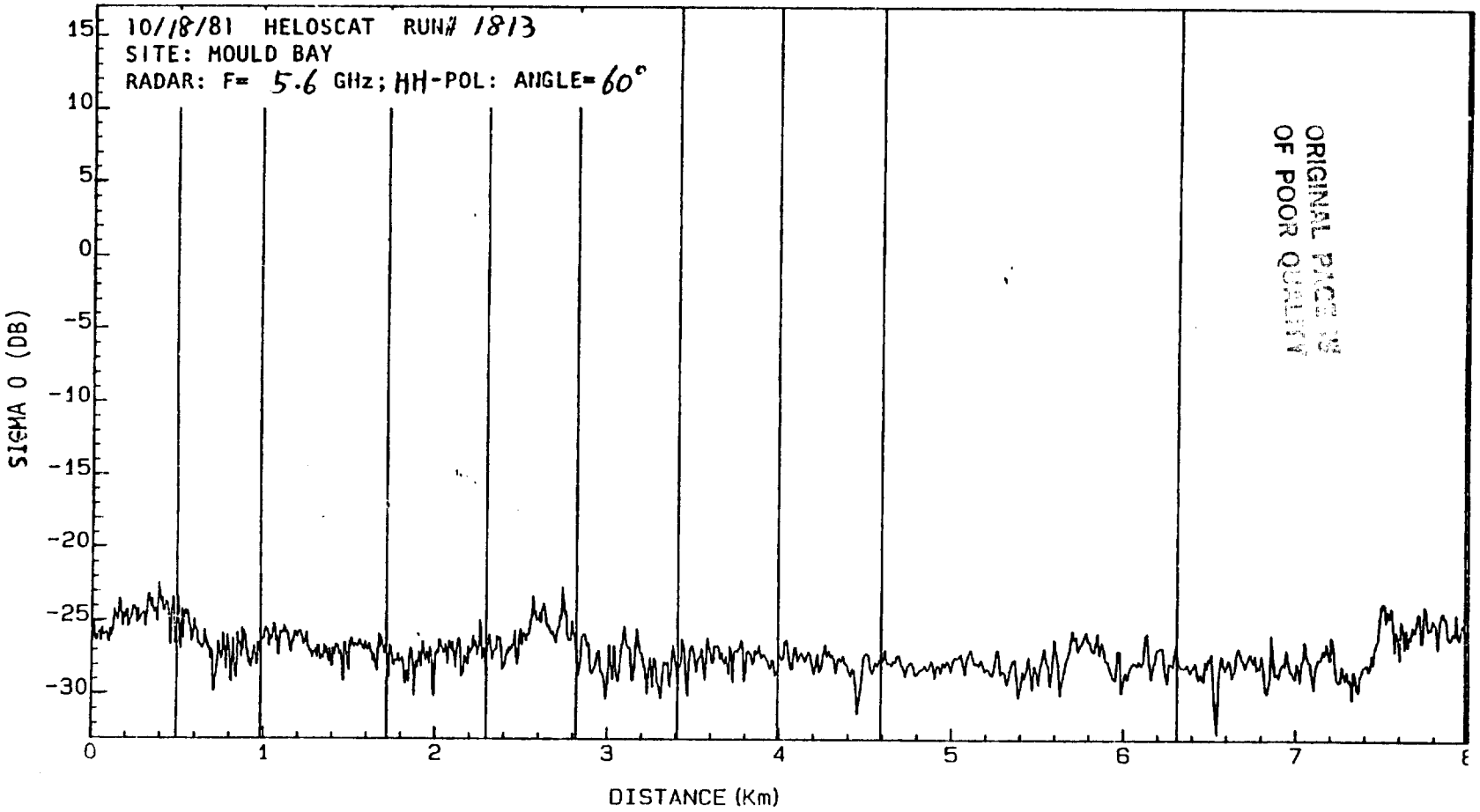

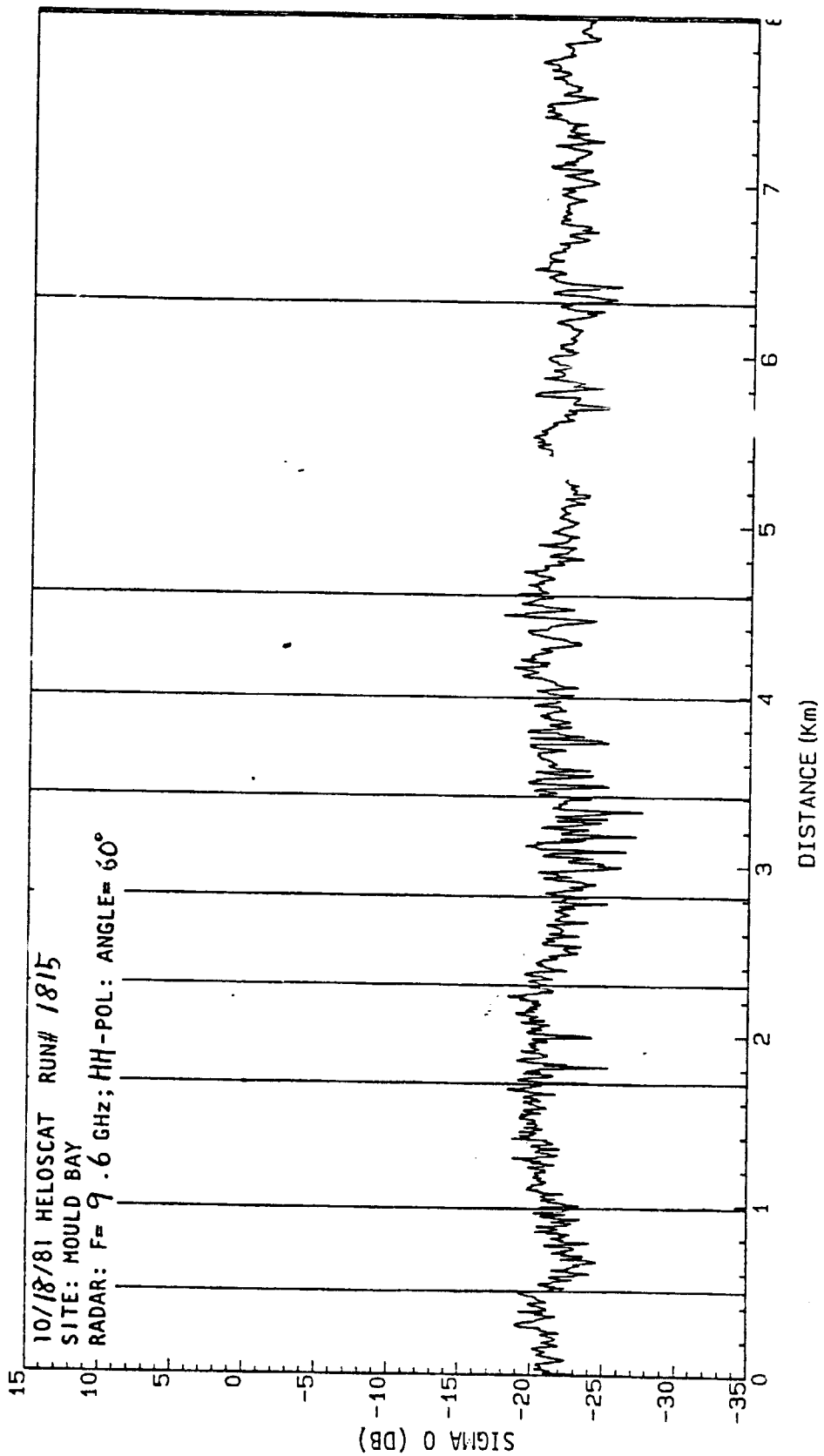

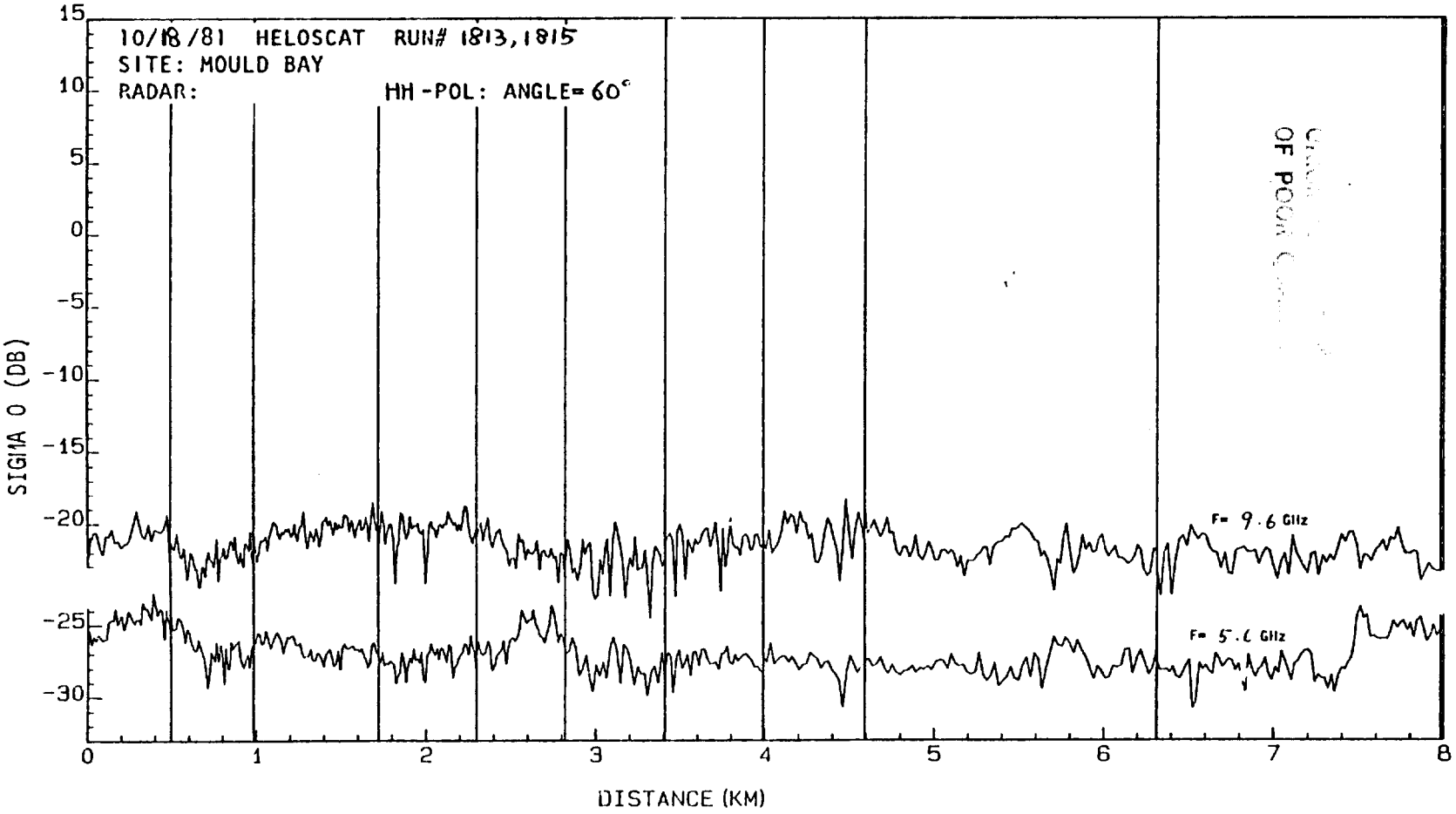
10/18/81 HELOSCAT RUN# 1813,1815
SITE: MOULD BAY
RADAR:
HH-POL: ANGLE= 60°
F= 9.6 GHz
F= 5.6 GHz
SIGMA 0 (DB)
DISTANCE (KM)
15
10
5
0
-5
-10
-15
-20
-25
-30
0
1
2
3
4
5
6
7
8

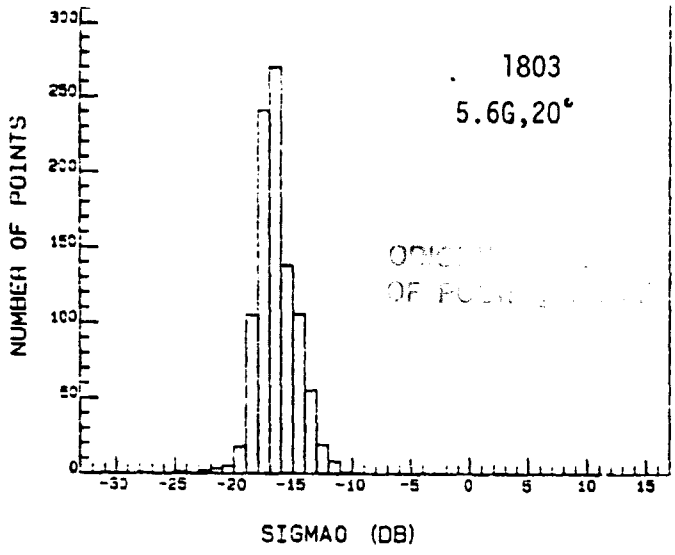
1803
5.6G,20°
NUMBER OF POINTS
SIGMA0 (DB)

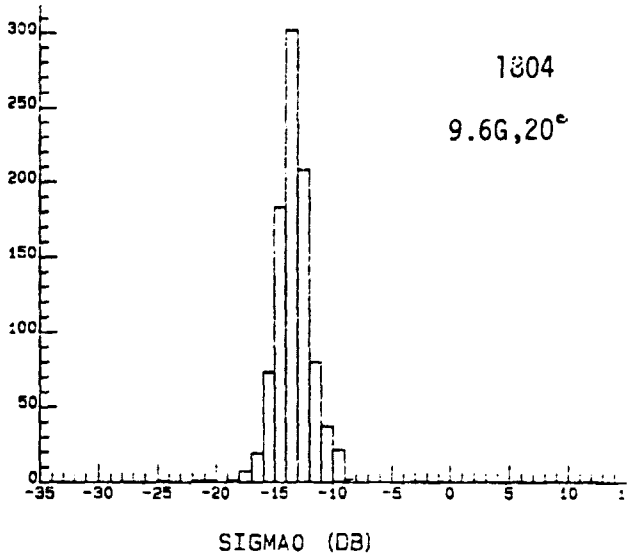
1804
9.6G,20°
SIGMA0 (DB)

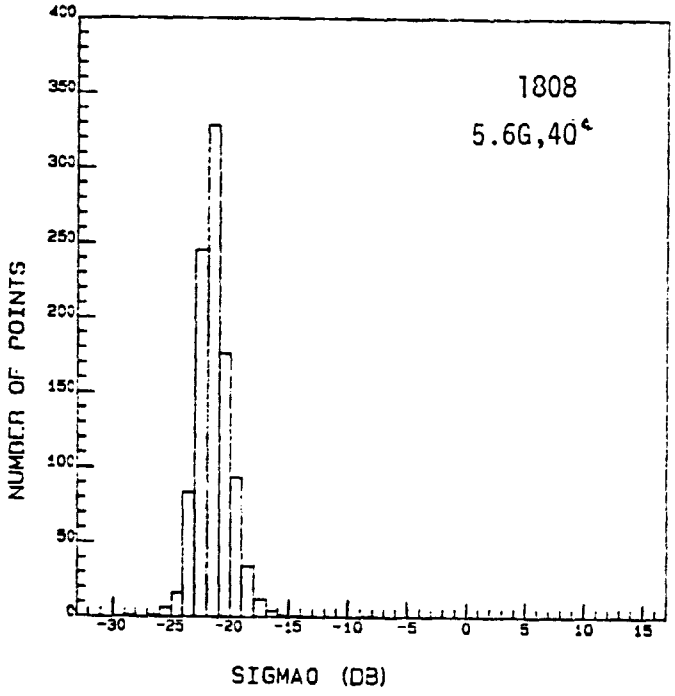
1808
5.6G,40°
NUMBER OF POINTS
SIGMA0 (DB)

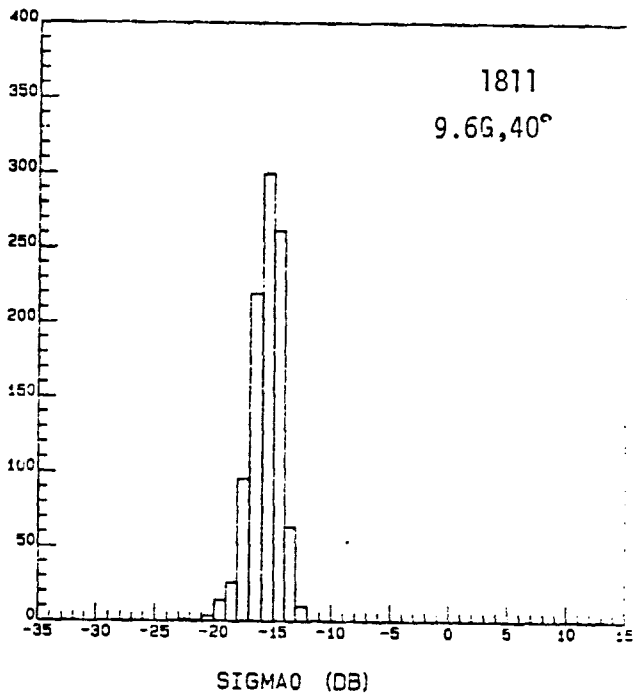
1811
9.6G,40°
SIGMA0 (DB)

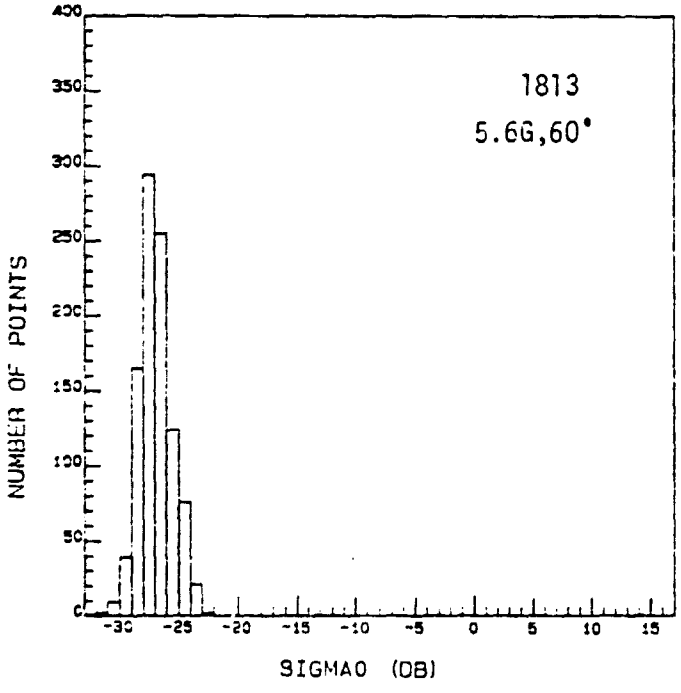
1813
5.6G,60°
NUMBER OF POINTS
SIGMA0 (DB)

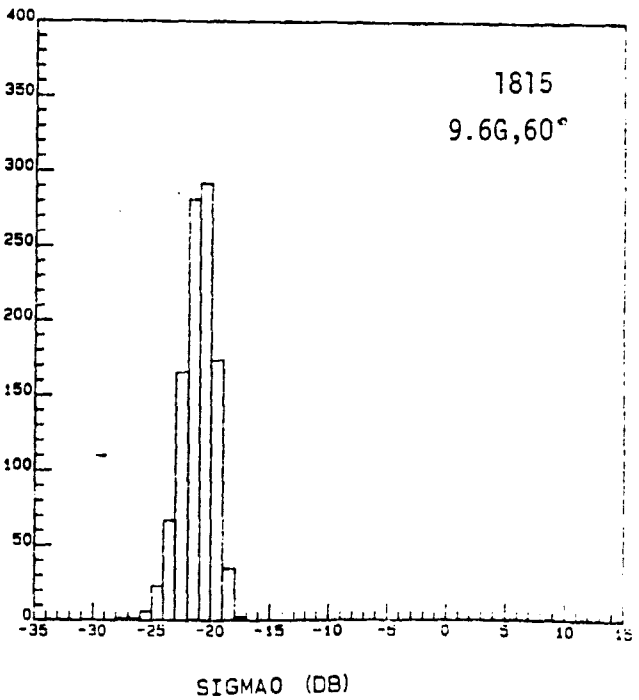
1815
9.6G,60°
SIGMA0 (DB)

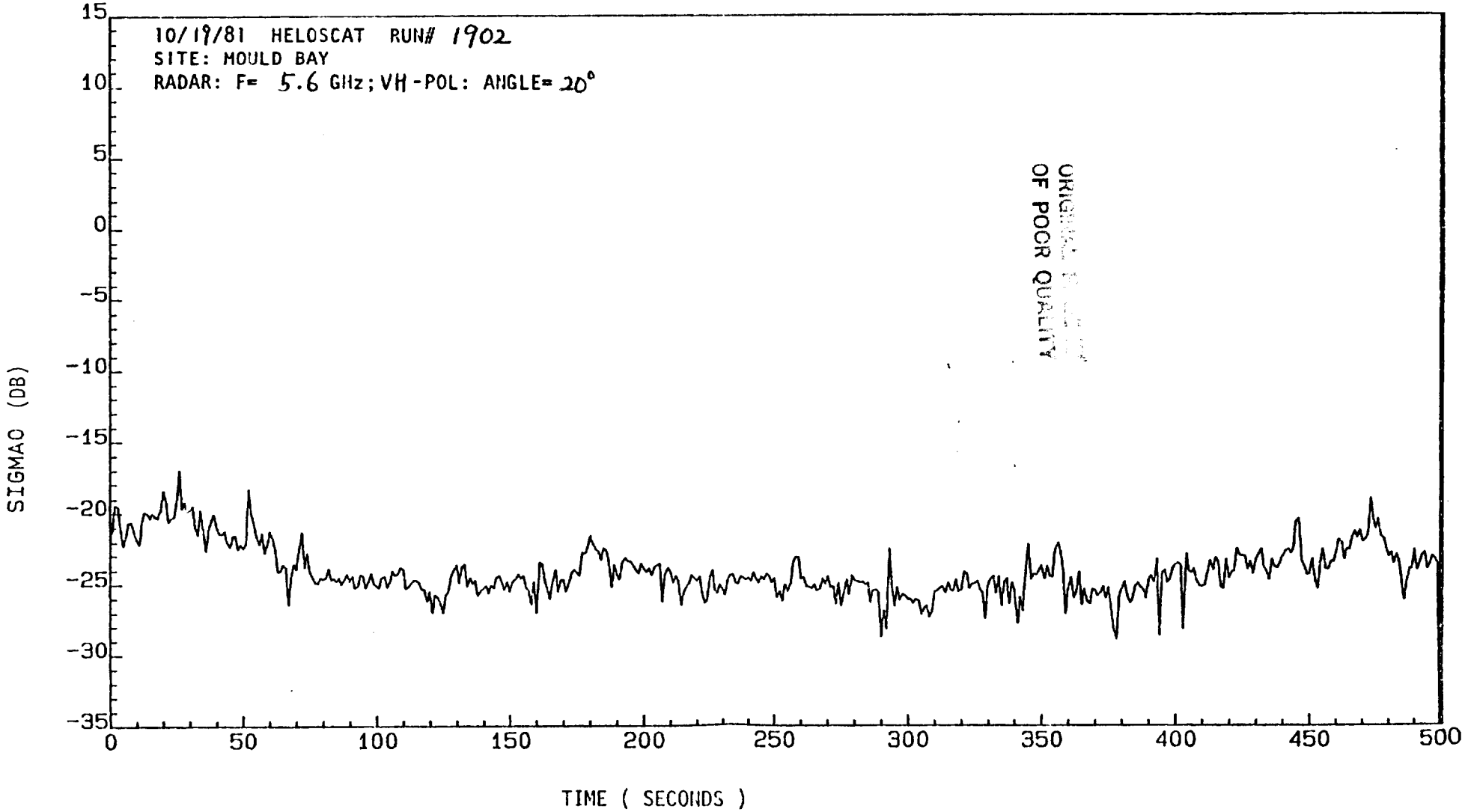

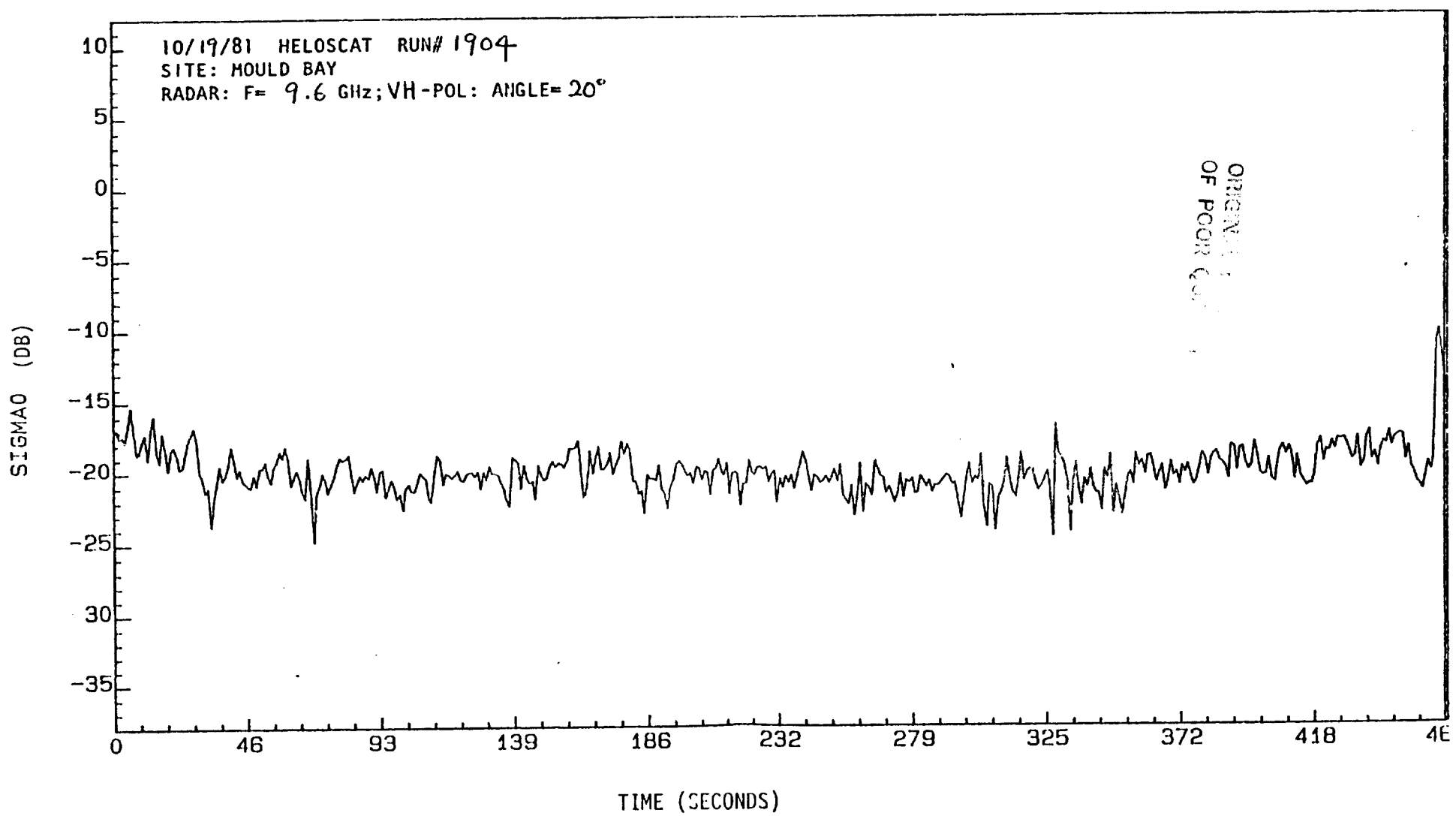
15
10/19/81 HELOSCAT RUN# 1904
SITE: MOULD BAY
RADAR: F= 9.6 GHz; VH-POL: ANGLE= 20°
10
5
0
-5
-10
-15
-20
-25
30
-35
SIGMA0 (DB)
0
46
93
139
186
232
279
325
372
418
TIME (SECONDS)

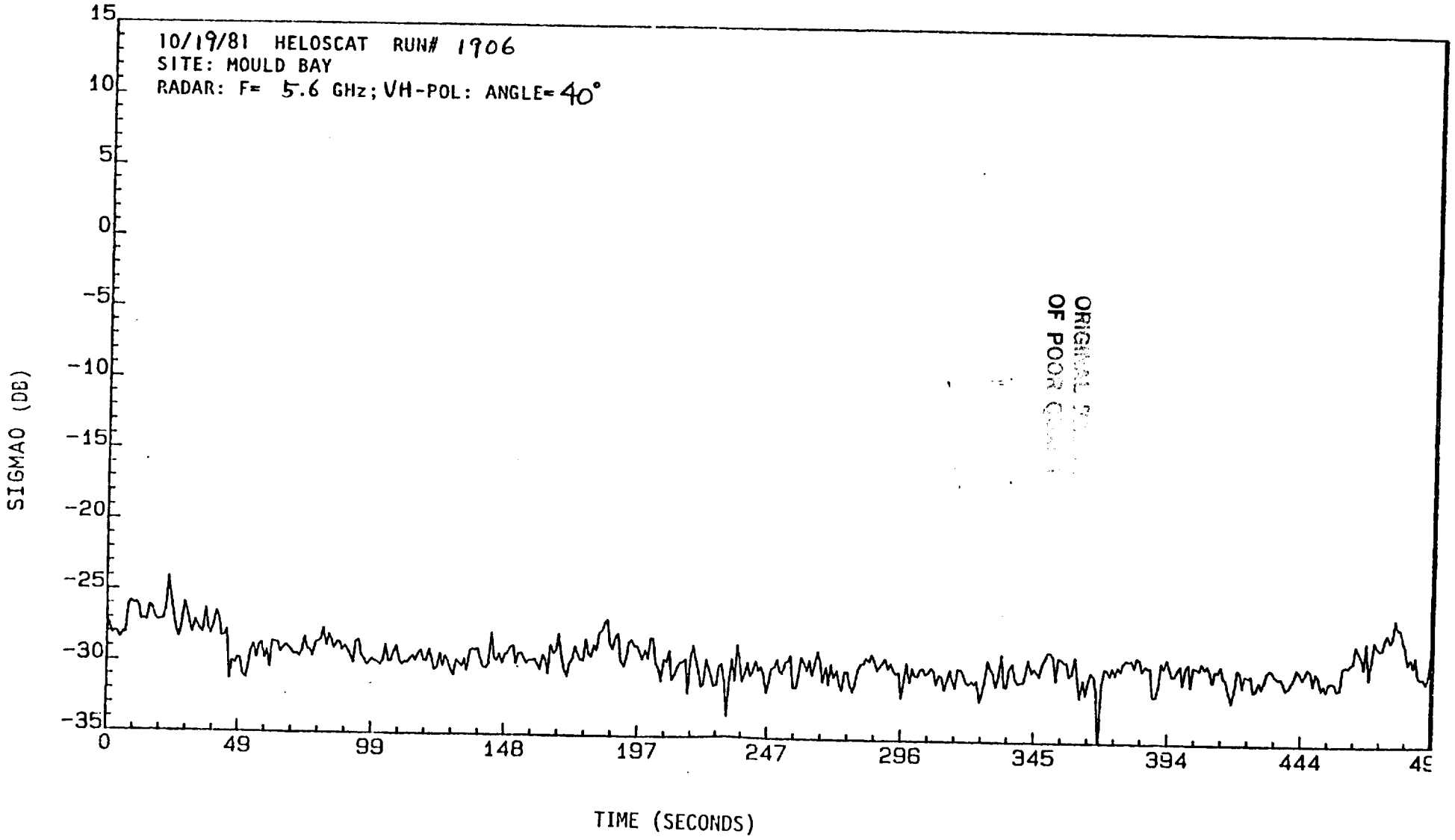

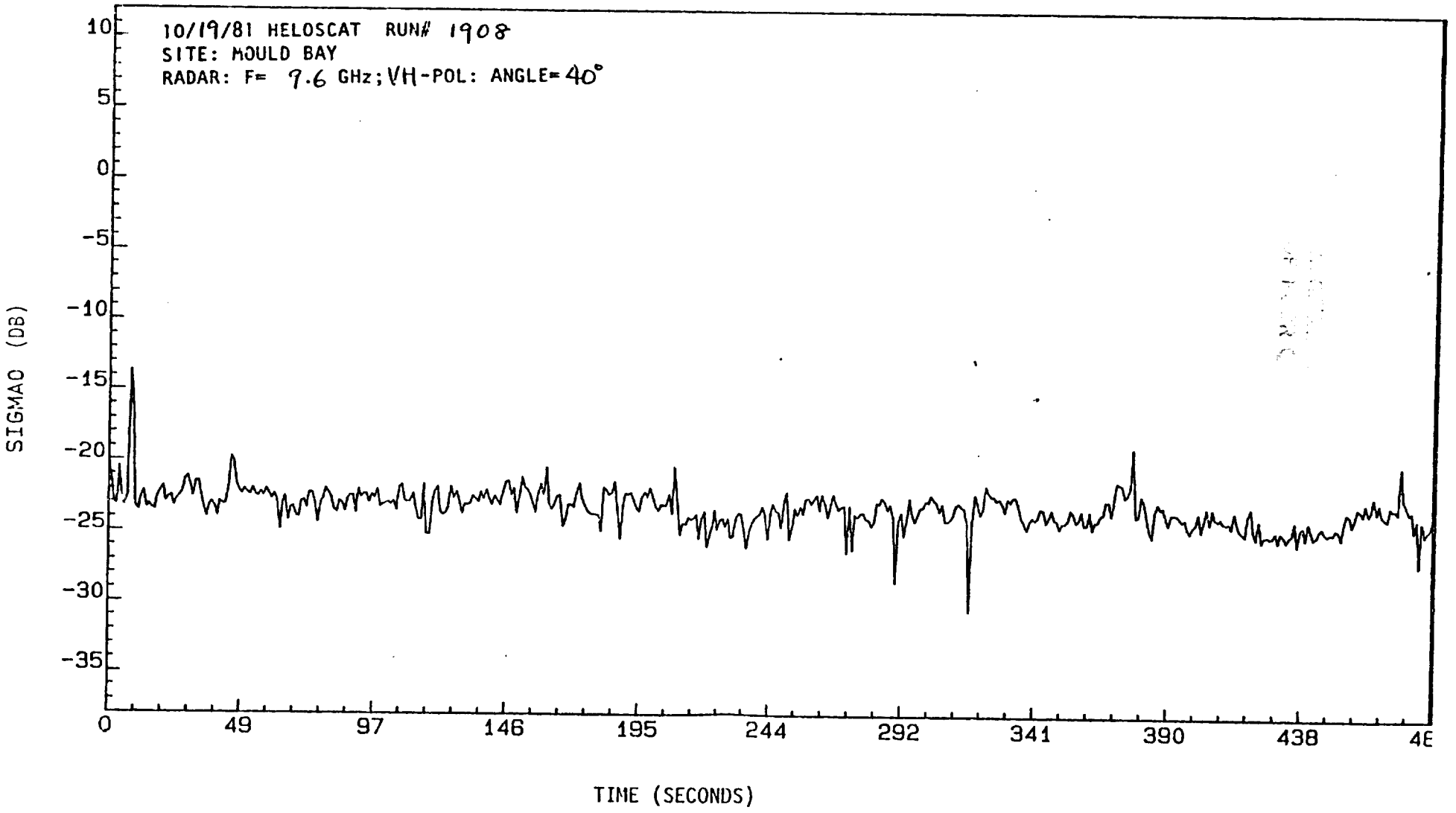
10/19/81 HELOSCAT RUN# 1908
SITE: MOULD BAY
RADAR: F= 9.6 GHz; VH-POL: ANGLE= 40°
10
5
0
-5
-10
-15
-20
-25
-30
-35
SIGMA0 (DB)
0
49
97
146
195
244
292
341
390
438
TIME (SECONDS)

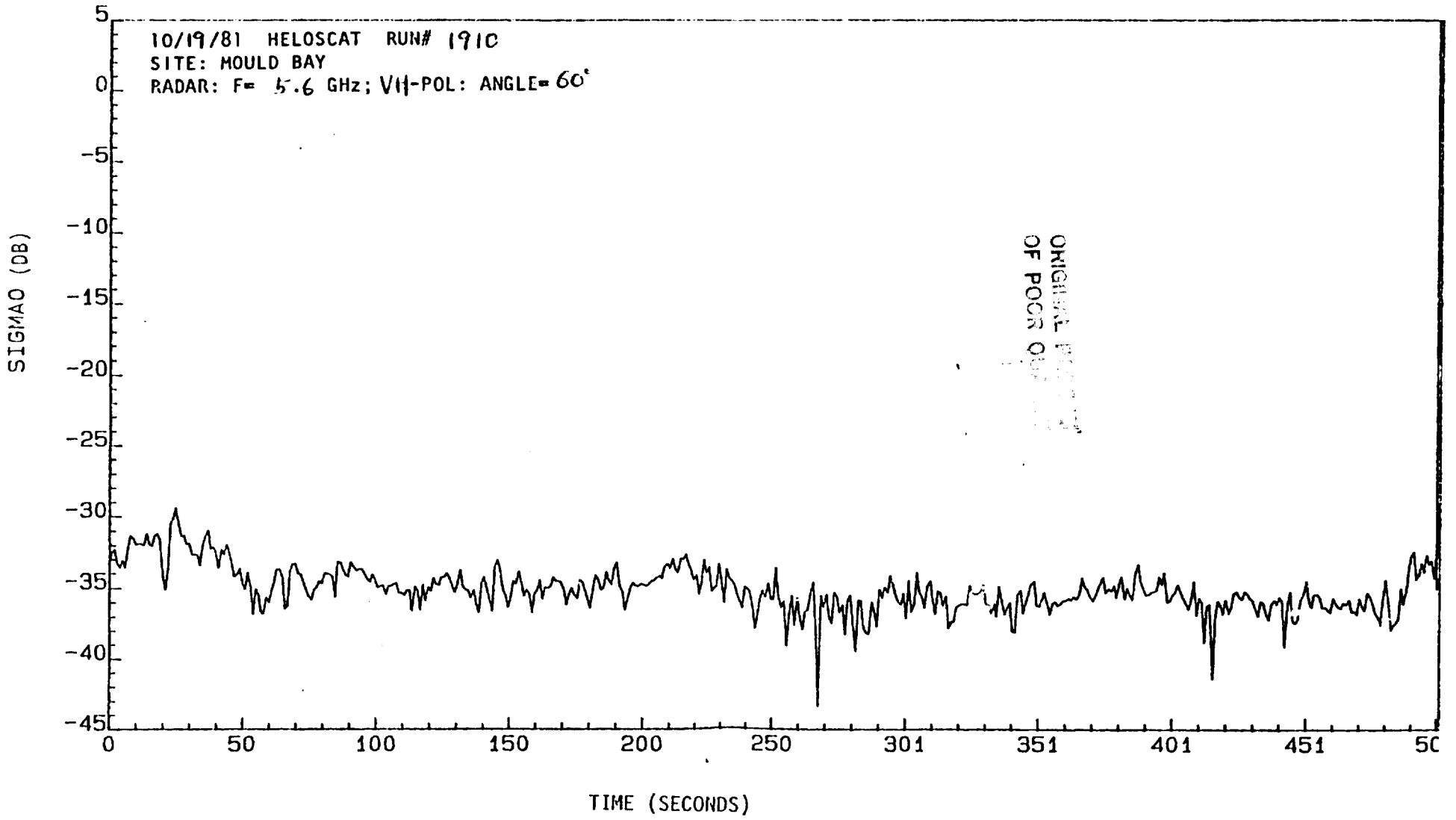
10/19/81 HELOSCAT RUN# 1910
SITE: MOULD BAY
RADAR: F= 5.6 GHz; VH-POL: ANGLE= 60°
SIGMAO (DB)
5
0
-5
-10
-15
-20
-25
-30
-35
-40
-45
0
50
100
150
200
250
301
351
401
451
TIME (SECONDS)

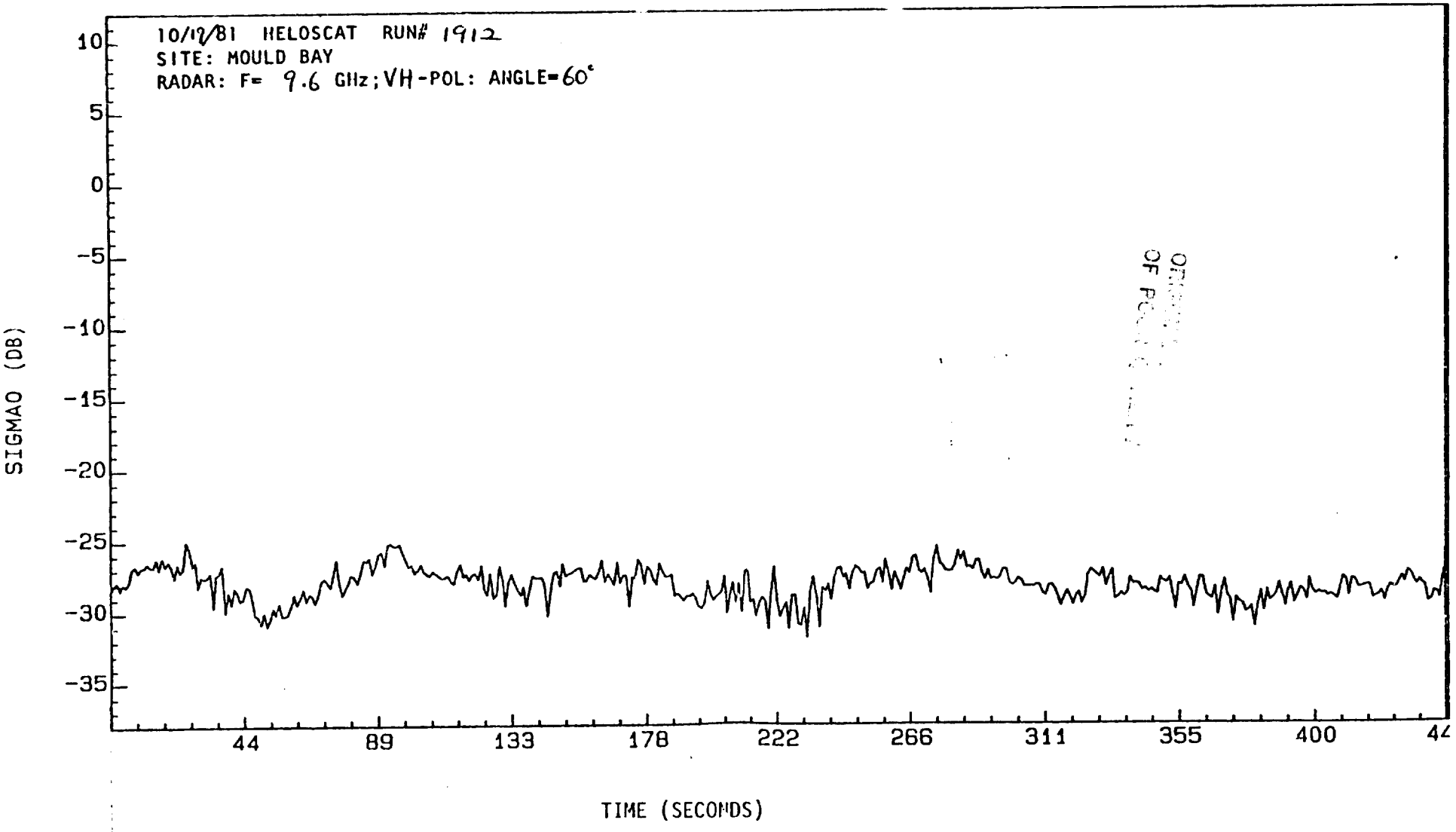
10/19/81 HELOSCAT RUN# 1912
SITE: MOULD BAY
RADAR: F= 9.6 GHz; VH-POL: ANGLE=60°
SIGMAO (DB)
10
5
0
-5
-10
-15
-20
-25
-30
-35
44
89
133
178
222
266
311
355
400
TIME (SECONDS)

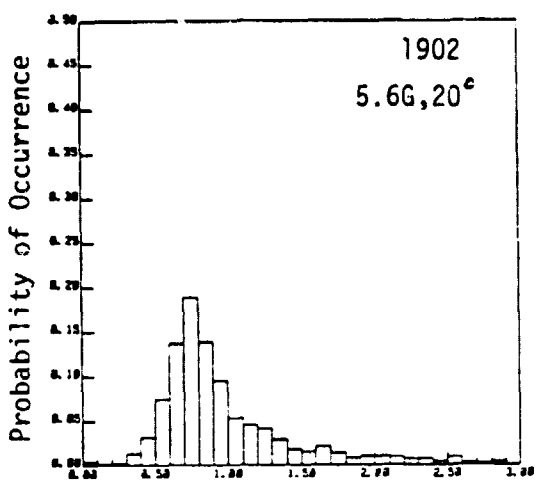
1902
5.6G,20°
Probability of Occurrence
SIGB NORMALIZED TO MEAN

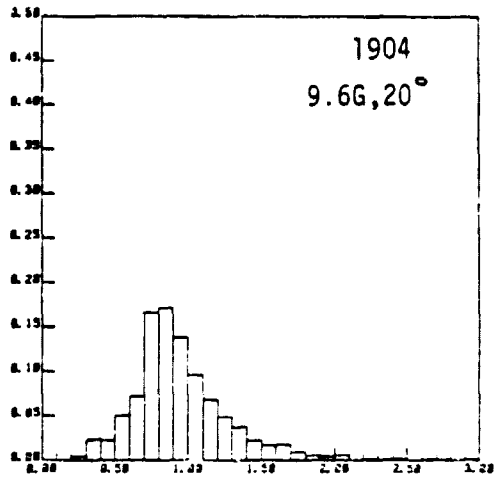
1904
9.6G,20°
SIGB NORMALIZED TO MEAN

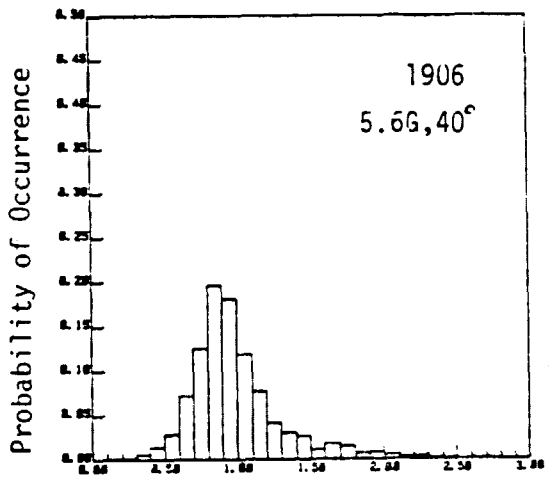
1906
5.6G,40°
Probability of Occurrence
SIGB NORMALIZED TO MEAN

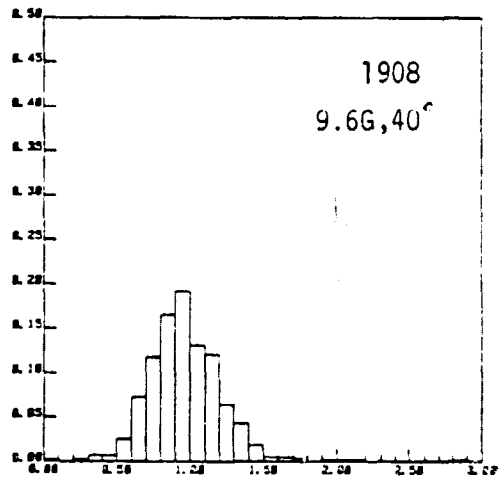
1908
9.6G,40°
SIGB NORMALIZED TO MEAN

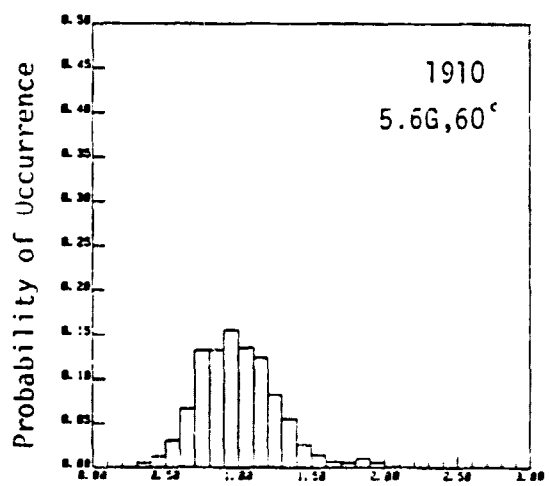
1910
5.6G,60°
Probability of Occurrence
SIGB NORMALIZED TO MEAN

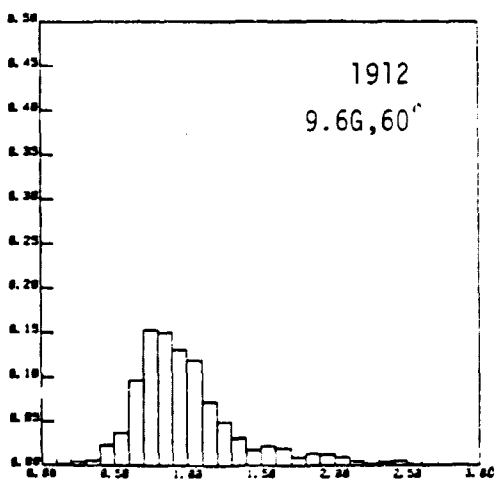
1912
9.6G,60°
SIGB NORMALIZED TO MEAN

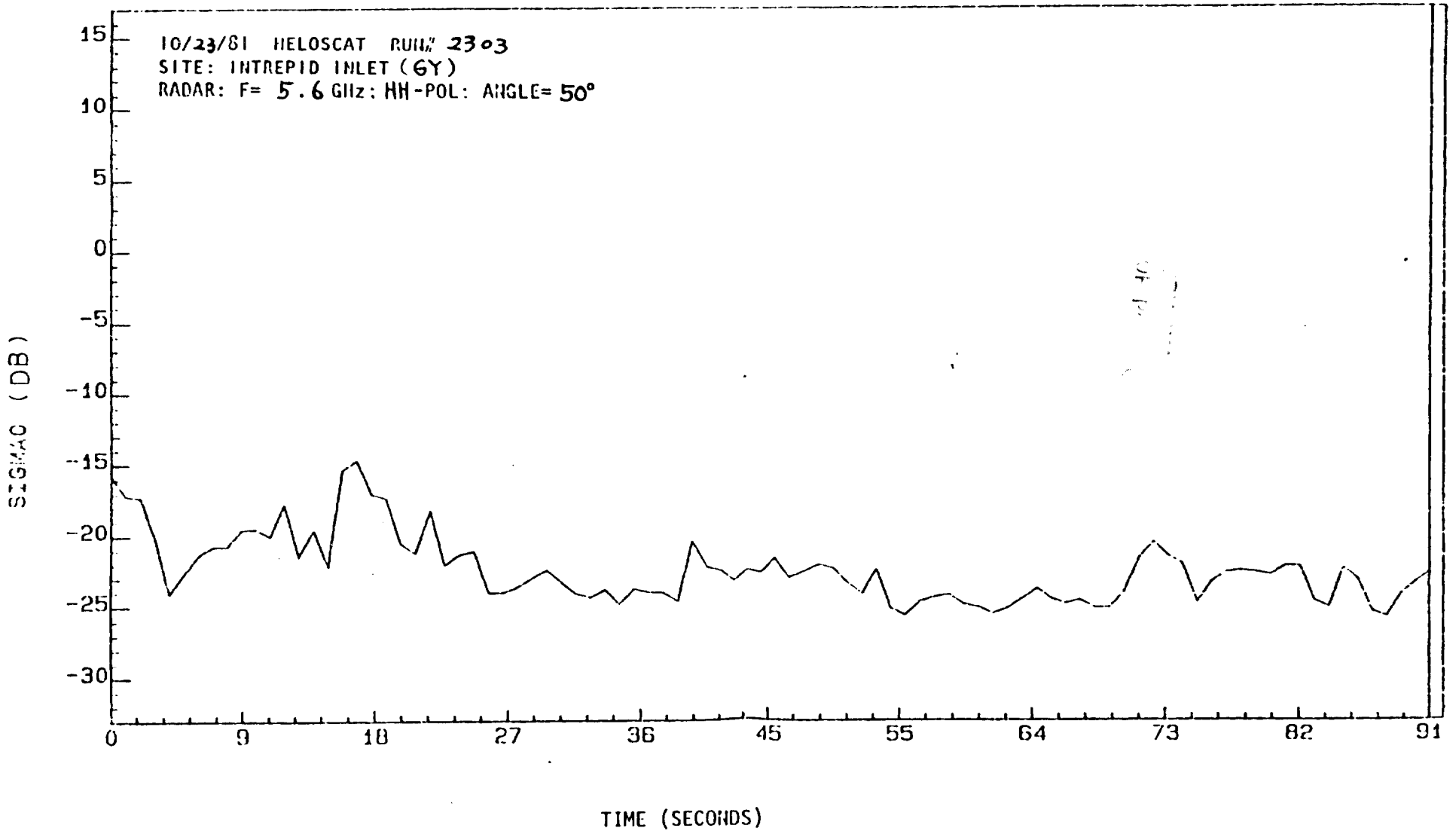
10/23/81 HELOSCAT RUN# 2303
SITE: INTREPID INLET (GY)
RADAR: F= 5.6 GHz: HH-POL: ANGLE= 50°
SIGMA0 (DB)
15
10
5
0
-5
-10
-15
-20
-25
-30
0
9
18
27
36
45
55
64
73
82
91
TIME (SECONDS)

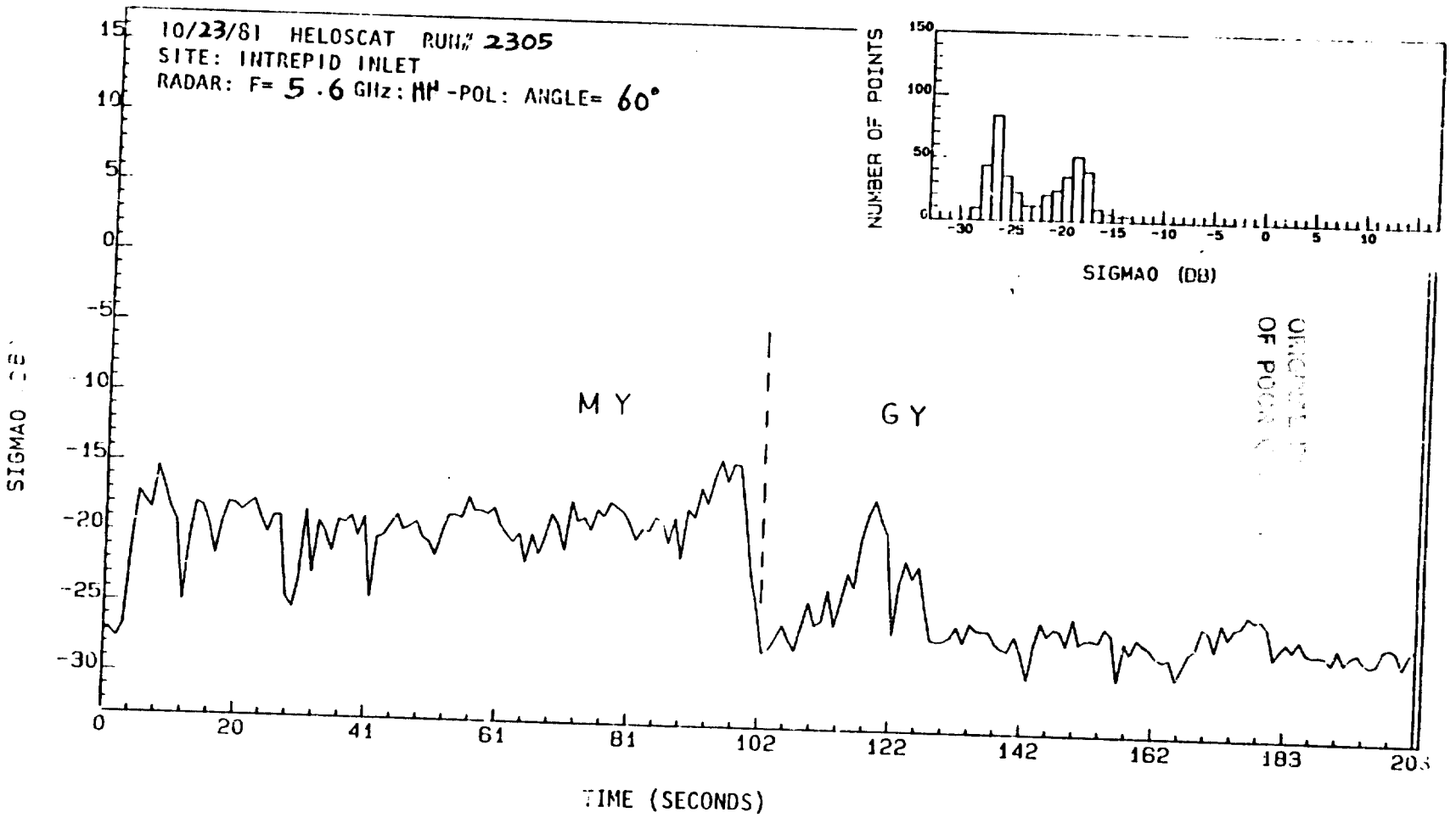
10/23/81 HELOSCAT RUN# 2305
SITE: INTREPID INLET
RADAR: F= 5 .6 GHz: HH -POL: ANGLE= 60°
SIGMAO (DB)
M Y
G Y
TIME (SECONDS)
NUMBER OF POINTS
SIGMAO (DB)

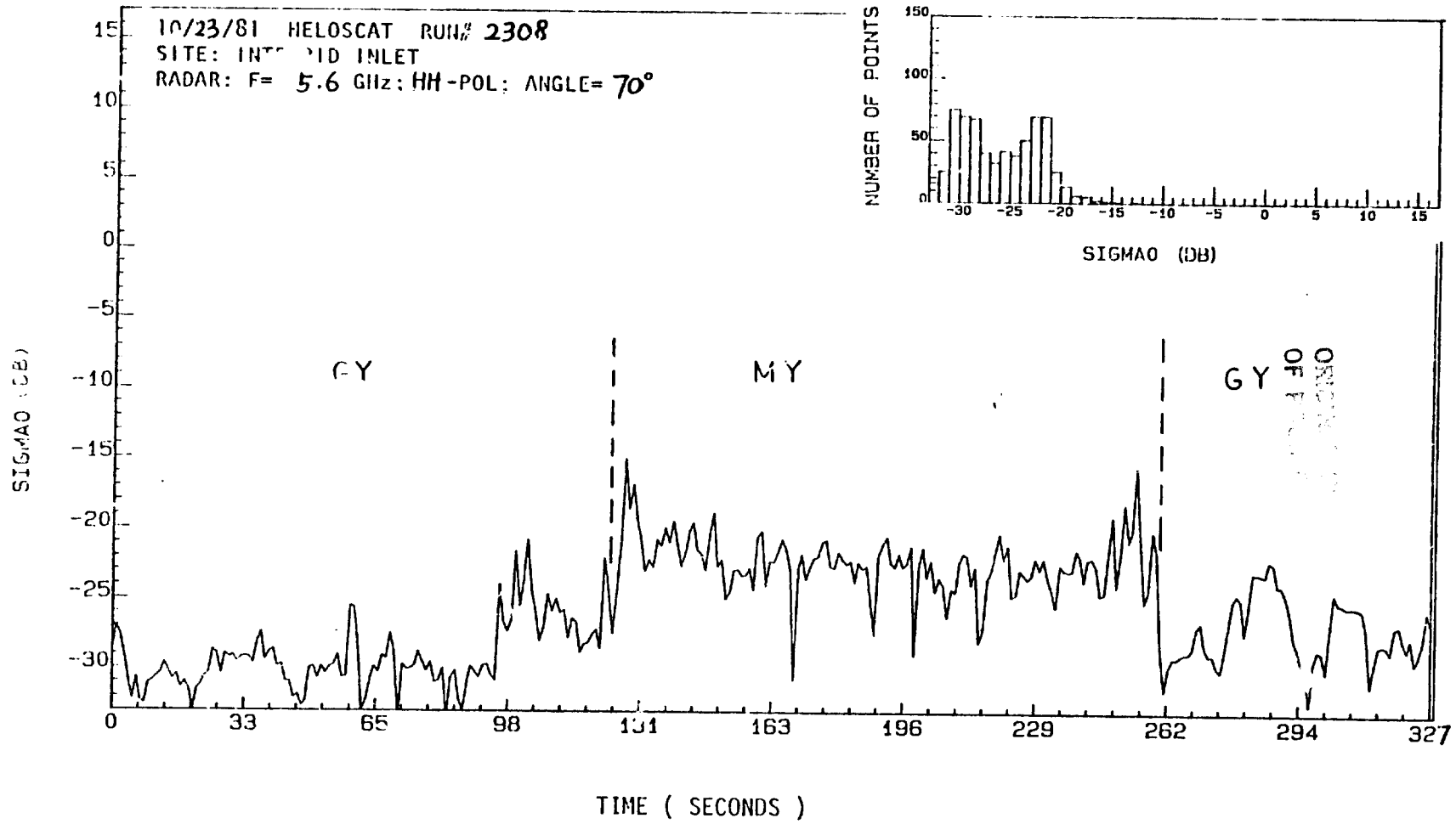
10/23/81 HELOSCAT RUN# 2308
SITE: INT' 'ID INLET
RADAR: F= 5.6 GHz; HH-POL; ANGLE= 70°
NUMBER OF POINTS
SIGMAO (DB)
SIGMAO (DB)
GY
MY
GY
TIME (SECONDS)

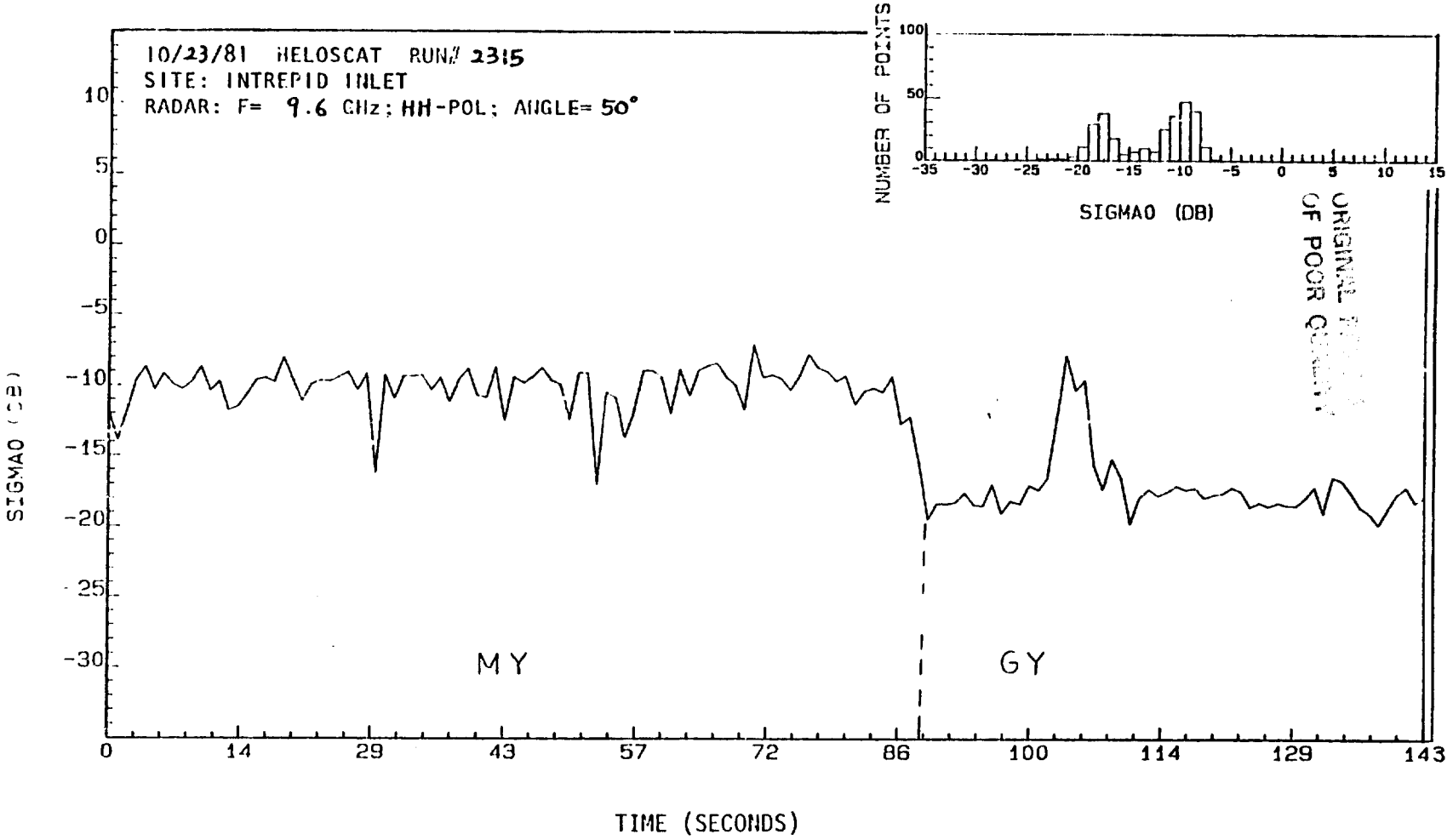
10/23/81 HELOSCAT RUN# 2315
SITE: INTREPID INLET
RADAR: F= 9.6 GHz; HH-POL; ANGLE= 50°
NUMBER OF POINTS
100
50
0
-35 -30 -25 -20 -15 -10 -5 0 5 10 15
SIGMAO (DB)
ORIGINAL PAGE IS
OF POOR QUALITY
SIGMAO (DB)
10
5
0
-5
-10
-15
-20
-25
-30
MY
GY
0 14 29 43 57 72 86 100 114 129 143
TIME (SECONDS)

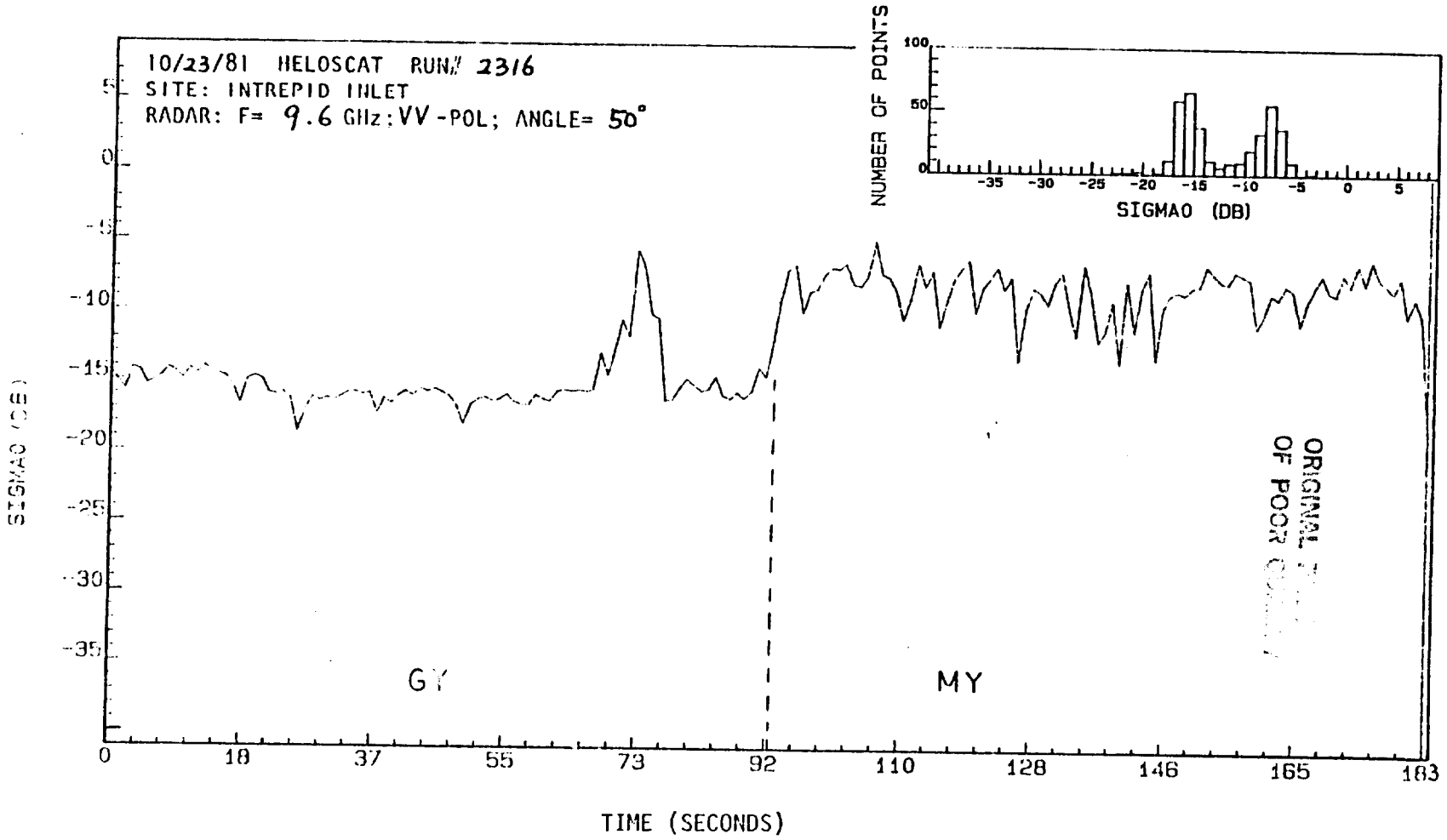
10/23/81 HELOSCAT RUN# 2316
SITE: INTREPID INLET
RADAR: F= 9.6 GHz; VV-POL; ANGLE= 50°
NUMBER OF POINTS
100
50
0
-35 -30 -25 -20 -15 -10 -5 0 5
SIGMAO (DB)
SIGMAO (DB)
5
0
-5
-10
-15
-20
-25
-30
-35
GY
MY
ORIGINAL PAGE IS OF POOR QUALITY
0 18 37 55 73 92 110 128 146 165 183
TIME (SECONDS)

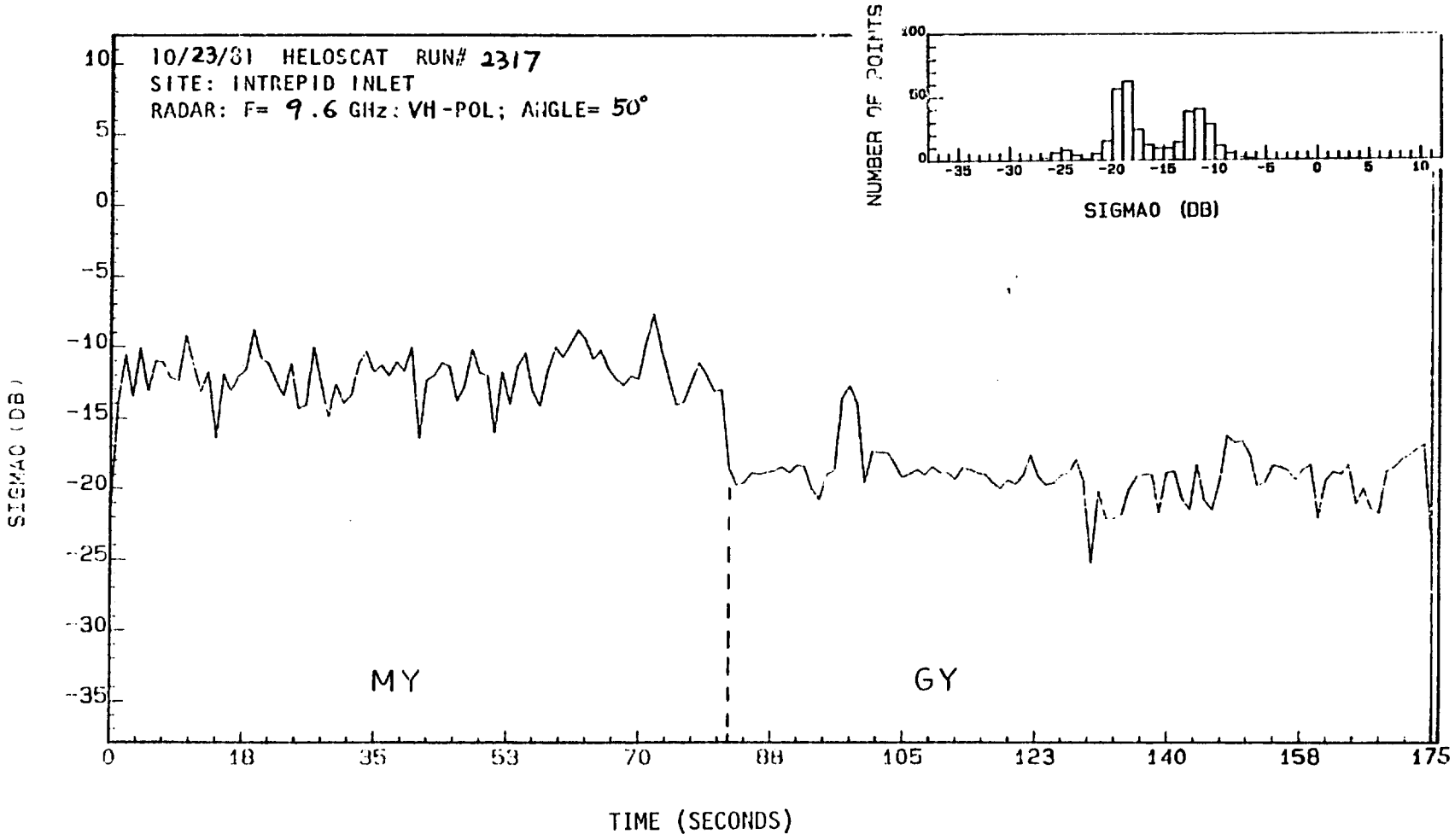

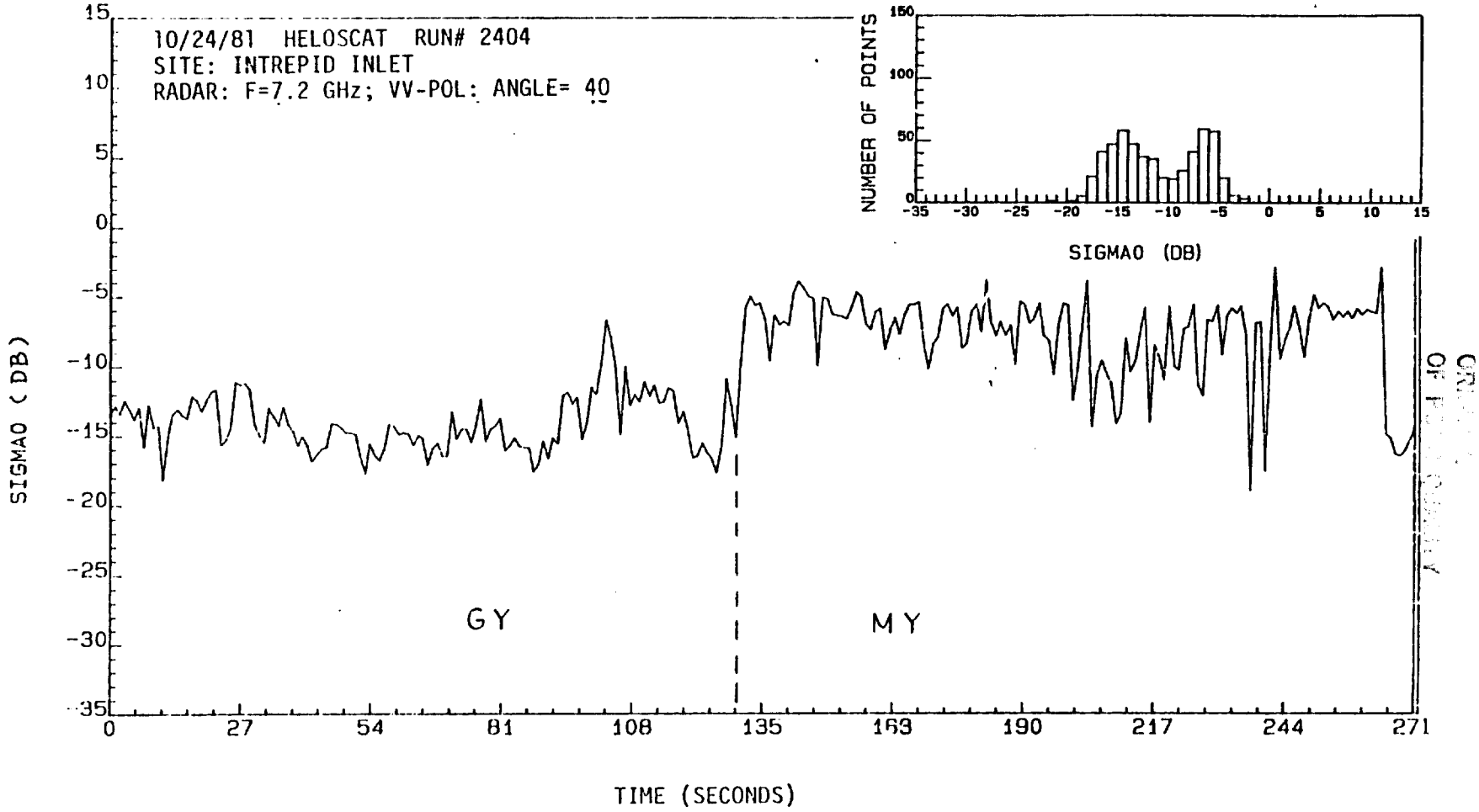
10/24/81 HELOSCAT RUN# 2404
SITE: INTREPID INLET
RADAR: F=7.2 GHz; VV-POL: ANGLE= 40
NUMBER OF POINTS
SIGMAO (DB)
SIGMAO (DB)
GY
MY
TIME (SECONDS)

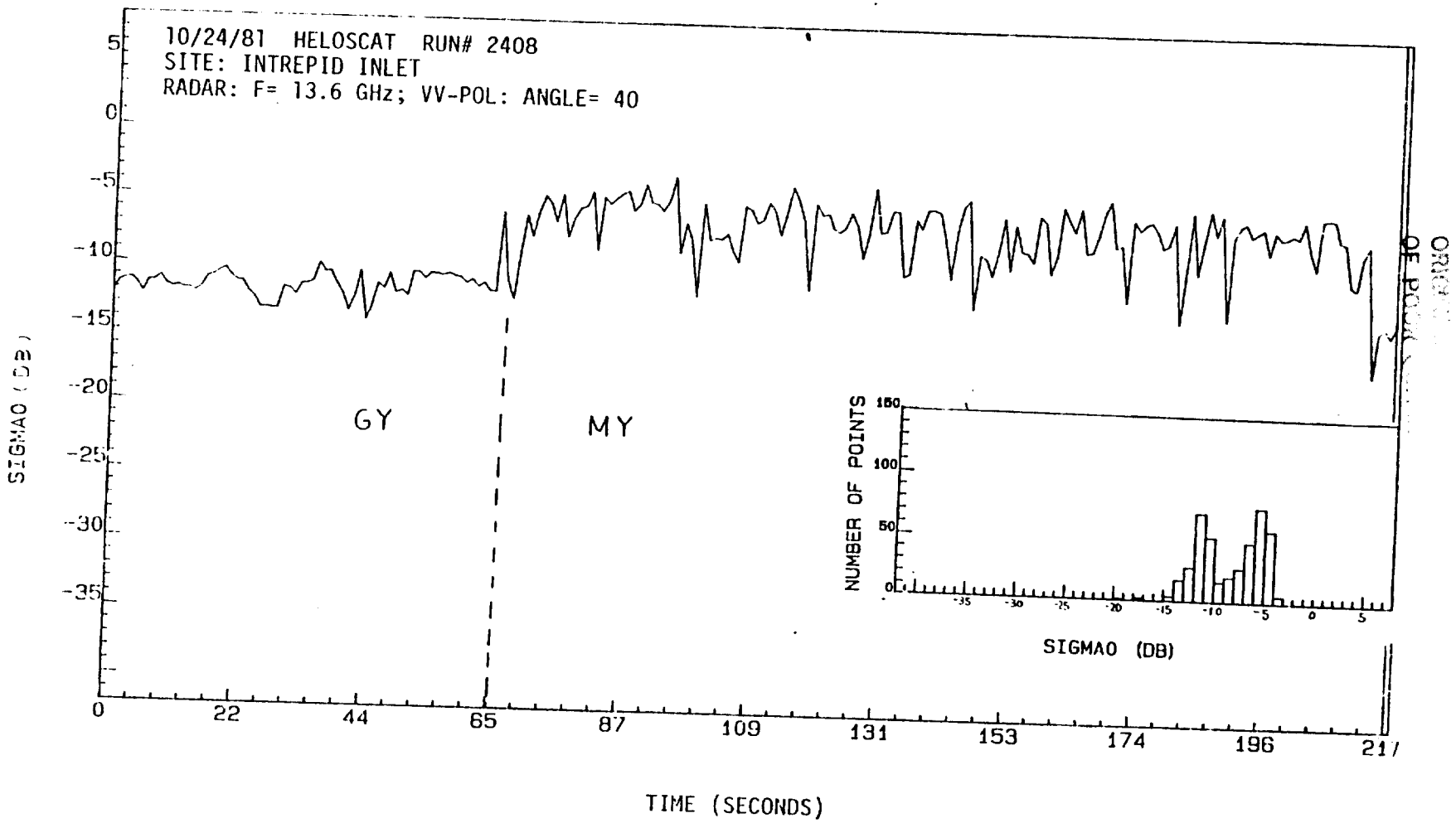
10/24/81 HELOSCAT RUN# 2408
SITE: INTREPID INLET
RADAR: F= 13.6 GHz; VV-POL: ANGLE= 40
SIGMAO (DB)
5
0
-5
-10
-15
-20
-25
-30
-35
GY
MY
0
22
44
65
87
109
131
153
174
196
217
TIME (SECONDS)
NUMBER OF POINTS
150
100
50
0
-35
-30
-25
-20
-15
-10
-5
0
5
SIGMAO (DB)

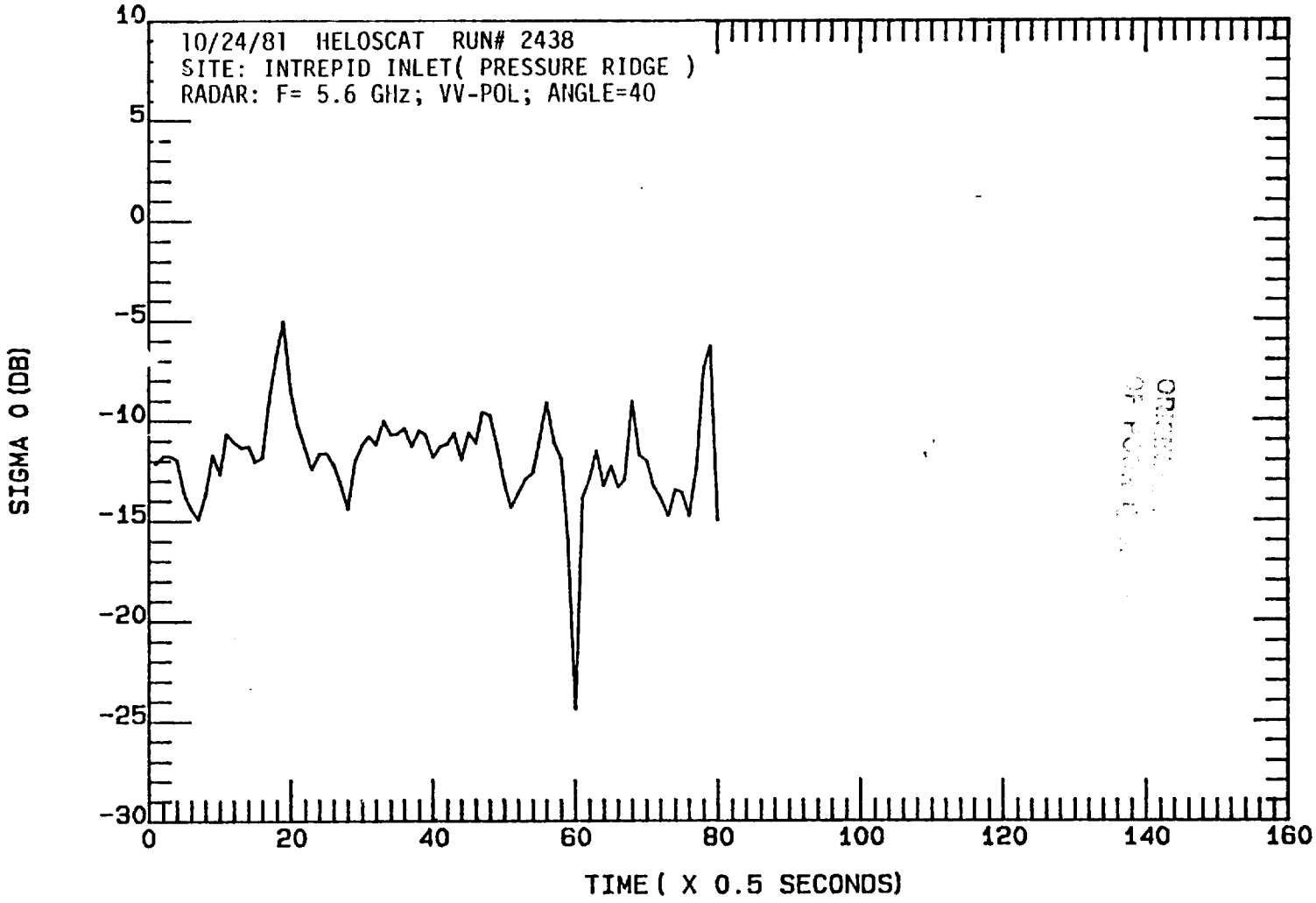
10/24/81 HELOSCAT RUN# 2438
SITE: INTREPID INLET(PRESSURE RIDGE)
RADAR: F= 5.6 GHz; VV-POL; ANGLE=40
SIGMA 0 (DB)
10
5
0
-5
-10
-15
-20
-25
-30
0
20
40
60
80
100
120
140
160
TIME (X 0.5 SECONDS)

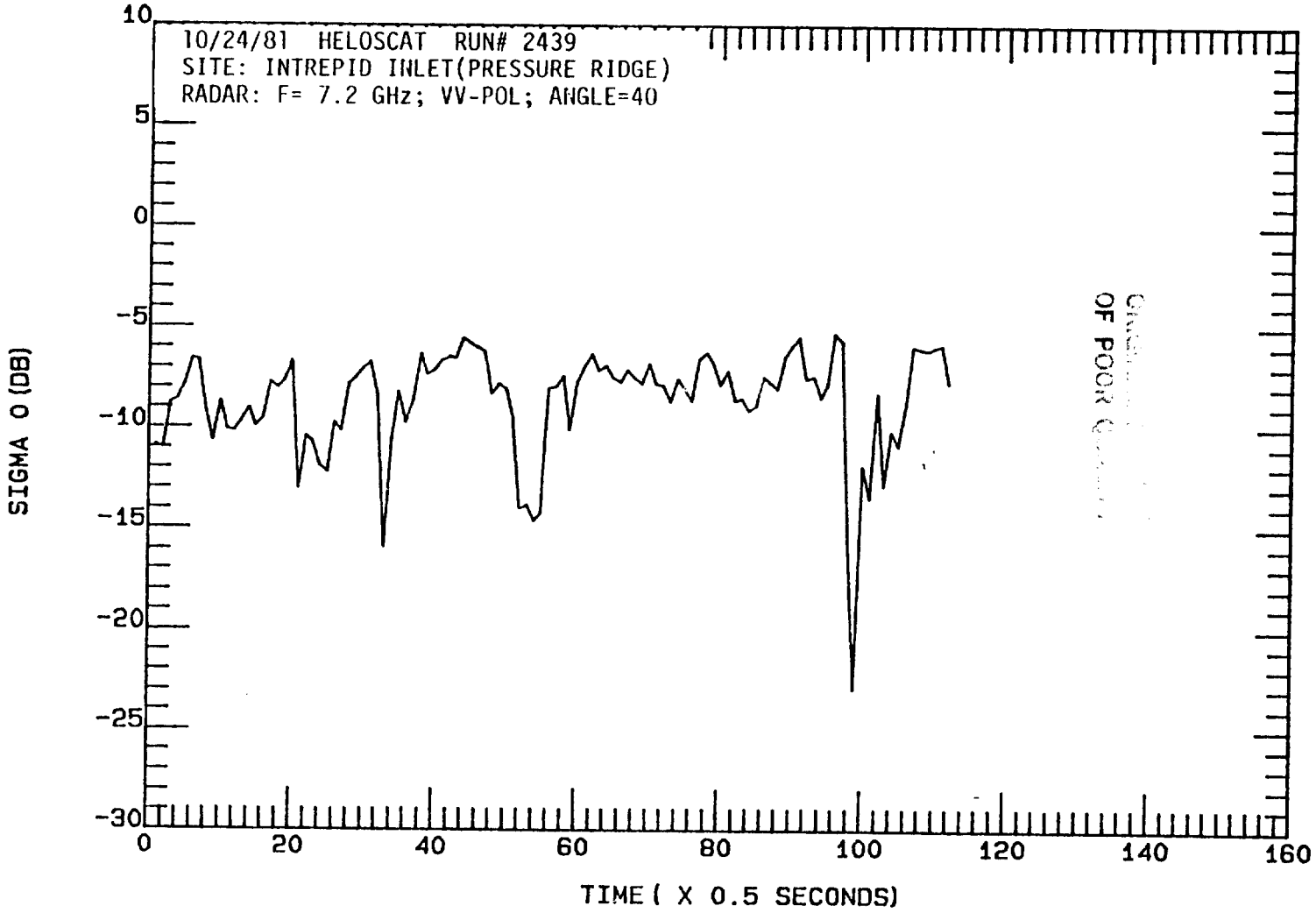
10/24/81 HELOSCAT RUN# 2439
SITE: INTREPID INLET(PRESSURE RIDGE)
RADAR: F= 7.2 GHz; VV-POL; ANGLE=40
SIGMA 0 (DB)
10
5
0
-5
-10
-15
-20
-25
-30
0
20
40
60
80
100
120
140
160
TIME (X 0.5 SECONDS)

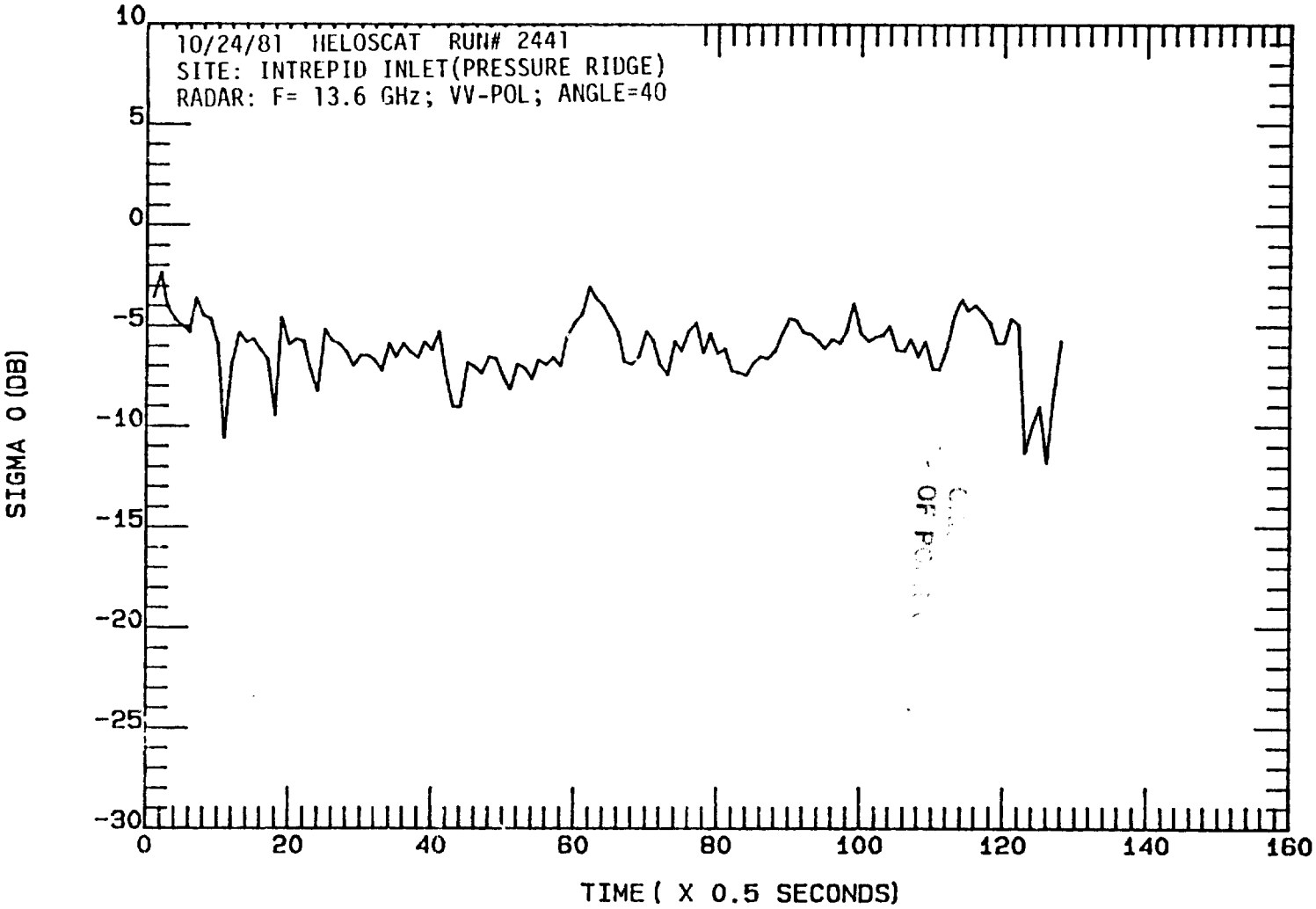
10/24/81 HELOSCAT RUN# 2441
SITE: INTREPID INLET(PRESSURE RIDGE)
RADAR: F= 13.6 GHz; VV-POL; ANGLE=40
SIGMA 0 (DB)
10
5
0
-5
-10
-15
-20
-25
-30
0
20
40
60
80
100
120
140
160
TIME (X 0.5 SECONDS)

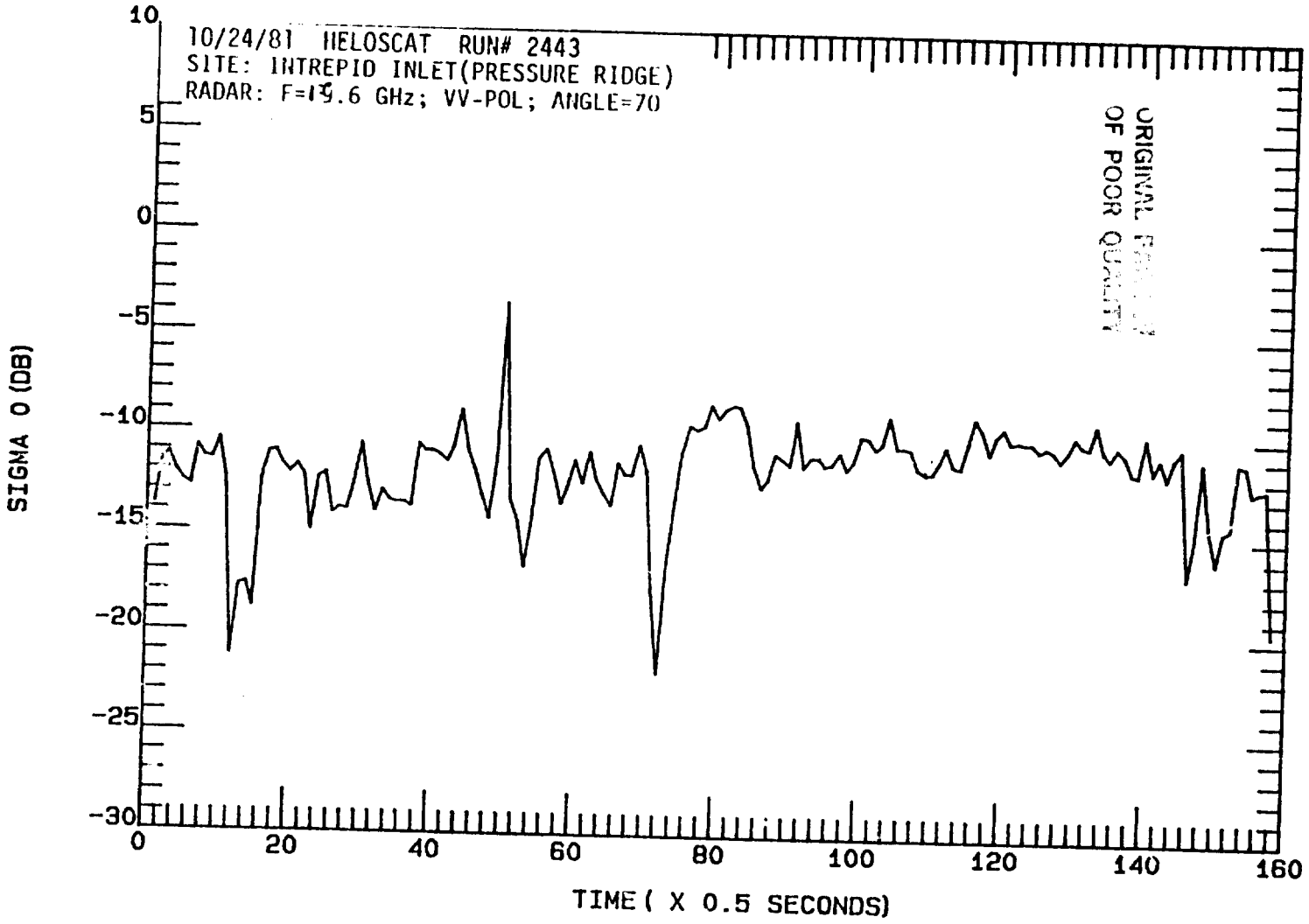

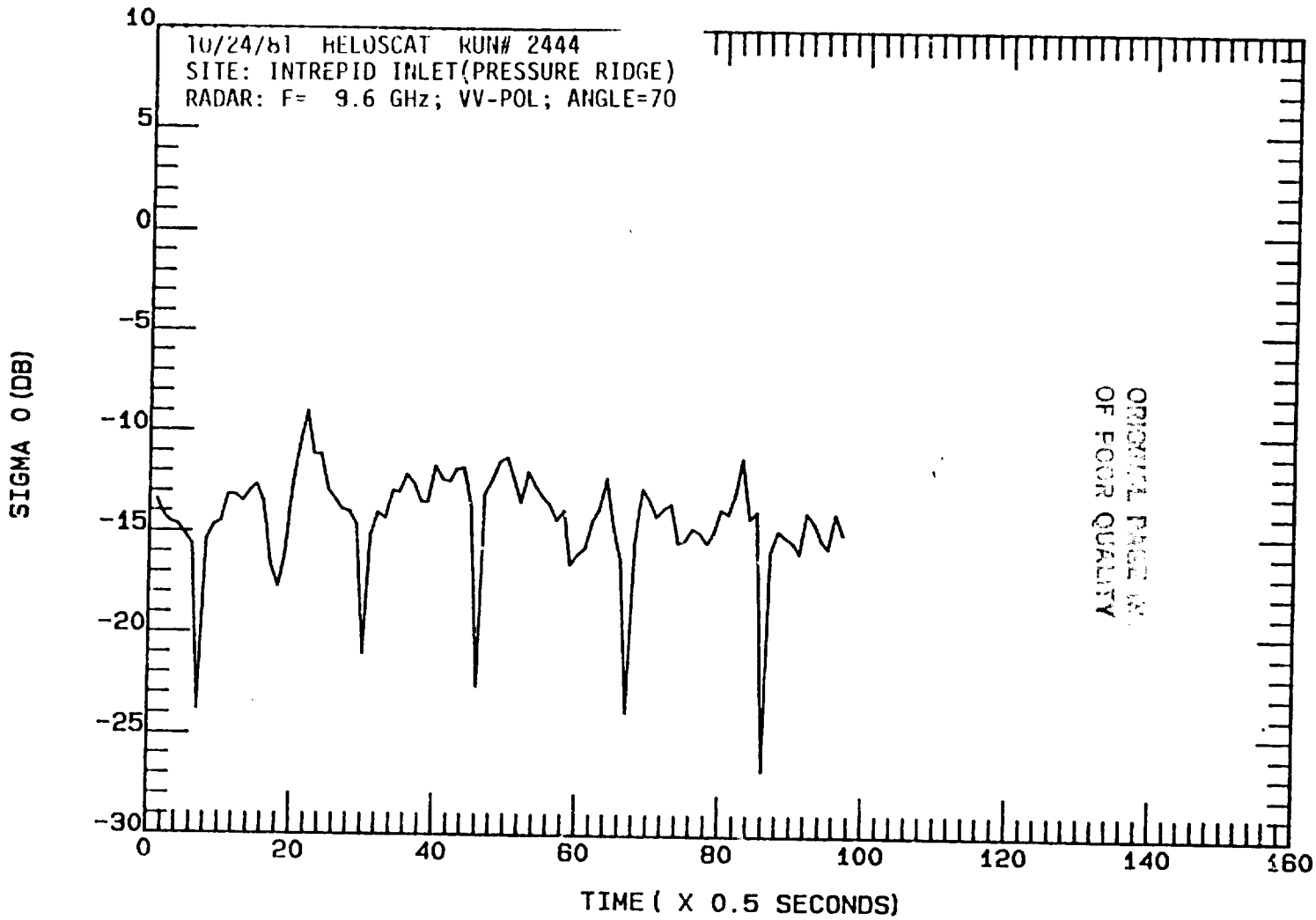

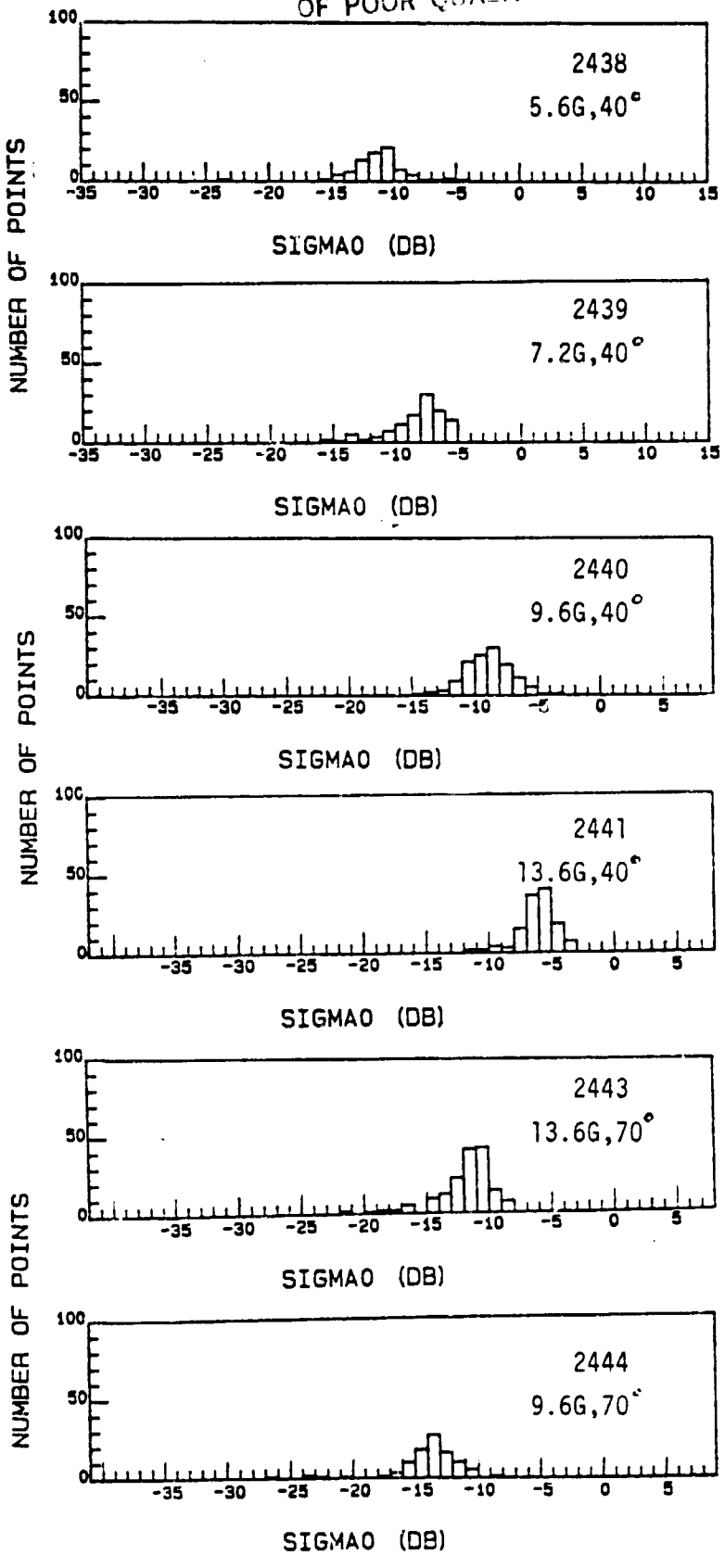

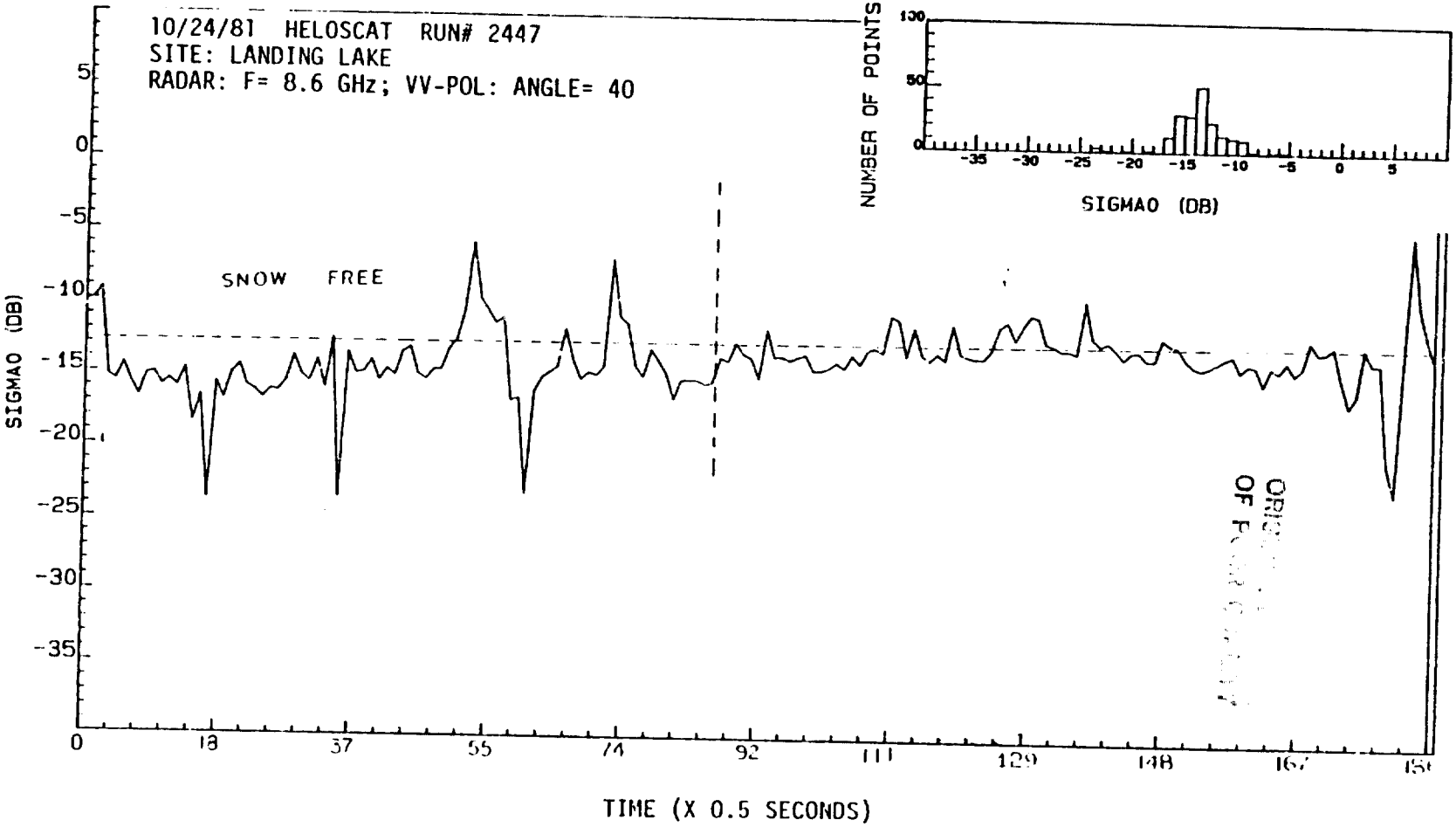
10/24/81 HELOSCAT RUN# 2447
SITE: LANDING LAKE
RADAR: F= 8.6 GHz; VV-POL: ANGLE= 40
SNOW FREE
SIGMAO (DB)
TIME (X 0.5 SECONDS)
NUMBER OF POINTS
SIGMAO (DB)

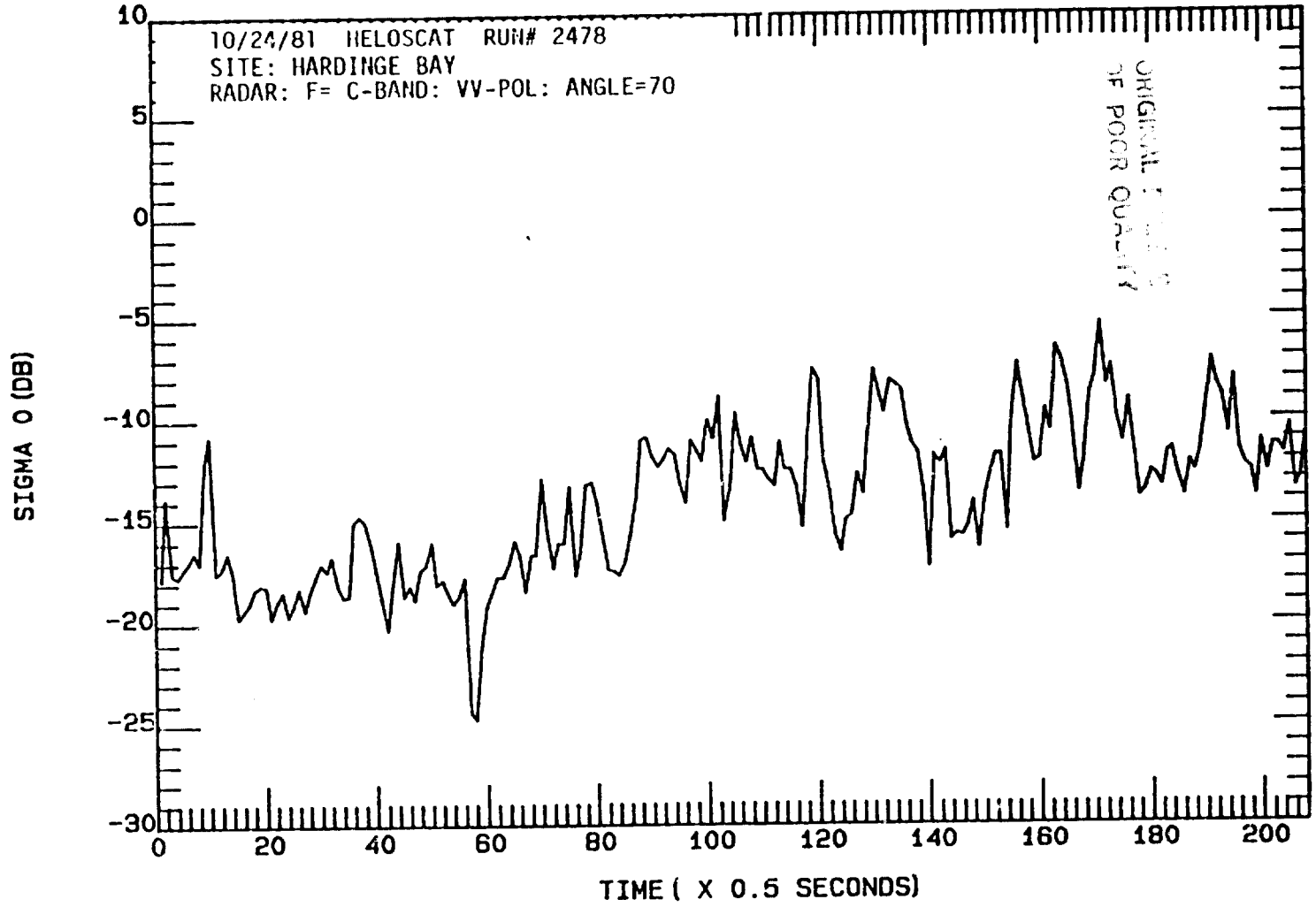
10/24/81 HELOSCAT RUN# 2478
SITE: HARDINGE BAY
RADAR: F= C-BAND: VV-POL: ANGLE=70
SIGMA 0 (DB)
10
5
0
-5
-10
-15
-20
-25
-30
0
20
40
60
80
100
120
140
160
180
200
TIME (X 0.5 SECONDS)

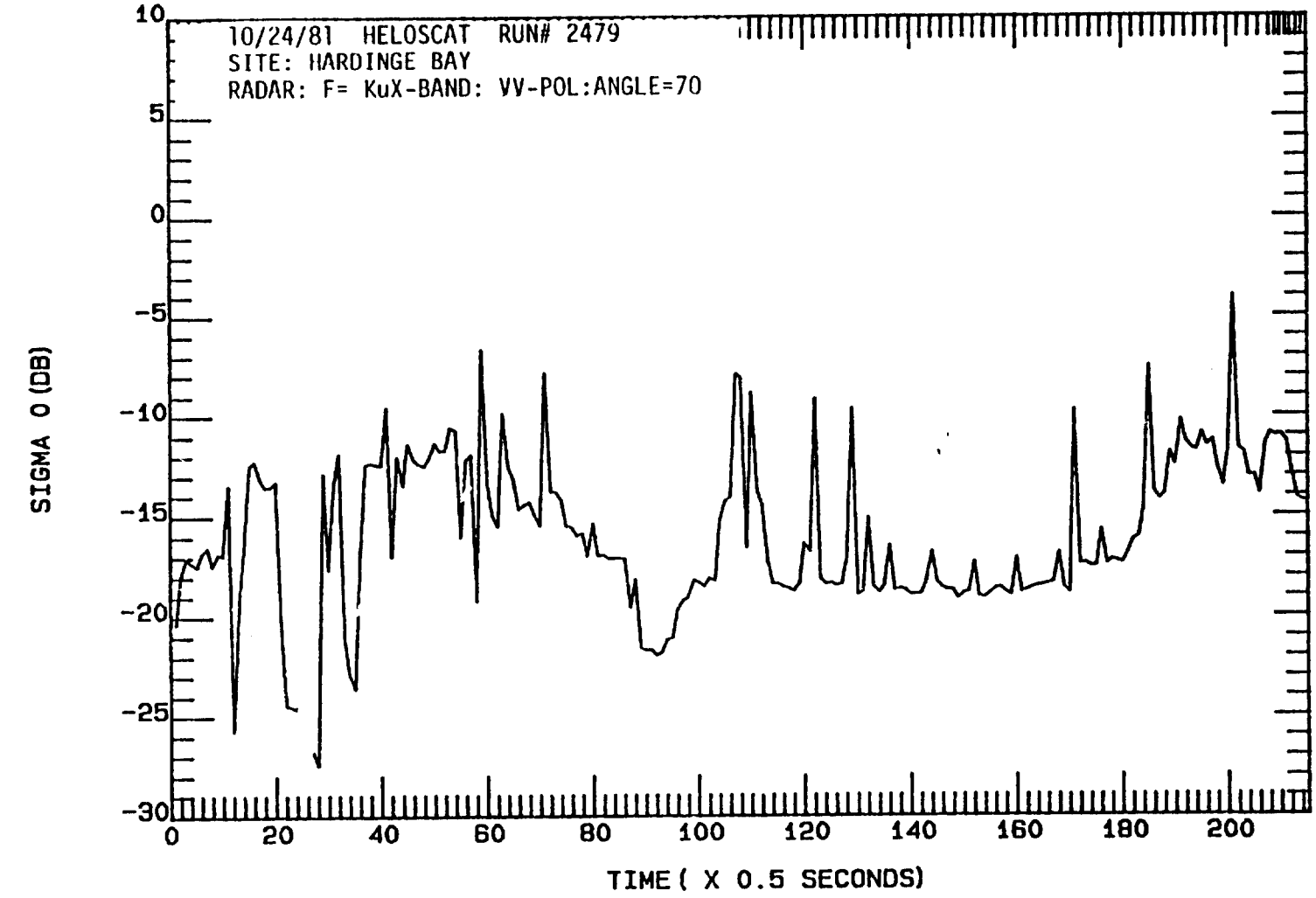

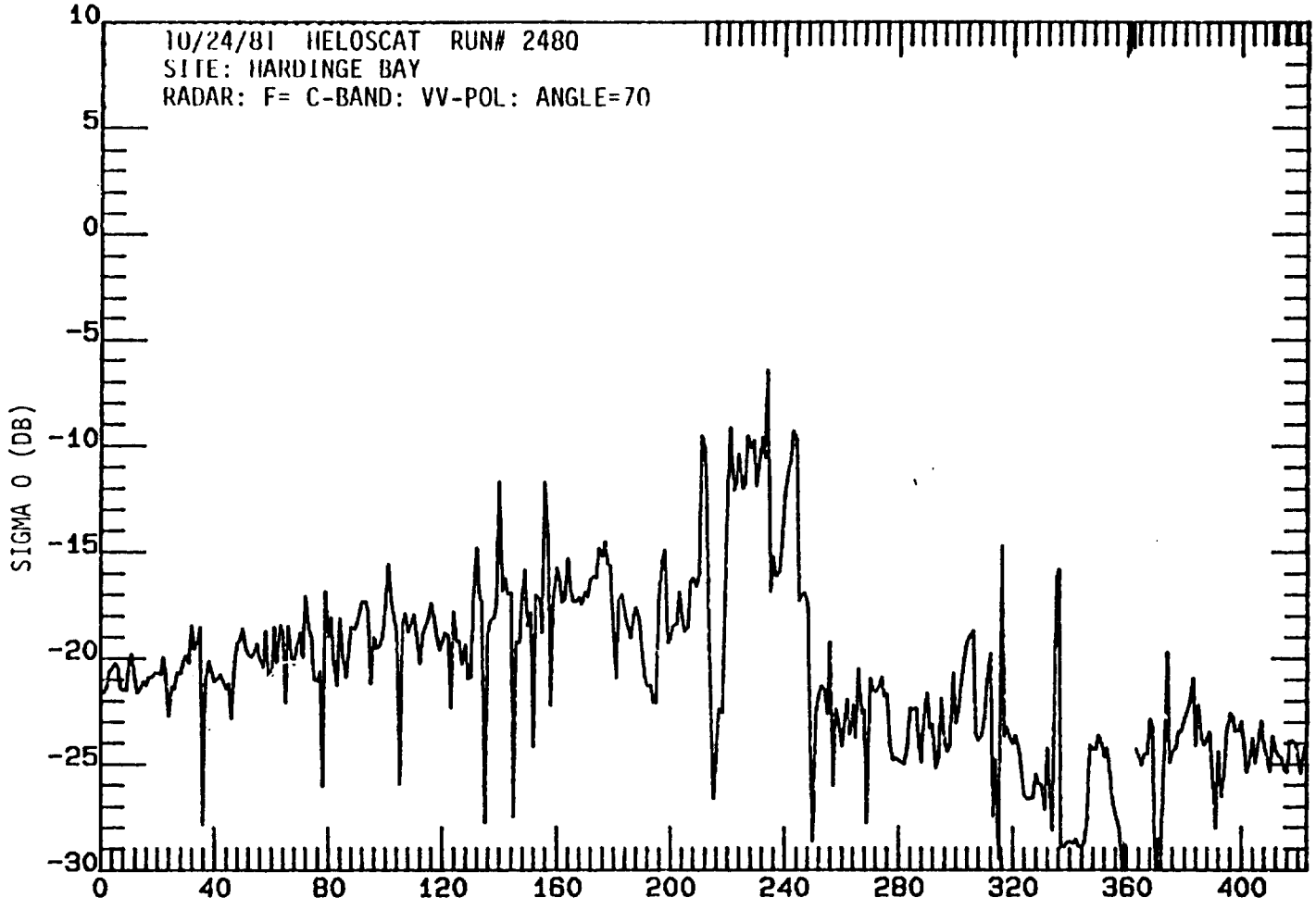

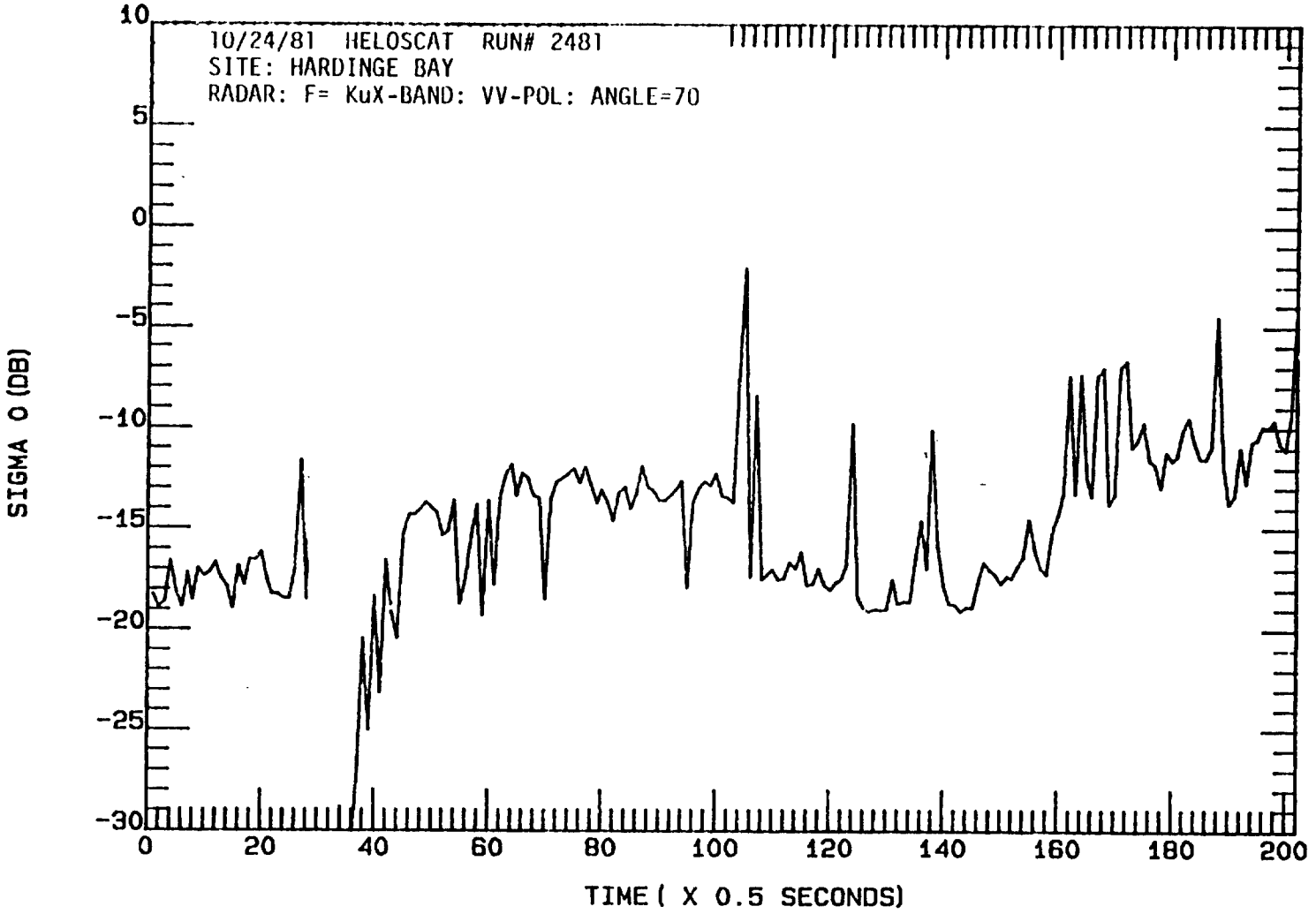
10/24/81 HELOSCAT RUN# 2481
SITE: HARDINGE BAY
RADAR: F= KuX-BAND: VV-POL: ANGLE=70
SIGMA 0 (DB)
10
5
0
-5
-10
-15
-20
-25
-30
0
20
40
60
80
100
120
140
160
180
200
TIME (X 0.5 SECONDS)